Development of a hybrid magnetic-inductive angular sensor with 360° range and stray field immunity

Faculty of Nanotechnologies for ICT

École polytechnique fédérale de Lausanne

author :

Bruno Brajon

Supervisors :

Eng. Lorenzo Lugani,
Prof. Catherine Dehollain
Prof. Matteo Cocuzza

Rome, 2020

A common mistake that people make when trying to design something completely foolproof is to underestimate the ingenuity of complete fools.

— Douglas Adams

To those who remembers…

Acknowledgements

Abstract

This report will show the results for my 6-months master project, which took place in Melexis, a semiconductor company in the Bevaix branch, Switzerland. I worked inside the Pre-Development team, specialized in the design of new concepts for angular position sensors.

This report will go through the development and the experimental evaluation of a novel angular sensor which features a combination of the two main types of sensors and present properties that are not met at the moment using a single device. This internship will produce the first proof-of-concept of this sensor will be developed on PCB using pre-existing ICs developed by Melexis.

The first part of the report will introduce the working principles of two of the main families of angular sensors (magnetic and inductive based sensors) for the automotive environment and will present the project background.

A second part will be dedicated to the presentation of the PCB layout and schematic which will feature the first concept of the hybrid angular sensor.

The third part will show the experimental results obtained with the novel sensor in different situations: in presence of an external magnetic field, metals close to the board, mechanical misalignments.

The fourth part will present a new study for a scaled-down version of the previous prototype, which will progress further the project toward the final concept originally thought by Melexis. The new miniaturized design of the inductive sensor has been produced and tested with satisfying results.

The presentation of the conclusions and the future developments will close the report.

Riassunto

Questa tesi illustrerà i risultati ottenuti nel mio stage di 6 mesi. Quest'ultimo si è svolto in Melexis, una società di semiconduttori, nella filiale di Bevaix, in Svizzera. Il lavoro è stato svolto all'interno del team di Pre-Development, specializzato nella progettazione di nuove proposte per sensori di posizione angolare.

Questo rapporto tratterà lo sviluppo e la sperimentazione di un innovativo sensore angolare che presenta una combinazione di due diversi tipi di sensori e presenta delle caratteristiche che al momento non sono soddisfatte utilizzando un unico dispositivo. Questo stage produrrà il primo proof-of-concept di questo sensore che sarà sviluppato su PCB utilizzando componenti già presenti nell'inventarion di Melexis.

La prima parte del rapporto introdurrà i principi di funzionamento di due delle più importanti famiglie di sensori angolari (sensori magnetici e induttivi) per l'ambiente automobilistico e presenterà il background del progetto.

Una seconda parte sarà dedicata alla presentazione del layout e schematico del PCB che presenterà il primo concept del sensore angolare ibrido.

La terza parte mostrerà i risultati sperimentali ottenuti con il nuovo sensore in diverse situazioni: in presenza di un campo magnetico esterno, metalli vicini alla scheda, disallineamenti meccanici.

La quarta parte presenterà un nuovo studio per una versione ridotta del prototipo precedente, che farà avanzare ulteriormente il progetto verso il concept finale originariamente pensato da Melexis. Il nuovo design miniaturizzato del sensore induttivo è stato prodotto e testato con risultati soddisfacenti.

La presentazione delle conclusioni e degli sviluppi futuri chiuderà la tesi.

Résumé

Ce rapport illustrera les résultats de mon projet de master de 6 mois qui s'est déroulé à Melexis, une entreprise de semi-conducting, dans le siège de Bevaix, en Suisse.J'ai travaillé au sein de l'équipe de pré-développement, spécialisée dans la modélisation de nouveaux concepts de capteurs de position angulaire.

Ce rapport abordera le développement et l'évaluation expérimentale d'un nouveau capteur angulaire qui combine deux principaux types de capteurs et qui possède des propriétés qui ne sont pas encore atteintes en utilisant seulement l'un d'entre eux. Ce stage permettra de produire la première démonstration de faisabilité de ce capteur qui sera conçu sur PCB en utilisant des circuits intégrés préexistants fournis par Melexis.

La première partie du rapport introduira les principes de fonctionnement des deux catégories principales de capteurs angulaires (capteurs magnétiques et inductifs) pour le secteur automobile et présentera le contexte du projet.

Une deuxième partie sera consacrée à la présentation du layout et du schématique du circuit imprimé et qui mettra en avant le premier concept de capteur angulaire hybride.

La troisième partie illustrera les résultats expérimentaux obtenus avec le nouveau capteur dans différentes situations : en présence d'un champ magnétique externe, de métaux proches de la plaque et de désalignements mécaniques.

La quatrième partie présentera une nouvelle étude pour une version du prototype précédent à échelle réduite, qui fera évoluer le projet vers le concept final envisagé par Melexis. La nouvelle conception miniaturisée du capteur inductif a été produite et testée avec des résultats satisfaisants.

La présentation des conclusions et des développements ultérieurs clôturera le rapport.

Contents

Contents

Development of a hybrid magnetic-inductive angular sensor: summary

Melexis is a company that develops microelectronic solutions for the automotive environment. In particular, a large size of its market is centered around angular sensors, which have a widespread use in automotive.

Two important typologies of angular sensors used in this field are magnetic and inductive sensors. Among the state of the art for these two families, however, it still doesn't exist a product which is able to have at the same time 360° range, very high accuracy and robustness, dimensions small enough to allow integration in a single microelectronic package and Stray Field Immunity (SFI). A stray field is an external magnetic field which can be generated by a high current wire in an automotive environment. This usually is the case for the engine environment of electrified cars, in which wires may drive large currents generating large magnetic fields. If a sensor is SFI then these external magnetic fields do not affect the measurement accuracy.
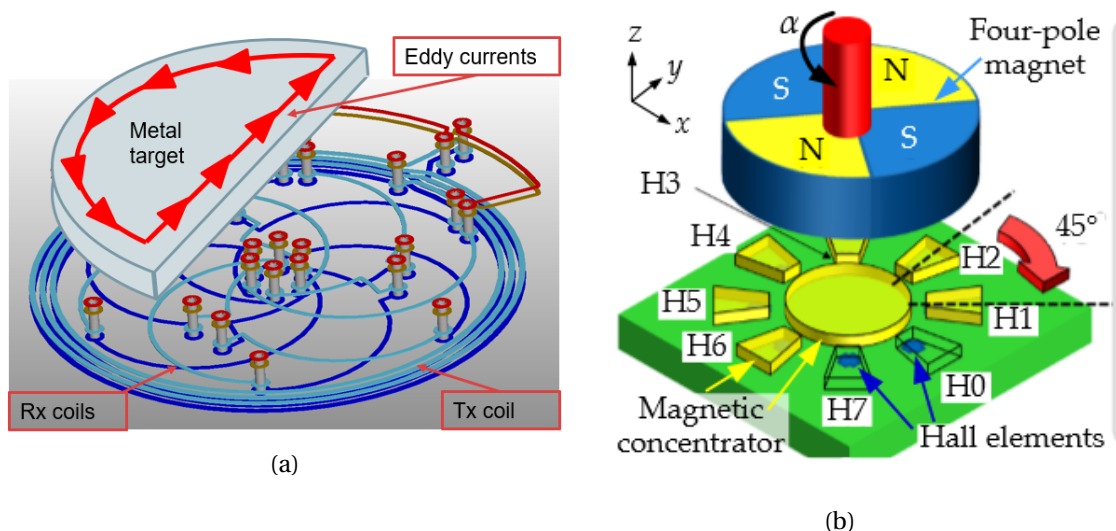

(a)

(b)

Figure 1 – (a) Example of the structure for an inductive sensor with 360° range. (b) The shape of the magnet for the SUN configuration together with the structure on a substrate.

Development of a hybrid magnetic-inductive angular sensor: summary

Most of the magnetic sensors in Melexis' portfolio detect the angular position of a magnet by exploiting the Hall effect, which is used to measure the amplitude of a magnetic field using a structure called Hall Plate (HP). On the other hand, we have the inductive sensor, that is composed of three main parts: the metal target is the rotating object whose angular position is going to be measured, the receiving (Rx) and transmitting (Tx) coils are the means used to retrieve the angular position [Figure 1a]. The Tx coil is put in oscillation generating an alternating magnetic field. This field will generate parasitic currents (or eddy currents) inside the metal target which, in turn, will generate a second magnetic field. This second magnetic field is the only contribution that will be detected by the Rx coils. These Rx coils will produce the signals processed by an IC to retrieve the angular position of the metal target.

In the years, Melexis developed a magnetic sensor that is SFI, very accurate and completely integrated in a single chip. This sensor is based on the SUN concept [Figure 1b] and it can detect the angular position of a 4-pole magnet by measuring the gradient of the magnet field. Due to the symmetry of the magnet, the SUN concept can cover a range of only 180°.

If a wider range is needed (E.g. 360°), one should exploit a second sensor giving a discriminating bit that can be used to understand in which 180° sector is the rotating object's position. Since we only need a discriminating bit, the error threshold for this second sensor will be very large (±90°). It is vital that the second sensor's presence shall not affect the measurements of the magnetic sensor.

The goal of this internship is to design, produce and characterize a proof-of-concept of a hybrid sensor that will use the SUN concept for the accurate angle (up to 180°) together with an inductive sensor with a 360°range for the discriminating bit. The reason behind the choice of the inductive sensor is that theoretically, it should not be able to interfere with the measurement of the magnetic sensor and vice-versa. This concept is illustrated in Figure 2.

Two designs have been developed in order to analyze different issues separately. The first design is a scaled-up version of the hybrid sensor's concept since an integrated version would have required a new IC development. This design was rather based on two already existing ICs: the MLX90377 magnetic sensor featuring the SUN structure and the MLX90510 inductive sensor. The PCB included the two chips together with the coil structure required by the MLX90510. The main two goals for this design were:

- To demonstrate that the two sensors operate completely independently one from the other
- To satisfy the requirements for the hybrid sensor (360° range, SFI, keeping the same performances of the SUN)

Four different tests have been performed on this design. The first test was in nominal working conditions. In the second test, the measurements were taken in the presence of a stray field generated by a neodymium magnet. In the third test, mechanical misalignments, such as off-axis, tilt and airgap variations, were introduced to observe their effect on the measurements. The last test was performed in presence of stray metals, which are pieces of metal which affect heavily the behavior of the inductive sensor.

The results satisfied all the requirements. It was demonstrated that the presence of the inductive sensor had no effect whatsoever on the outcome of the magnetic sensor's measure. The final accuracy of the hybrid sensor in case of mechanical misalignments, stray field and stray metals remained that of the magnetic sensor.
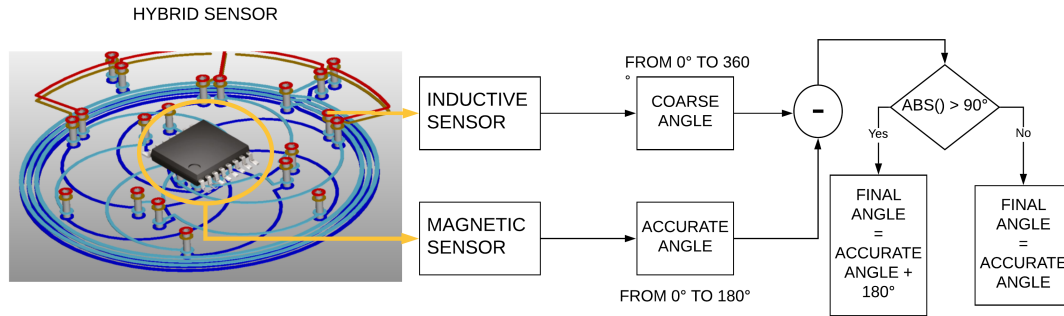

Figure 2 – The working principle behind the Hybrid sensor.

After the promising results obtained with the first design, the project followed with an analysis of the consequences for the miniaturization of the inductive sensor. In this second PCB, a scaled-down version of the inductive sensor that could fit a single package (5mm x 5mm region) was designed. This design did not include the magnetic sensor for two main reasons. First, we demonstrated the orthogonality between magnetic and inductive sensors, therefore, the two channels can be analyzed separately. Second, the magnetic is already developed in CMOS technology and does not need any further miniaturization. In the future development of the sensor, the magnetic part of the IC would be just copied as it is.

The integration of the inductive sensor is the main source of risk for the project. In fact, the amplitude of the signal and the robustness against mechanical misalignments drop drastically with the decreasing of the coil structure's dimensions. However, the goal of this prototype was to understand if the angular error could be kept under the threshold of ±90°, a necessary requirement to be employed in the hybrid sensor.

To work with the same IC of the previous prototype was one of the main design challenges for this new prototype since the MLX90510 has not been designed to work with such a small coil structure.

However, after the promising results of the analytical analysis and the simulation of the new PCB design, it has been decided to proceed with the fabrication of the scaled-down version. A measurement campaign similar to the first one has been performed and the inductive sensor satisfied the requirements to work in the hybrid sensor.

This master project advanced the Technology Readiness Level (TRL) for the hybrid sensor's project by creating the first working proof-of-concept for this type of sensors. Moreover, It has been demonstrated that an integrated version of the inductive sensor is possible to be employed in a hybrid concept. The next step of the project will be to create the first concept included in a single package, with a dedicated IC for both magnetic and inductive parts.

Introduction

Location

The Master project took place in the Swiss branch of Melexis in Bevaix. Melexis is a Belgian microelectronics manufacturer for mixed-signal IC and integrated sensor ICs. Its main field of expertise is the automotive and transportation sector but it is also expanding to smart buildings, industrial and medical applications. The branch in Bevaix, Switzerland is focused mainly on the design and development of position sensors.

Basics of position sensing

Information about the position of an object is crucial, especially in automotive applications. When considering a car, it is required to evaluate, often with high accuracy, the position of a series of mechanical objects for safety and/or performance reasons. Some key examples are the throttle valve, the acceleration pedal, the steering wheel, the transmission gear, and many others. However, position sensors have a wider range of applications, extending well beyond the automotive sector. This is also the reason why a large variety of sensing principles exist among this family.

One of the most common and inexpensive position sensors is simply the potentiometer. Very often used in electronics as a variable resistor, a potentiometer is usually composed of a resistive element along which slides a conductive wiper which shorts part of the resistance. If the current across the resistance is fixed the electric potential across it will vary according to the position of the wiper. Therefore, by measuring the voltage we can evaluate the wiper's position.

Another example of a position sensor is the capacitive displacement sensor. In this case, similarly to the case of the potentiometer, the position of the object will be found by evaluating the variation of a capacitance instead of resistance. The capacitance, if one considers a parallel plate model, is defined as $C = \epsilon_0 \epsilon_r A/d$ where ϵ_0 is the permittivity of free space constant, ϵ_r is the dielectric constant of the material in the gap, A is the overlapping area of the metal plates, and d is the distance between the plates. The variation of the relative position of the two plates will vary either d or A, depending on the type of motion. By evaluating the variation of the capacitance we can then quantify the displacement.

Optical sensors (e.g. photoelectric sensor, Laser rangefinder, etc.) are common as well. These

sensors emit an electromagnetic wave and look for changes in the return wave. They are largely used in industrial manufacturing and also to measure very long distances up to tens of kilometers.

The types of sensors mentioned above are not usually used in automotive environments (E.g. the motor compartment of a car). The continuous movement of a car will inevitably produce e.g. dust or oil drops which will affect the measurement of both an optic sensor and a capacitive sensor. For the former, the particles will act as an obstacle, altering the measurement. For the latter, they will change the permittivity of the air gap between the two plates, hence the capacity to be evaluated. The potentiometer, on the other hand, is not adequate since, after several uses, the tip of the wiper will wear out. Moreover, it is required a sensor that could sustain near-engine areas temperatures, which can go as high as 160°C when the car is running, but it should be able to withstand equally temperatures down to -40°C when the engine is turned off in cold climates. The two types of sensor best suited for this type of employment are magnetic sensors and inductive sensors. Both of these sensors are contact-less, thus preventing damage due to wear and insensitive to dust or oil, making them more reliable.

Among the magnetic sensors' family, the most common are magnetoresistive sensors and Hall sensors. The magnetoresistive sensors can detect the position of a magnet by measuring the resistance of a magnetoresistive material which has the property to change its resistivity if immersed in a magnetic field. Hall sensors, on the other hand, exploit the Hall effect to detect the presence and direction of a magnetic field. Hall sensors can be completely integrated (E.g. using $0.18\mu m$ CMOS technology) making them very cheap and suitable for narrow spaces applications.

Inductive sensors can be divided into two main categories. A first class exploits the measure of the variation of the inductance of a coil with the motion of an object. As an example, when a coil is approached by a metallic object, its inductance will vary according to the proximity of the metal. A high-frequency magnetic field is generated by coil L in the oscillation circuit. If a metal object is put close to the coil, parasitic currents will flow inside it, becoming an external load for the oscillating circuit. By measuring the amplitude variation or alternatively the frequency variation of the oscillating signal, we are able to evaluate the distance of the metal object from the coil.

The other class of inductive sensors is based on the transformer principle. These sensors comprise a primary or transmission(Tx) coil and a set of secondary or receiving(Rx) coils. The coupling between the Tx and Rx coils is modulated by a movable metallic target where eddy currents (or parasitic currents) are excited by the Tx coil.

In particular, this Master project will focus on Hall sensors from the magnetic sensors family and the transformer-based sensors from the inductive sensors family. The two technologies will be presented in reference to the detection of the angular position of an object.

Master project

The goal of this master project is to develop a proof of concept for an innovative hybrid angular sensor that will combine the inductive and magnetic sensors' principles. The first prototype will be a scaled-up version of the final concept and it will be used to show the independence of the two measurement principles. A second prototype will be produced in order to assess the effects of miniaturization on the inductive part of the hybrid sensor to fit a single package.

Structure of this report

chapter 1: presentation of the working principle of the two types of sensors that will be used for the proof of concept. In particular, there will be presented the properties of both magnetic Hall angular sensors and eddy current based inductive angular sensors. The chapter will also explain what is the final goal of the project and what role has this internship for its completion.
chapter 2: presentation of the design that will be produced on PCB with a special focus on the chips used for the magnetic and inductive sensors. The schematic of the prototype will be presented together with the PCB layout of the test board.
chapter 3: presentation of the experimental results for the measures on the test board. A total of 4 tests will be performed to assess the correct behavior of the sensor and to demonstrate that the two measurement systems are independent.
chapter 4: presentation of the results for the analysis of the consequences for scaling down the inductive part of the hybrid sensor. After a simulation of a possible miniaturized concept, a new prototype featuring only the inductive part of the hybrid sensor was built. A set of measurements have been taken in order to assess the behavior of this scaled-down version.
chapter 5: presentation of the conclusions obtained from the internship together with the perspectives for the future of the project.

1 Magnetic & inductive sensors

The Hall-based angular sensor and the inductive angular sensor are the two main components of the final hybrid sensor. This chapter will present their respective working principles and their major advantages and defects. Finally, there will be a section dedicated to the challenges addressed in this thesis and how they relate to the final goal of the project.

1.1 Magnetic Hall Sensors

1.1.1 Introduction

The Hall effect was discovered by Edwin H. Hall in 1879. Figure 1.1 shows a conductive slab in which a current flow is injected using the generator V_X connected on the sides of the slabs perpendicular to the X-axis which generates an electric field (E_x) along the length of the conductor. On the sides of the slab perpendicular to the Y-axis, a voltmeter (V_H) is connected
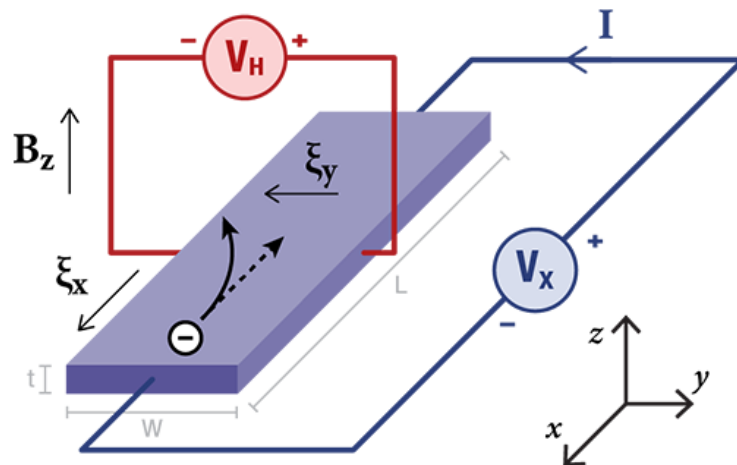

Figure 1.1 – The principle behind the Hall effect phenomenon.

which in presence of a magnetic field will sense a difference of potential.

The current passing through the slab generated by the application of V_X is equal to:

$$I_x = J_x w t = n q v_x w t \tag{1.1}$$

where J_x is the current density ($J_x = \sigma E_x$ where σ is the conductivity of the slab), w is the width of the slab, t is its thickness, nq is the slab's charge density and v_x is the drift velocity of the carriers (defined as $v_x = \mu_e E_x$ where μ_e is the electron mobility in the slab). If we now assume the presence of a magnetic field (B_z), then the moving charges will be subjected to the Lorentz force $\vec{F} = q\vec{v} \times \vec{B}$. This force will deviate the charges perpendicularly to both its direction and the direction of the applied magnetic field. As a result, there will be a charge accumulation on one side of the slab which will create an electric field in the y-direction. The force of this electric field on the charges ($\vec{F} = q\vec{E}$) has to be balanced with the force of the magnetic field when the steady-state is reached. It is easy to show that this condition is achieved if $E_y = v_x B_z$ [(1)]. The Hall potential will, therefore, be equal to :

$$V_H = -\int_0^w E_y \, dy = -E_y w = -v_x B_z w = -\mu_e E_x B_z w = -\frac{I_x B_z}{nqt} \tag{1.2}$$

V_H is used to evaluate the intensity of the magnetic field perpendicular to the metal slab. For modern Hall sensors, the slab of metal is replaced with a doped semiconductor region. This is the basic component of Hall sensors: the Hall Plate (HP).

The sensitivity for these HP is defined as:

$$S_v = \frac{V_H}{V_b B} \tag{1.3}$$

where V_B is the biasing voltage of the Hall device. Since V_H depends on the electron mobility, in order to reach very high sensitivity [Equation 1.2], one can use high-electron-mobility materials such as InSb, GaAs, or low-doped Si.

Two different types of HP can be used: vertical and horizontal. The horizontal HP (Figure 1.2a) is composed of four contacts placed on a sheet of n-doped (or sometimes p-doped) semiconductor. Through the first two contacts(C_1 and C_3) will pass the current, while across the other two contacts(C_2 and C_4), perpendicular to the firsts, will be generated a potential(V_H) in presence of a magnetic field (B). The HP would ideally have a fourfold symmetry. In reality, small misalignments will always be introduced during fabrication depending on the resolution of the lithography tools. This leads to a misalignment of the position of the electrodes both on the x_1 and x_2 axis with respect to the doped well. These misalignments will cause the carriers to flow closer to an electrode even in the absence of an external magnetic field. This is the source of an offset on the sensing electrodes that can reach also 1mV. According to the sensitivity of the HP (in the case of integrated horizontal HP we go up to $0.120\,T^{-1}$(4)), this is translated with an error on the measured magnetic field that can range from 5 mT to 10 mT. This offset can be removed using the 4-phases spinning-current method [(4)]. This method consists of adding a selector circuit which can exchange the roles of the 4 electrodes:

- Phase 1: the current will flow from C_1 to C_3, while the Hall voltage will be measured
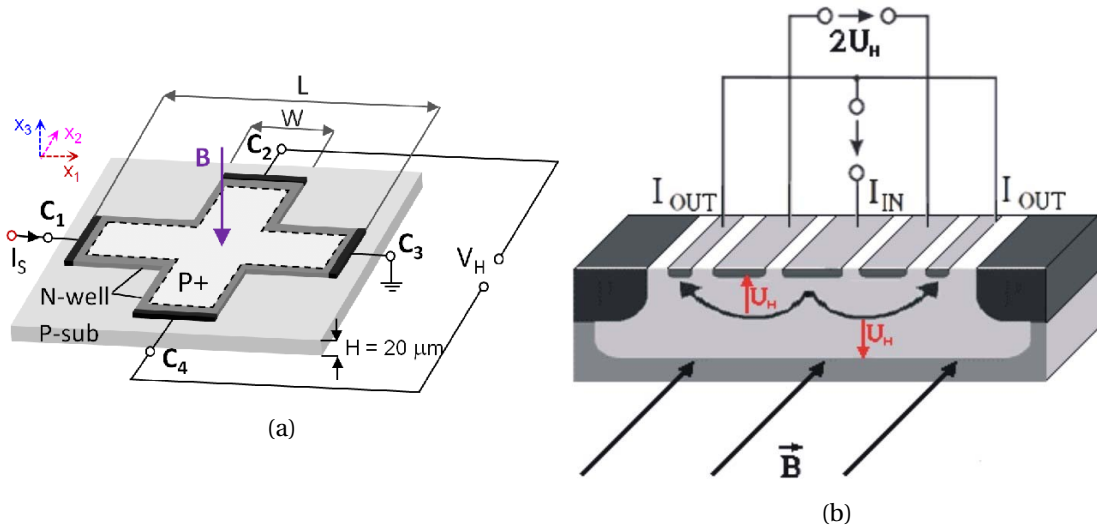
Figure 1.2 – (a) Example of a horizontal Hall plate[(2)]. (b)Example of a vertical Hall plate[(3)]

across C_2 and C_4

- Phase 2: the current will flow from C_4 to C_2, while the Hall voltage will be measured across C_1 and C_3
- Phase 3: the current will flow from C_3 to C_1, while the Hall voltage will be measured across C_2 and C_4
- Phase 4: the current will flow from C_2 to C_4, while the Hall voltage will be measured across C_1 and C_3

For all cases, the Hall voltage will remain the same while the offset will change its sign maintaining its amplitude. Most of the offset component is therefore easily removed from the final signal by averaging the 4 voltage, leaving only a residual offset of few micro-volts (about $1\mu T$ error on the magnetic field).

The horizontal HP alone is able to detect only the component of the magnetic field that is perpendicular to the horizontal plane (along the x_3 axis). On the other hand, the vertical HP can detect only the component that is parallel to the horizontal plane(Figure 1.2b).

The vertical HP is composed of the same conductive semiconductor sheet but the electrodes are all on the same side. One of them will inject the current that will flow equally to the two output electrodes placed on the two different sides of the input electrode. The two sensing electrodes are placed in between the two couple of output electrodes and the input electrode. Since the current will be flowing in different directions, upon application of the magnetic field, the current flow will get closer to the sensing electrode on one side and further on the other side. This is how the difference of potential is generated between the two sensing electrodes. This type of HP allows sensing the in-plane field (with respect to the wafer). However, this type of HP presents generally lower offset rejection and lower sensitivity (usually around 0.01 T^{-1} (4)) with respect to the horizontal HP. From the above considerations, it is clear that the

horizontal HP is preferable over the vertical HP. However, when using horizontal HP, the field of interest might be in a direction for which the HP cannot detect it. In this case another component is required: an Integrated Magnetic Concentrator(5) (IMC).
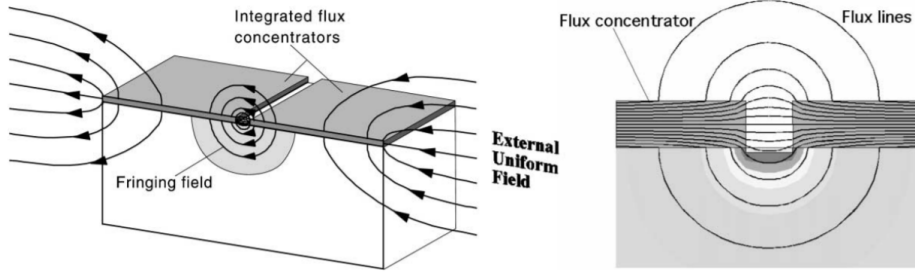

Figure 1.3 – The IMC presented in (5)

The IMC is a high permeability ferromagnetic layer that is able to bend and concentrate external magnetic field lines. The concentration of the field lines provides a gain factor (usually referred to as g_c) that in some cases can be even higher than 5 (4). This structure alone can be deposited above the HPs to bend the horizontal field lines in order to generate a perpendicular component that can be detected by the HPs. In some configurations, two IMCs can be placed close to each other forming a small airgap fissure at the center (Figure 1.3) to increase even more the IMC gain. The parallel field lines get concentrated by the ferromagnetic material and the gap causes the bending of the field lines transforming them from parallel to perpendicular. Placing an IMC above a horizontal HP we achieve the detection of the parallel field and an increase of the signal provided by the IMC gain factor.

The intrinsic noise of a magnetic Hall sensor, which will define its maximum accuracy, is described by its Noise-Equivalent Magnetic Field spectral density (NEMFsd). The physical limit for this noise is defined as follows:

$$NEMFsd, min \geq \frac{\sqrt{4kTR_H}}{g_c S_v V_b} \tag{1.4}$$

where k is the Boltzmann constant, T the absolute temperature and R_H the resistance of the HP. In order to minimize this value, devices with high-carrier-mobility can be used to reduce the resistance and increase the sensitivity. V_b is usually a strongly limited quantity in modern microelectronics (usually between 2V and 4V)(4). Even if a low resistance of the plate will result in high robustness to thermal noise, it is advised to use HP with few $k\Omega$ of resistance in order to limit the current drain and, consequently, the power consumption. Since the $NEMFsd, min$ depends on the sensitivity of the HP, it will be higher for vertical HP (around $400nT/\sqrt{Hz}$) compared to horizontal HP (around $125nT/\sqrt{Hz}$)(4).

1.1.2 Hall effect based angular sensors

The Hall effect can be employed by an angular magnetic sensor in order to evaluate the absolute angular position of a magnet. The Melexis' Triaxis products are based on a magnetic sensor technology capable of very precise three-axis magnetic field measurements. The magnet is usually attached to the movable part for which we are interested to know its angular position. At this time the third generation of these sensors has been reached.
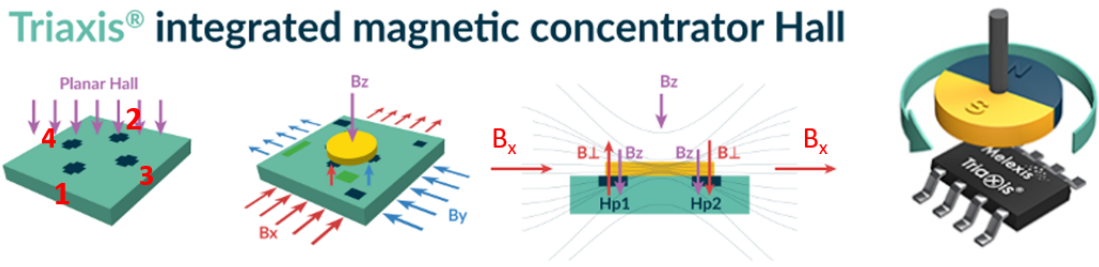
Triaxis Single-disc

Figure 1.4 – The working principle of the Triaxis Single-disc configuration

The first example for these magnetic angular sensors will be the Triaxis II Gen, or Triaxis Single-disc. [fig.1.4]. This device is a 360° range magnetic sensor able to detect the absolute position of a dipolar magnet. It is composed of four horizontal HP (in dark blue in Figure 1.4) and a magnetic concentrator (in yellow) at the center. Two HP will be placed along the X-axis and two others will be placed on the Y-axis. Let's consider the B_x component of the magnetic field. In this case, the magnetic concentrator will bend the B_x field, creating a new $B_{\perp x}$ component on the HPs on the X-axis. The $B_{\perp x}$ field on the second HP will have the same amplitude but opposite direction with respect to the $B_{\perp x}$ on the first HP. Therefore, by making the difference between the two signals, we obtain a strong, differential signal on both the X and Y axes. On the other hand, the signal from both HP3 and HP4 will be zero. For this field component we will have the following signals:

$$
\begin{cases}
V_a = V_{hp1} - V_{hp2} = 2S_v V_b B_{\perp x} = 2S_v V_b g_c B_x \\
V_b = V_{hp3} - V_{hp4} = 0
\end{cases}
\tag{1.5}
$$

In the case of the B_y component we will be in the complementary situation:

$$
\begin{cases}
V_a = V_{hp1} - V_{hp2} = 0 \\
V_b = V_{hp3} - V_{hp4} = 2S_v V_b B_{\perp y} = 2S_v V_b g_c B_y
\end{cases}
\tag{1.6}
$$

Since the reading is differential,it is easy to see that any B_z component will be rejected. The final evaluation of the angular position of the dipolar magnet is done using the following

expression:

$$\alpha = \arctan\left(\frac{\sin\alpha}{\cos\alpha}\right) = \arctan\left(\frac{B_x}{B_y}\right) = \arctan\left(\frac{V_a}{V_b}\right) \tag{1.7}$$

The main drawback for this concept is that it is not immune to stray fields. A stray field is an external magnetic field generated by a source other than the magnet outside the chip. Especially in electrified cars, large stray fields in the order of 1 to 5 mT are very common [(6)]. The critical parts which can generate such fields are the high current cables between the battery and the electrical motor. A sensor is called Stray Field Immune SFI if it is insensitive to the effect of a stray field.

Going back to the Triaxis Single-Disc configuration, an external contribution to the in-plane field will inevitably affect the measurement of the sensor since it is unable to distinguish between a stray field and the field generated by the magnet.

1.1.3 Stray-field immune options

dBz mode

An alternative configuration for the Triaxis Single-Disc structure involves the removal of the magnetic concentrator, keeping only the 4 HPs. This configuration is called dBz mode [Fig.1.5]. In this configuration, the horizontal HP will detect only the perpendicular component of the
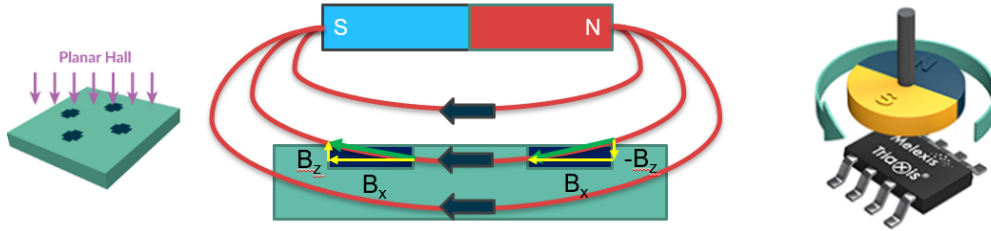
Figure 1.5 – The working principle of the dBz mode. $B_\perp$ will be the only contribution to V_H (7).

field lines coming from the magnet. The signals from the the two couples of HP will be:

$$\begin{cases} V_a = V_{hp1} - V_{hp2} = 2S_v V_b B_z \\ V_b = V_{hp3} - V_{hp4} = 0 \end{cases} \qquad \begin{cases} V_a = V_{hp1} - V_{hp2} = 0 \\ V_b = V_{hp3} - V_{hp4} = 2S_v V_b B_z \end{cases}$$

    When the magnet is aligned   When the magnet is aligned

    with respect to the X-axis   with respect to the Y-axis

Despite the fact that the differential reading, as clearly visible from Figure 1.5, the B_z component is really small and it is not concentrated by any IMC. Thus, the accuracy of the sensor is worse compared to other concepts since the signal coming from the Hall plates is low. However, it is a Stray Field Immune solution since a uniform external field applied in the

in-plane direction will not be detected by the horizontal HP and a constant field perpendicular to the plane will be removed by the differential reading.

This solution allows the detection of the angular position of a dipolar magnet on a full 360° range using the same expression shown in Equation 1.7.

SUN configuration

The alternative SFI solution is the so-called "SUN" structure and it has been deployed since the Triaxis III Gen. products. This concept makes use of a 4-poles magnet as shown in Figure 1.6. For the described magnet the field lines on a plane parallel to the sensor plane will be in the shape of Figure 1.8.
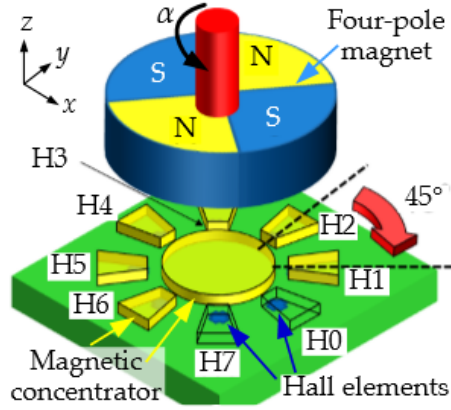

Figure 1.6 – The shape of the 4-pole magnet for the SUN configuration together with the structure on a substrate (6).

A larger IMC is placed at the geometrical center of the structure and it is surrounded by eight different Hall plates. Upon each one of them is placed a magnetic concentrator in order to bend and concentrate the in-plane field as shown in Figure 1.7.

To better understand the working principle of the structure, Table 1.1 will show the values of the signals retrieved by the HPs for different fields contributions.

In the first case of Table 1.1 the magnet is in its starting position (0°). The in-plane magnetic field line (in black in Figure 1.8) are parallel with respect to the IMC placed upon HP1, HP3, HP5 and HP7. For this reason the field is not bent upward by the IMC and therefore we do not have any contribution from these HPs. On the other hand, on the other 4 HPs, we have a strong signal $V_H = S_v V_b g_c \frac{\partial B_x}{\partial x} \frac{\Delta x}{2}$ (Δx is shown in table Figure 1.8, due to symmetry we can say $\Delta x = \Delta y$).

The signals which will be used to retrieve the angular position of the sensor are described by the following equation:

$$\cos 2\alpha = V_{H0} - V_{H2} + V_{H4} - V_{H6} = 2 S_v V_b g_c \left(\frac{\partial B_x}{\partial x} - \frac{\partial B_y}{\partial y} \right) \Delta x \qquad (1.8)$$

$$\sin 2\alpha = V_{H1} - V_{H3} + V_{H5} - V_{H7} = 2S_v V_b g_c \left(\frac{\partial B_x}{\partial y} - \frac{\partial B_y}{\partial x} \right) \Delta x \qquad (1.9)$$

$$\alpha = \frac{1}{2} \arctan \left(\frac{\sin 2\alpha}{\cos 2\alpha} \right) \qquad (1.10)$$

In the second case the magnet is rotated by 45°(Figure 1.9). Here the role of the HP are inverted with respect to the first case and therefore the sine wave will be maximum this time and the cosine wave will be zero.

The other cases are used to demonstrate that this configuration is SFI.

Field	HP								Signals	
	0	1	2	3	4	5	6	7	$\cos 2\alpha$	$\sin 2\alpha$
4pole(0°)	$+V_H$	0	$-V_H$	0	$+V_H$	0	$-V_H$	0	$4V_H$	0
4pole(45°)	0	$+V_H$	0	$-V_H$	0	$+V_H$	0	$-V_H$	0	$4V_H$
$\partial B_z/\partial x$	$-V_{H1}$	$-V_{H2}$	0	$+V_{H2}$	$+V_{H1}$	$+V_{H2}$	0	$-V_{H2}$	0	0
$\partial B_z/\partial y$	0	$+V_{H2}$	$+V_{H1}$	$+V_{H2}$	0	$-V_{H2}$	$-V_{H1}$	$-V_{H2}$	0	0
B_x	$-V_{X1}$	$-V_{X2}$	0	$+V_{X2}$	$+V_{X1}$	$+V_{X2}$	0	$-V_{X2}$	0	0
B_y	0	$-V_{Y2}$	$-V_{Y1}$	$-V_{Y2}$	0	$+V_{Y2}$	$+V_{Y1}$	$+V_{Y2}$	0	0
B_z	$+V_Z$	$+V_Z$	$+V_Z$	$+V_Z$	$+V_Z$	$+V_Z$	$+V_Z$	$+V_Z$	0	0

Table 1.1 – This table shows how the SUN structure behaves in presence of different magnetic fields

Third and fourth case demonstrate the insensitivity of the structure for gradients on the z-axis, (E.g. like the ones produced by a dipole magnet like in (Figure 1.5)). In this case the gradient will be symmetrical with respect to the center of the structure. The gradient can be split in the two components on the X-axis and the Y-axis. Taking in consideration the X-axis the highest

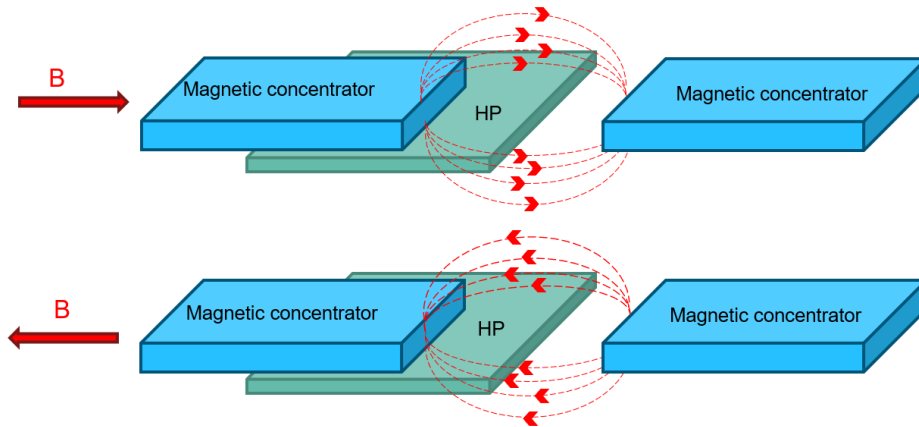Figure 1.7 – The mechanism whereby the magnetic concentrator bends the magnetic field. Since we are considering horizontal HPs, the field that will cause the Hall voltage will be the one perpendicular to the HP. Depending on the direction, the HP will generate signals of opposite signs.
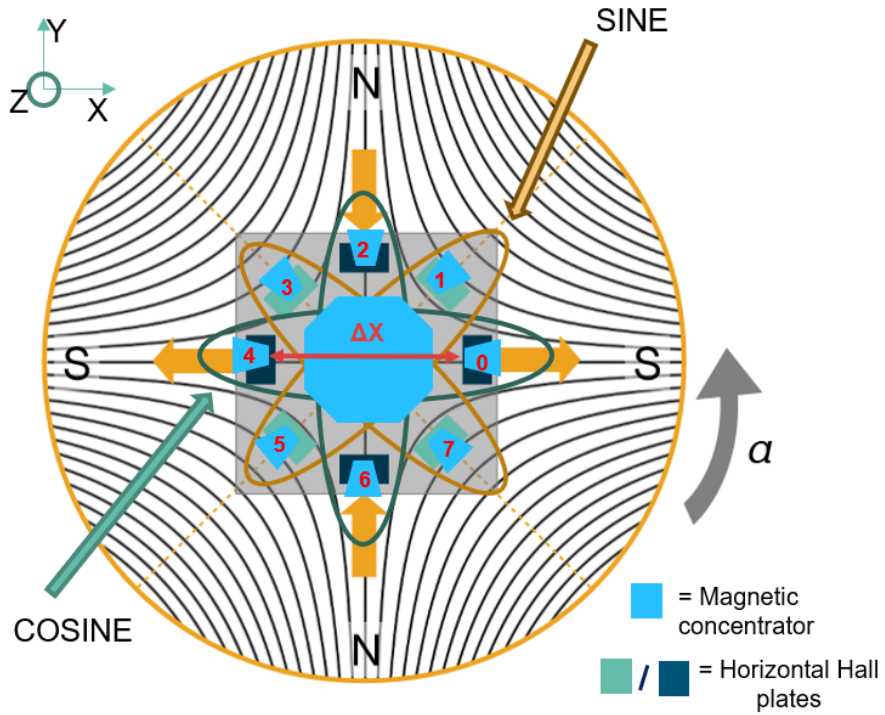
Figure 1.8 – The SUN structure. 4-pole magnet's angle equal to 0°.

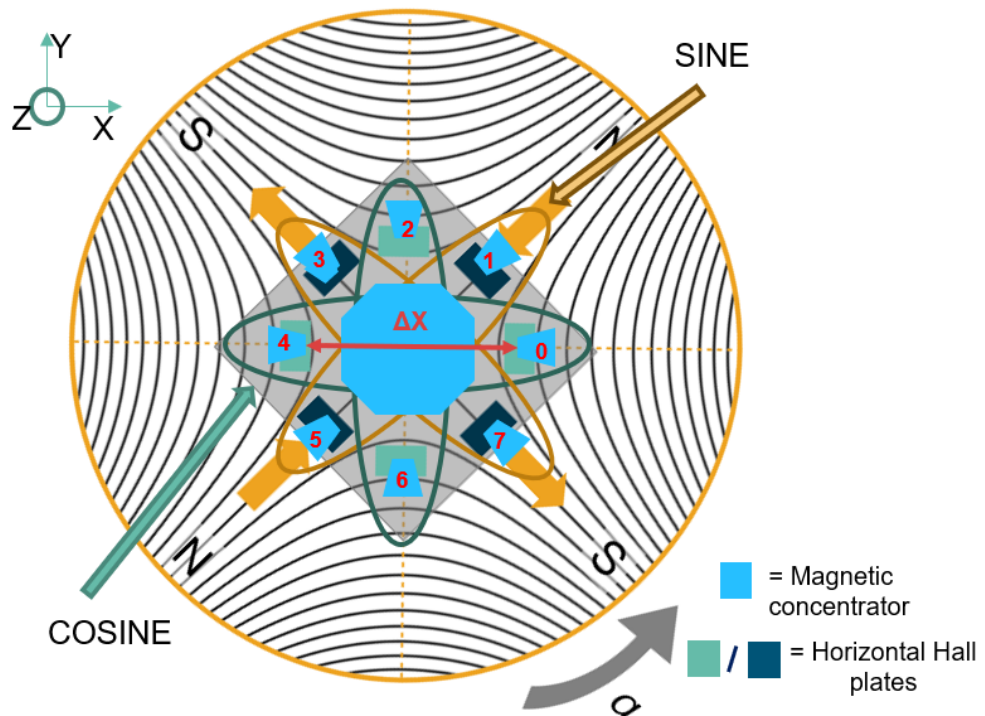Figure 1.9 – The SUN structure. 4-pole magnet's angle equal to 45°.

contribution V_{H1} will be given by HP0 and HP4. On the other hand, the contribution on HP1, HP3, HP5 and HP7 will be different from V_{H1} but, due to the symmetry of the structure, the amplitude will always be the same (V_{H2}). In fact, the contribution on the HPs is balanced for both the component on the x-axis and the y-axis respectively. By using equations eqs. (1.8) and (1.9), It is easy to observe that there will be no contribution on the final measure.

The last three cases cover the case of a constant external magnetic field. All the constant components on any axis is rejected, giving no contribution to the sinusoidal signals. Let's consider the X-axis as example. When the magnetic field is not passing through both the central IMC and the IMC above the HP, the field lines are not bent and, therefore, they are not detected by the horizontal HPs. Therefore the contribution from HP2 and HP6 is zero. Part of the magnetic field passing over HP1, HP3, HP5 and HP7 will be detected and they will provie a contribution as shown in Table 1.1. We will have the highest contribution for HP4 and HP0 for which the magnetic field is totally bended ($V_{X1} > V_{X2}$).

The same argument can be applied for the other two axes. The final contribution for these constant magnetic fields is null to the final measure.

It's easy to understand, both from the periodicity of the magnet and of Equation 1.10, that the range of this sensor only reaches 180°.

Despite this drawback, the SUN configuration is overall more robust than the DBz mode. It works with stronger signals than the latter, due to the presence of the magnetic concentrators. All these characteristics grant to the design a high accuracy (error lower than 0.8° for thermal drift).

It is worth mentioning that another version of the SUN exists. It is called Bubble and the structure is identical to the SUN version except for the absence of the central octagonal magnetic concentrator. This configuration provides a lower g_c avoiding the saturation of the signal from the HPs if very strong magnets are employed for angular detection.

This magnetic concept, and all the others presented in this chapter, are composed of multiple HPs. The signals that are used for the evaluation of the angular position of the magnets come from the difference between the signals from two or more HPs. For all configuration, it has been assumed that every HP is equal to each other and have the same sensitivity to a magnetic field [Equation 1.3]. This is an ideal assumption and, in reality, the main source of error on the angular position will be due to sensitivity mismatches between the HPs.

One of the conditions that could induce a change in the sensitivity in the HPs is a thermal gradient along the sensor structure. The mobility of the carriers in the HP's semiconductor has a strong dependence on the temperature. The conductivity of the HP will vary accordingly. This change in the conductivity will affect the Hall potential sensed by the HP since the current across the plate will also vary [Equation 1.2].

The carriers' mobility has a strong dependence also on the stress on the semiconductor. The stress can be induced by the aging of the package and have different contributions on each HP. Thus, this is another source of sensitivity mismatch.

The SFI versions of magnetic sensors have a limit for the amplitude of the stray-field before it starts affecting the measurement. In particular, magnetic fields higher than $5mT$ will increase the angular error of the sensor that would bring its measurement out of specs. The reason

behind this limit is the sensitivity mismatch between the HP. If the field is too high, even if the sensitivity of two differential HPs are lightly mismatched, the difference between the output signals will include a component due to the stray field. Also, the presence of a gradient in the stray field can increase further the angular error since it is not rejected by the differential reading of the signals.

1.2 Inductive Sensor

1.2.1 Introduction

The basic principle, on which this type of angular sensor is based, is the law of induction. This effect was firstly discovered by Faraday in 1831 and Maxwell expressed it in differential form:

$$\nabla \times \vec{E} = -\frac{\partial \vec{B}}{\partial t} \tag{1.11}$$

Where $\vec{E}$ is the electric field and $\vec{B}$ the magnetic field. To better understand the meaning of Eq.[1.11], let's apply the Stokes' theorem and retrieve the integral form of the law:

$$\oint_\Gamma \vec{E} \cdot d\vec{s} = -\int_S \frac{\partial \vec{B}}{\partial t} \cdot \vec{n} \, dA = -\frac{\partial}{\partial t} \int_S \vec{B} \cdot \vec{n} \, dA \tag{1.12}$$

where Γ is any closed curve and S is any open surface that has Γ as an edge. The second expression ($\frac{\partial}{\partial t} \int_S \vec{B} \cdot \vec{n} \, dA$) of the electric field circulation over Γ ($\oint_\Gamma \vec{E} \cdot d\vec{s}$) is the most meaningful to understand the relation between $\vec{E}$ and $\vec{B}$: a variation of the flux of a magnetic field across a surface S will determine the presence of an electromotive force along the closed line Γ. The electromotive force will generate a current along the line if it is included inside a conductive material. This principle is essential to understand the origins of Foucault's currents which are the basis of the principle of the inductive sensor.

The Foucault's currents, also called eddy currents, are the result of the interaction between a magnetic field and a conductor. In order to observe eddy currents inside a conductor, there must be a variation of the magnetic field or of the position of the metal with respect to a fixed magnetic field. Let's consider a varying magnetic field and a fixed metal slab perpendicular to the direction of the field. According to Equation 1.12, if one is to take closed lines inside the metal, non zero electric field circulation will appear on these lines. The electric field will exercise an electromotive force on the free carriers of the metal which will move accordingly and generate these parasitic currents. Due to the minus sign of the Faraday's law, the currents will be oriented so that they will produce a field in the opposite direction to the original one. This principle is at the basis of many applications, E.g. magnetic breaks and magnetic levitation[(8)]. In our case, we will take advantage of this effect to detect the angular position of a metal object inside a varying magnetic field.

1.2.2 Eddy currents in angular sensors

The main components of an inductive sensor for angular position sensing are a Transmitting (Tx) coil, a set of Receiving (Rx) coil and a metal object (target) on top of the structure [Figure 1.10]. The sensor will be able to evaluate the angular position of the metal target.

For the following examples, we will analyze a fully 360° range sensor which will be the version designed during the project. For this sensor, the shape of the metal target will be a half-moon. A high-frequency oscillating current is excited in the Tx Coil that generates a varying magnetic
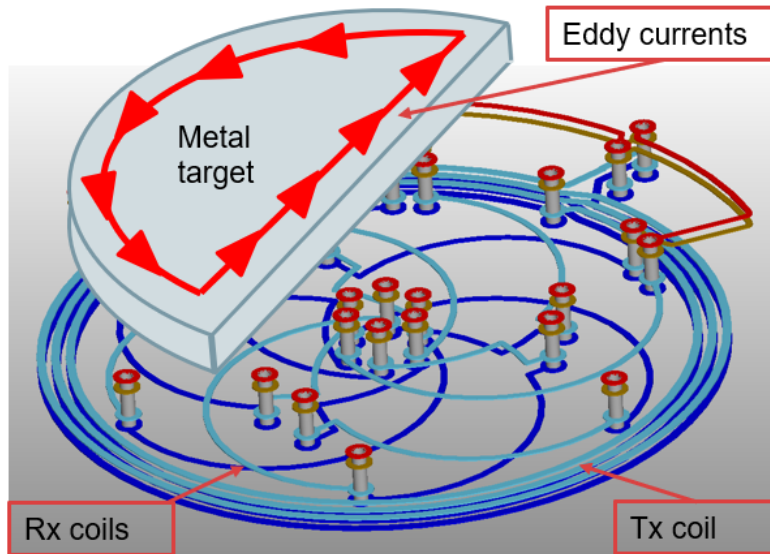
Figure 1.10 – Example of the structure for an inductive sensor with periodicity N=1. The range of this sensor will be 360°. In red it is highlighted the eddy current.

field. This magnetic field will generate in return eddy currents inside the metal target according to Equation 1.11.

The Rx coils are connected to high impedance nodes and therefore they will generate a modulated voltage signal. These high impedance nodes avoid also the generation of a magnetic field from the Rx coils by preventing current flows.

As a first approach, we consider an Rx coil composed of a single winding positioned as in Figure 1.11(a). The eddy currents inside the metal target will generate a modulated magnetic field that will oppose the magnetic field generated by the Tx coil. To simplify the concept one can imagine a current flowing along the edge of the metal target in a direction for which the field generated is in an opposite direction to the Tx coil's field. Finally, the Rx coil will collect the total magnetic field that will depend on the position of the metal target.

When the target will be exactly above the Rx coil, the amplitude of the total magnetic field in that region will be minimum and therefore the voltage signal will be minimum. When there is not the contribution of the metal target on the magnetic field above the Rx coil, the voltage signal will be maximum [Figure 1.11(a)]. This configuration is useful to understand the basic principle for this type of sensors, however, it is affected by various defects. In this configuration, the signal will have a fixed offset due to the constant contribution of the Tx coil field. Moreover, a single Rx Coil will not provide a 360° range but only a 180° range since within one period of the signal we have 2 possible values of the angle for the same amplitude, therefore at least a second Rx coil is necessary for the full range requirement.

In order to solve the offset problem an anti-winding is added to the Rx coil as shown in Figure 1.11(b). The field generated by the Tx coil will have the same contribution on the two winding but since the windings have opposite turning directions this contribution will be canceled. In this way, the magnetic field generated by the Tx coil will not affect the signal of
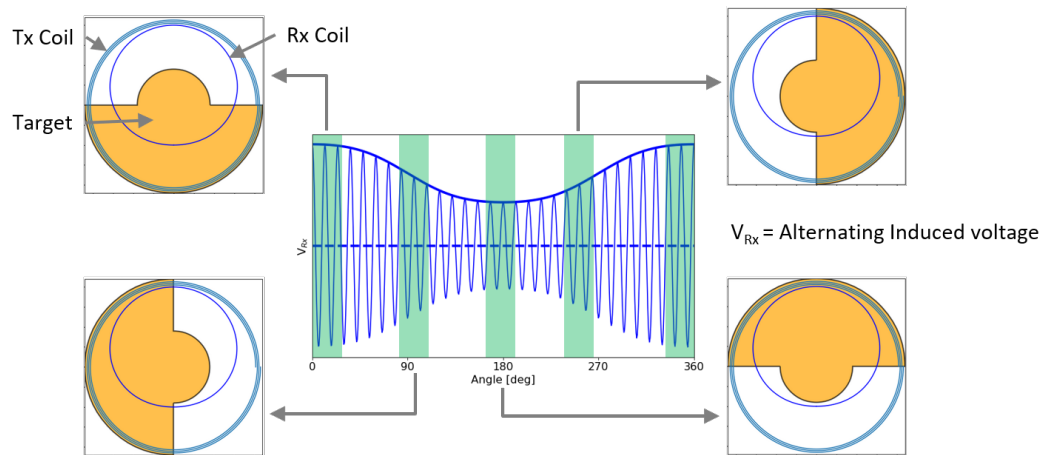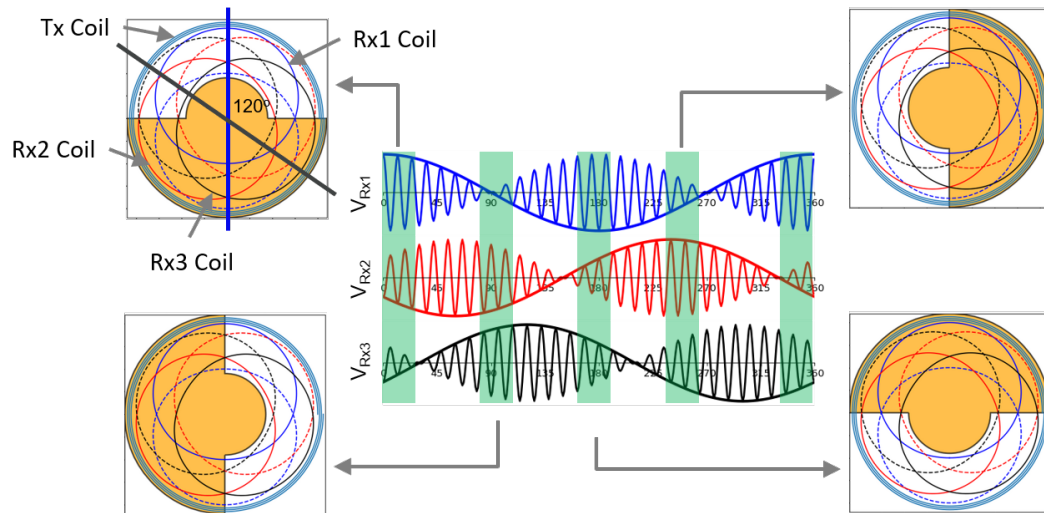
(a) First Approach Inductive coils configuration
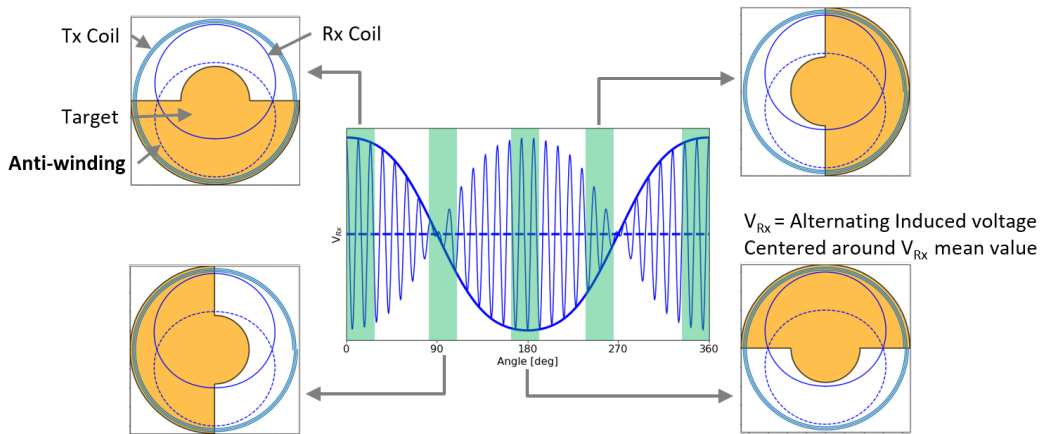
(b) Second approach Inductive coils configuration

(c) Final Inductive coils configuration

Figure 1.11 – Design steps for a 360° inductive angular potion sensor (7).

the Rx coil which will be generated exclusively by eddy currents inside the metal target. The signal will be bipolar due to the opposite winding directions of the coils.

In order to solve the full range problem at least a second Rx coil is needed. One option is to place perpendicularly with respect to the first one. Similarly to the case of the magnetic sensors, This couple of coils will provide us the sine and cosine of the angular position of the metal target. In this way, by simply applying arctan(sin α / cos α) it is possible to retrieve the value of the rotation angle.

Nevertheless, Melexis uses a three-phase design for the Rx coils [Figure 1.11(c)] since it has a particular benefit on the accuracy of the measurement. The reason for this choice comes from the fact that the signals generated by an individual winding-antiwinding pair are not perfectly sinusoidal but inevitably contain some unwanted harmonics, as illustrated in Figure 1.12. The harmonics of odd order are on the other hand not removed. The intensity of the various harmonics diminishes with their order.
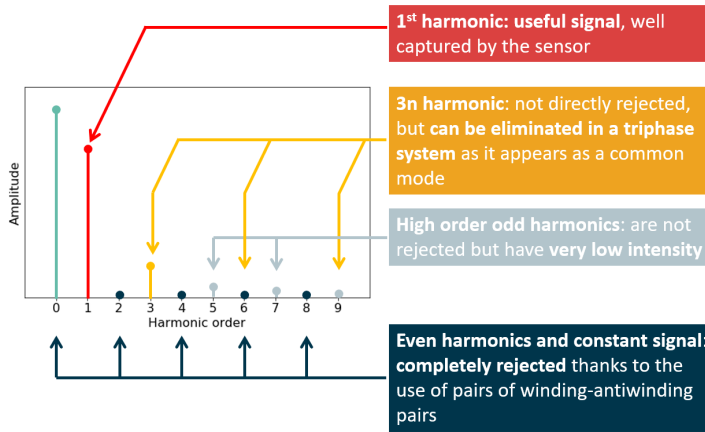
Figure 1.12 – Fourier analysis of the signal coming from the Rx coils complete of description

One can observe that, due to the symmetry of the metal target and the winding-antiwinding pairs, the harmonics of even order have negligible amplitude. The 1st harmonic is the signal we are interested in. The 3rd harmonic is the highest contributor after the 1st harmonic. By using a simple two-coils configuration this parasitic signal would be impossible to reject and it would cause angular error. Using instead a three-phase system, the 3rd harmonic appears as common mode and it is consequently canceled.

In a triphase system we retrieve three different signals from the three Rx coils:

- The first coil will give us the signal A, equal to $A = V_{R_x} \cos \alpha$
- The second coil will gives us the signal B, equal to $B = V_{R_x} \cos \left(\alpha + \frac{2\pi}{3} \right)$
- The third coil will gives us the signal C, equal to $C = V_{R_x} \cos \left(\alpha + \frac{4\pi}{3} \right)$

For these signals, α is the rotation angle of the target and V_{R_x} is the amplitude of the voltage signal generated by an Rx coil.

The rotation angle of the target can, therefore, be retrieved by the IC using:

$$\alpha = \arctan\left(\frac{\sqrt{3}(A-M)}{B-C}\right) \tag{1.13}$$

where: $M = \frac{A+B+C}{3}$. The amplitude of the Rx coils (V_{Rx}) is simplified in the final expression of the angle. However, the signal must be converted in a digital value before proceeding to the signal processing. This is the reason why the amplitude of the signal from the Rx coils plays an important role in the sensor's accuracy.

According to a parametrization derived from a series of COMSOL simulations, the expression for V_{Rx} can be written as:

$$V_{R_x} = V_{T_x}\frac{0.28}{n_{T_x}}\left[1-\left(\frac{r-r_0}{1-r_0}\right)^p\right]e^{-k\left(\frac{z}{D_{Rx,ext}}\right)^m} \tag{1.14}$$

where:

- z is the air gap between the coils and the metal target
- p is a parameter that depends on the air gap : $p = 0.0625z^2 - 0.7z + 3.5375$
- V_{T_x} is the amplitude of the voltage across the Tx coil
- n_{T_x} is the number of turns of the Tx coil
- r is the ratio between the inner Rx coil diameter ($D_{Rx,int}$) and the outer Rx coil diameter ($D_{Rx,ext}$). These two diameters will define the region in which the Rx coils appear. This formula is valid as long as $r > r_0$. Otherwise, the expression is still valid but using $r = r_0$ to eliminate the corrective factor.
- r_0, k, and m are all hand fitting parameters that depend only on the periodicity of the metal target. For a 360° sensor we have: $r_0 = 0.217$, $k = 10$, $m = 0.83$

The accuracy of this sensor is, therefore, strictly related to its geometry which is unaffected by temperature variations. Therefore, variations in the temperature have very little effect on the signal. This makes the inductive sensor very robust against thermal drift error.

Since the detection of the position of the metal target is achieved using a modulated high-frequency magnetic field, they are SFI by design and therefore any external field will have no effects on the measurements whatsoever.

The main drawback of inductive sensors is their dimensions. While the control unit can be integrated into a single chip, the coil dimensions are usually in the order of tens of millimeters. These dimensions imply that the receiving and transmitting coils should be printed on a Printed Circuit Board (PCB).

A second drawback of inductive sensors is their sensibility to stray metals. It is called stray metal any conductive object close enough to the coils to affect the measurement. Usually, these objects are perceived by the inductive sensor as a "parasitic" metal target and consequently, they can bring easily the sensor's measurement out of specs.

Mechanical misalignment between the metal target and the coils on PCB is also a possible source of error. However, for this discussion, we need to distinguish between inductive sensors

having a target with a periodicity equal to 1 (360° range) and inductive sensors having a target with a periodicity equal to N, with N>1 (360°/N range).

When a mechanical tilt is present, there will be a region in which the metal target is closer and a region in which it will be more distant from the Rx coils. When the target gets closer to the Rx coils, they will see a stronger magnetic field, and therefore the centroid of eddy's currents (which correspond approximately to the peak of the magnetic field) will be off-centered towards this region [Figure 1.13a]. In the case of 360°range inductive sensors, we will observe a considerable angular error when the target is rotated of 0° and 180°.

A similar argument applies to Off-axis errors. When an off-axis misalignment is present the centroid of the eddy currents will be displaced with respect to the aligned case towards the off-axis direction[Figure 1.13b]. Also in this case, a 360°range inductive sensor will suffer a large error in the 0° and 180° positions.

In the case of higher periodicity, we have more centroids for eddy's currents and they will move as in Figure 1.13c and Figure 1.13d. However, the effect of the misalignment on one lobe will be compensated by the others since we are taking the average of the angles measured between the different target periods to retrieve the final angle estimation.

In general, 360° range inductive sensors are much more sensitive to mechanical misalignment than higher periodicity inductive sensors.

The amplitude of the off-axis error depends also on the size of the metal target: the larger the target the lower the error since it increases as the target edge gets closer to the Tx coil.

The dimension of the cylindrical metal support for the teeth (essential if we have periodicity higher than one) will influence the off-axis error. The smaller the central cylinder the lower the error [(9)].
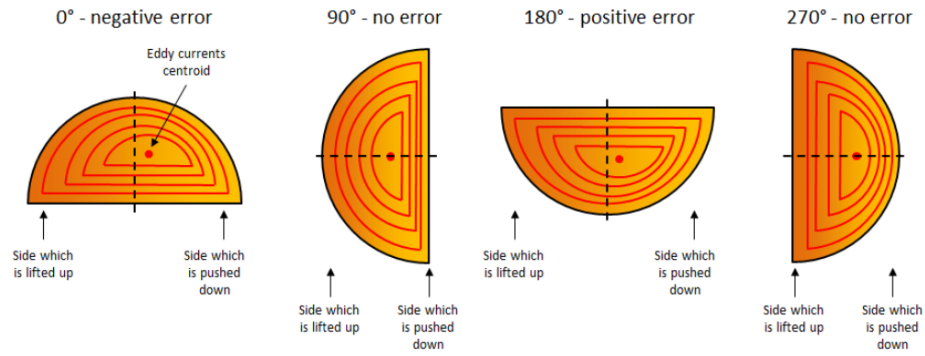
(a) centroid position in case of tilt for a full 360° sensor
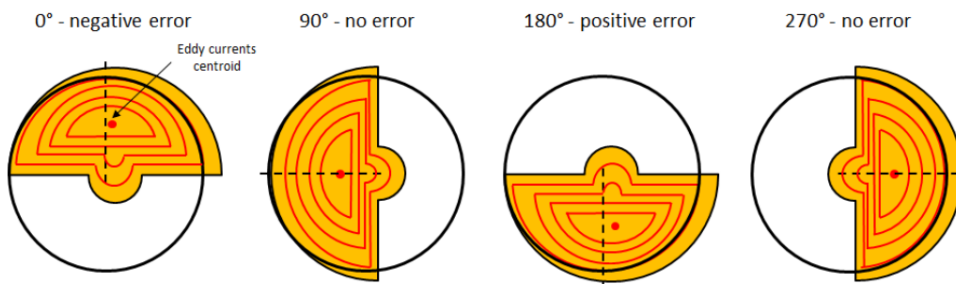
(b) centroid position in case of off-axis for a full 360° sensor
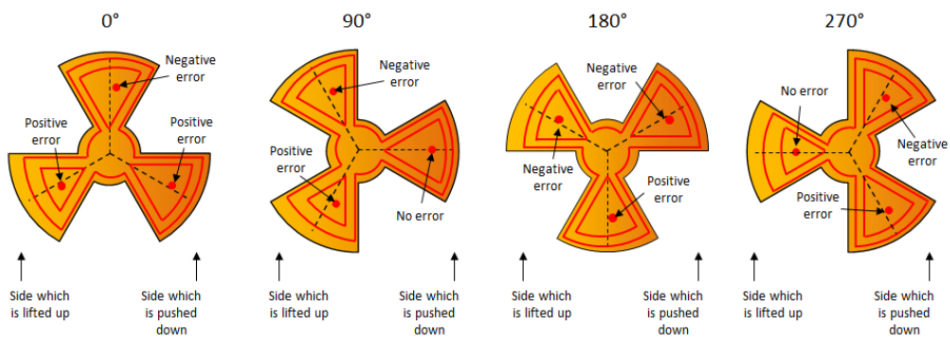
(c) centroid position in case of tilt for a 120° sensor (Periodicity = 3)
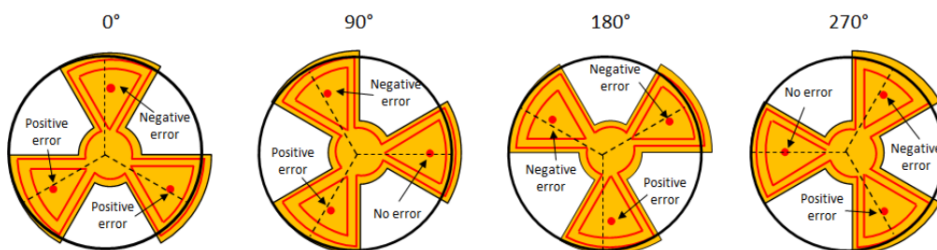
(d) centroid position in case of off-axis for a 120° sensor (Periodicity = 3)

Figure 1.13 – This figure shows in detail how the position of the centroid of the eddy currents inside the metal target is modified by the introduction of tilt or off-axis misalignments (9).

1.3 Inductive and magnetic sensors: a comparison

The properties of the two types of sensors have been summarized in Table 1.2. Inductive sensors are competitive in terms of performance providing higher accuracy, better thermal robustness and total stray field immunity with respect to magnetic Hall sensors. However, Inductive sensors with 360° range are heavily affected by mechanical misalignments.

Hall based magnetic sensors are made from semiconductor material and therefore can be integrated directly on-chip, reducing size and costs. Even PCB-less versions of these sensors have been developed making possible to mount it directly on a platform using metal pins. Therefore they are very much suitable for applications that require sensors to be placed in small spaces. Also, for the state of the art, only the magnetic Hall sensor can be used to detect the object position on a 3D space (Joystick), while the inductive sensor is limited to planar sensing.

If stray field immunity is required, the SUN configuration is a better choice than the dBz mode sensor. Its only defect is that its range is limited to 180°.
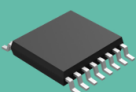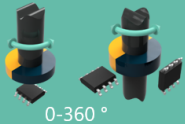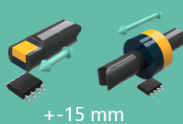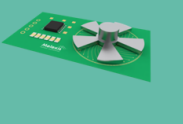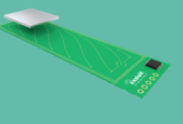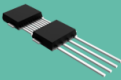
Figure 1.14 – A comparison between inductive sensors and magnetic sensors (7)

Property:	Hall Sensors			Inductive sensors	
Structure:	dBz	SUN	Triaxis SD	Periodicity N = 1	Periodicity N > 1
Range:	360°	180°	360°	360°	360°/N
Stray field immunity:	up to 5mT		No	by design (infinite)	
Signal strength:	low	high		depends on air gap and dimensions	
Misalignment sensitivity:	high	low		high	low
Thermal drift:	moderate			low	
Dimensions:	Small (all-in IC)			Big(PCB is required)	

Table 1.2 – Summary of the properties for the two types of angular sensors

1.4 Project Goal

A sensor featuring **at the same time** the following properties has not been developed yet:

- Stray-field immunity
- angular error less than 1°
- 360° range
- fitting inside a single package

The final goal of the Melexis' project is to develop a magnetic-inductive 360° range SFI hybrid sensor inside a single package [Figure 1.15] that can meet the previously stated requirements. In order to reach this goal, the SFI magnetic sensor mounting the SUN structure will be used
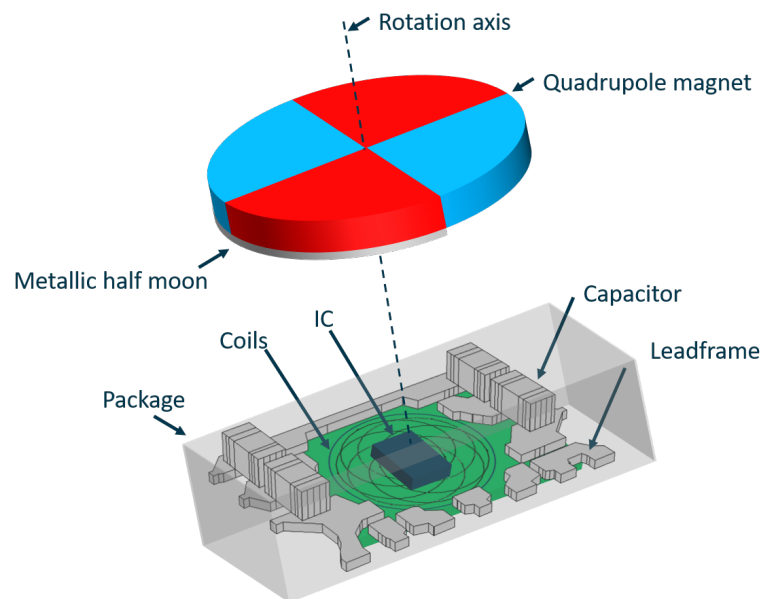
Figure 1.15 – A depiction of the final design (10)

for the accurate measurement of the angle but only in a limited range of 180 °. The full range discrimination will be provided by a complementary 360 °range inductive sensor which will be used for the coarse angle measurement. Basically, it will be used as a discrimination bit to distinguish between the two 180 ° sectors. By merging the two measurements, a full 360 ° range SFI sensor with the performance of a 180° magnetic sensor will be developed [Figure 1.16]. This configuration leaves large freedom for the design of the inductive sensor. In fact, we can allow a very large error for this channel without decreasing the final accuracy which will be given by the magnetic sensor (Table 1.3). This is the reason why the entire concept could fit a single package despite the fact that, usually, it is not the case for inductive sensors. The very low signals coming from very small receiving coils should be acceptable if the error threshold is very permissive.
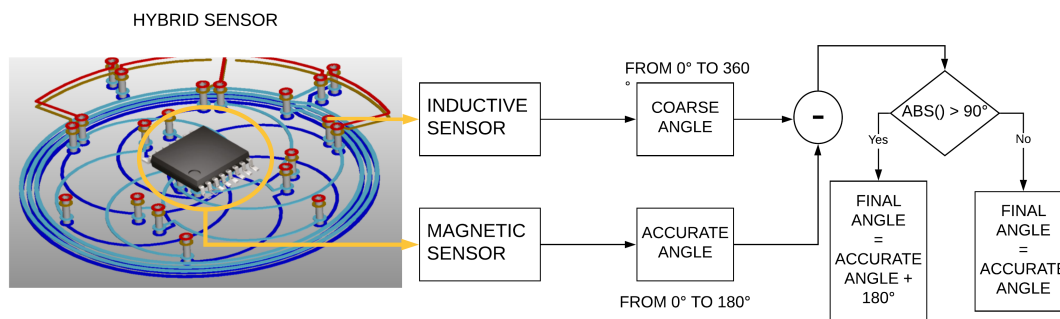
Figure 1.16 – The working principle of the hybrid sensor.

1.4.1 Internship Goal

This master thesis will progress the Technology Readiness Level (TRL) of this project from the theoretical formulation of the concept (TRL2) to an experimental proof of concept (TRL3) [Appendix A].
A scaled-up version of the final concept will be developed on PCB. This prototype, featuring both an inductive and a magnetic sensor, will be used to provide the proof that such a hybrid concept will work as intended extending the range of the SUN structure up to 360°. It will also be used to demonstrate that the two technologies can coexist without affecting each other's performances.
Upon review of the results from this first concept, a second design will be developed to test the feasibility of including the entire structure inside a single package.
The requirements to be matched by the hybrid sensor has to match the one described in Tab. 1.3 in order to achieve the TRL3.

REQUIREMENTS	TARGET	COMMENTS
Range	360 °	By design
Angular error	0.8 °	Performance of the Sun structure
5 mT stray field-induced error	0.4 °	Performance of the Sun structure
2 °tilt error	<<1 °	We expect the magnetic sensor to be tilt insensitive
Angular error for second channel	<90 °	Very large error allowed

Table 1.3 – Requirements for the internship's design

2 Hybrid sensor: design

In order to demonstrate the thesis presented in subsection 1.4.1, we chose to develop a scaled-up version of the final hybrid sensor's concept. The main goal of this prototype, other than demonstrate the correct behavior of the sensor, is also to demonstrate that the two sensors, inductive and magnetic, work completely independent one from the other.

Therefore, a PCB featuring both inductive and magnetic sensors has been designed in order to obtain the first proof of concept of the hybrid sensor. This prototype will mount both an MLX90510 (inductive sensor IC) and an MLX90377 (magnetic Hall sensor IC). Most of the design will be focused on shaping the tracks for Rx and Tx coils printed on the PCB, the position of the components and their interconnections on the board.

2.1   MLX90377

The MLX90377 is a magnetic position processor IC developed by Melexis [(11)]. This sensor can be used in different modes of application. The first application mode is the SUN configuration, the 180° range SFI sensor that we analyzed in subsection 1.1.3. The second application mode allows the chip to detect the angular position of a dipolar magnet via the classical Triaxis Gen.II mode [subsection 1.1.2] for a full 360°range of detection but without SFI. The third application allows us to detect the linear position of a dipolar magnet. This prototype made use of the SUN mode.

For this prototype, it has been used the SUN mode TSSOP-16 version (16 pins). This package mounts two full redundant dies, both featuring a Hall sensor with SUN structure, analog to digital signal conditioner, advanced Digital Signal Processing (DSP) and an output stage driver[Figure 2.1]. This version has been chosen, instead of a single die SOIC-8 package, due to availability reasons. However, for our prototype, only one die is needed. The pins of the package connected to the other die will be all grounded as advised by the data-sheet.

The IC of the sensor can be interfaced with a PTC-04. The PTC-04 is an instrument developed by Melexis to communicate, debug and calibrate its sensors [more about the applications in section 3.1].

The sensor will use the Single Edge Nibble Transmission (SENT) protocol to communicate

with the PTC-04. Each message will contain:

- A synchronization period to determine the time base of the SENT frame (56 clock ticks)
- 4-bit Status and Serial communication nibble pulse
- up to six 4-bits data nibbles representing the value of the signal to be transmitted
- 4-bit Checksum nibble pulse
- optional pause pulse

Using this protocol, the sensor is able to send information directly from its RAM to the device used for the communication. Among the various readable cells, the most important are the ones related to the information on the angular displacement of the magnet and the internal conditions of the chip (Internal temperature, virtual gain, etc.).

As explained in subsection 1.1.3, the temperature will affect the sensitivity of the sensor's HP introducing angular error due to sensitivity mismatches. The thermal drift error has been quantified to ±0.67° for this sensor.
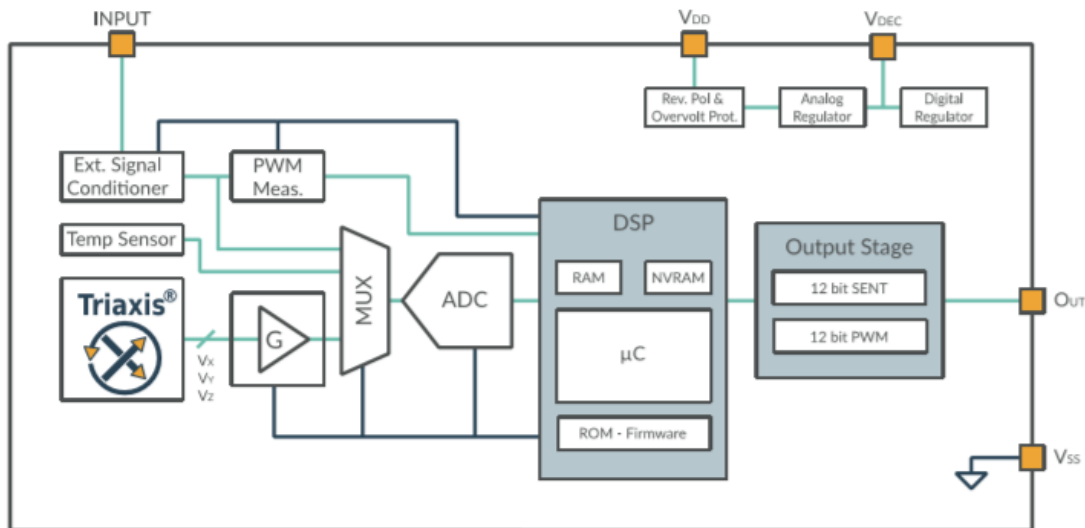
Figure 2.1 – The block diagram of the internal structure of the IC of the MLX90377 (11)

2.2   MLX90510

The MLX90510 [Figure 2.2] is an IC designed to control the signals of the inductive coils for an inductive position sensor used for absolute rotary motion/position sensing in automotive and industrial applications [(12)]. It provides two differential analog outputs that vary like $\sin\alpha$ and $\cos\alpha$ where α is the angular position of the metal target. This IC requires a connection to a Tx coil and three 120°-shifted Rx coils.

The IC will put in oscillation the external LC circuit formed by the Tx coil and external SMD

capacitors connected to the LCP and LCN pins. The inputs IN0, IN1 and IN2 are the signals
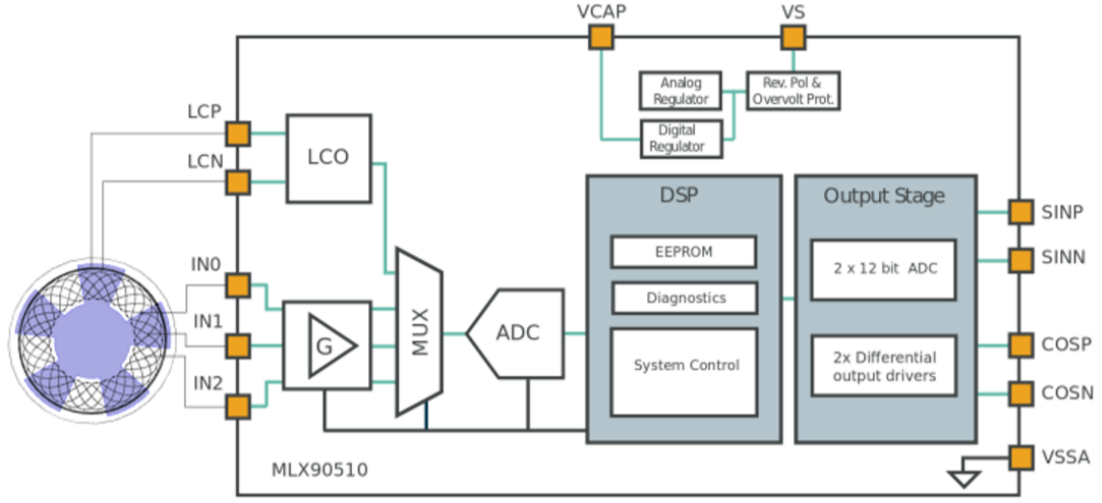
Figure 2.2 – The block diagram of the internal structure of the IC of the MLX90510 (12).

coming from the three Rx coils. These signals are filtered through an Electromagnetic Compatibility (EMC) filter to suppress high-frequency noise. The differential amplifier stage will remove the common mode for the input signals caused by the coupling with the Tx coil. The output of the amplifier is rectified and further filtered. The signal is subsequently converted to a digital signal for further digital processing. Finally, the output signals are converted by two DAC and buffered by 2 differential output buffers which provide $\sin\alpha$ and $\cos\alpha$.

The design on PCB should respect the conditions of the LCO (LC oscillator) of the IC. From the specifications of the datasheet, the inductance is typically equal to $4\mu H$. However, a range from $0.5\mu H$ to $10\mu H$ is also supported. In case the coil is built on a multilayer PCB, such as in this case, we can refer to the following formula:

$$L_{Tx} = \frac{0.8R^2 n_{Tx}^2}{25.4(6R + 9l + 10w)} \tag{2.1}$$

where l is the vertical length (depth) of the coil, R is the average coil radius in mm, w is the width of the coil and n_{Tx} is the number of turns ((13)). For this formula, the units of measure for the lengths must be expressed in [mm] and the inductance will be expressed in $[\mu H]$.

The frequency (f) of the LCO should be kept between 2 and 5 MHz according to the component's datasheet. We can control the oscillation frequency by selecting the correct size for the capacitor of the oscillator: $C_{Tx} = 2/(L_{Tx}(2\pi f)^2)$.

The specified typical quality factor Q is equal to 18. A higher Q factor will ensure lower power consumption. However, for a fixed Q factor, the power consumption increases drastically with the decrease of the inductance [Figure 2.3]. The quality factor of the oscillating circuit is defined as:

$$Q = \frac{2\pi * f * L_{Tx}}{R_{Tx}} \tag{2.2}$$
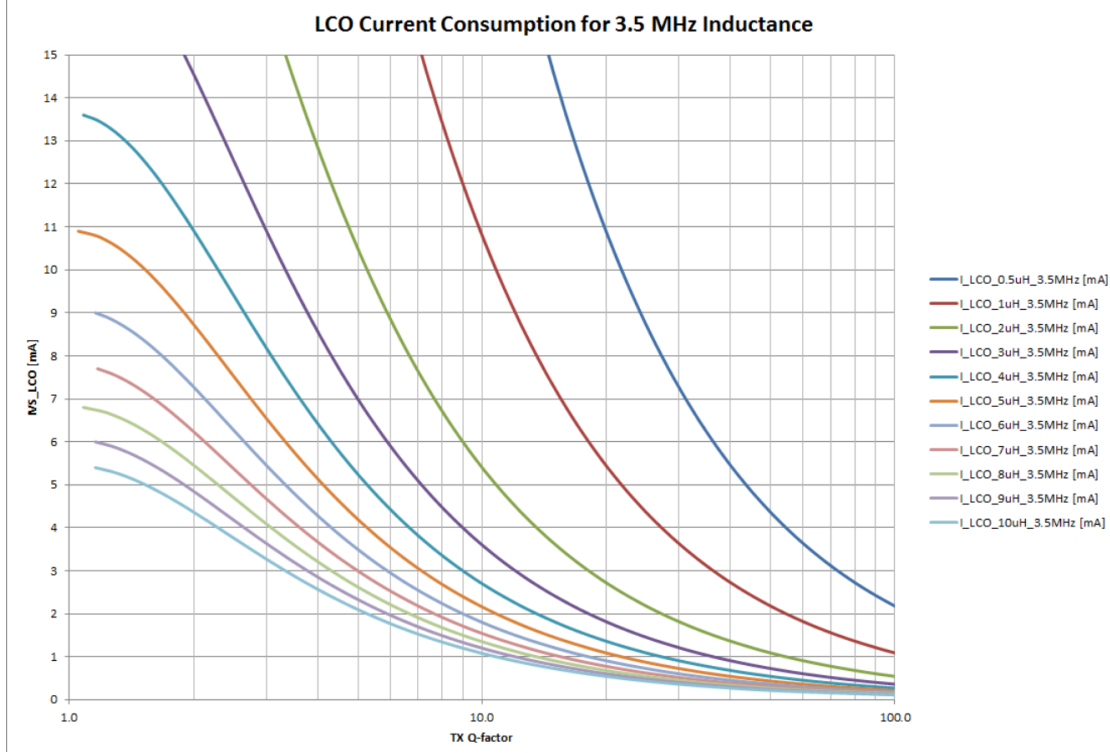
Figure 2.3 – This plot shows how the current drained by the oscillating circuit varies with the inductance of the Tx coil and the Q factor of the circuit

where R_{Tx} is the resistance of the Tx coil, defined as :

$$R_{Tx} = \frac{2\pi n_{Tx} D}{W_{Tx} T_T \sigma} \tag{2.3}$$

where W_{Tx} is the width of the track. T_T is the thickness of the track and in standard PCB it may vary between internal and external layers. Therefore, it is advised to take an average thickness for T_T. σ is the conductivity of the material of the track (usually copper is used and its conductivity is equal to $6 * 10^7 S/m$).

In addition to the requirements related to the LCO operation, the inductive sensor needs to respect some requirements in terms of signal strength. In particular, in order to respect the performances presented on the datasheet (positional accuracy equal to $\pm 0.3°$), we expect an amplitude for the Rx coil signal (Equation 1.14) greater or equal to 2.9 mV at the chosen airgap. Actually, another common way to refer to the signal from the Rx coil is the rotor amplitude (A_rotor). This quantity is defined as the maximum difference between the potential of two receiving coils: $A\_rotor = max(IN_x - IN_y)$ where IN_x and IN_y are the signal coming from two different Rx coils in the three-phase system). The following relation is always valid in a three-phase system: $A\_rotor = \sqrt{3} V_{Rx}$. Therefore, from the datasheet of the MLX90510, the minimum value for A_rotor is 5 mV. Nevertheless, even if the Rx coils signal drops below this threshold the MLX90510 will still continue to provide the metal target's angular position but

with an error range which is no more guaranteed by the inductive sensor's datasheet. This IC, likewise the MLX90377, can be interfaced with the PTC-04 to perform the calibration of the sensor (more details in section 3.1). One of the analog outputs (E.g. SINP) is used as an input/output pin for communication with this tool.

2.3 Schematic

The schematic of the circuit(Fig.2.5) has been designed using Altium 19.1.5 schematic tool. Most of the connections for the two ICs have been performed following the recommended application diagrams in the respective Datasheets. Let's analyze first the connections for the MLX90510 [Figure 2.4a].

(a)

(b)
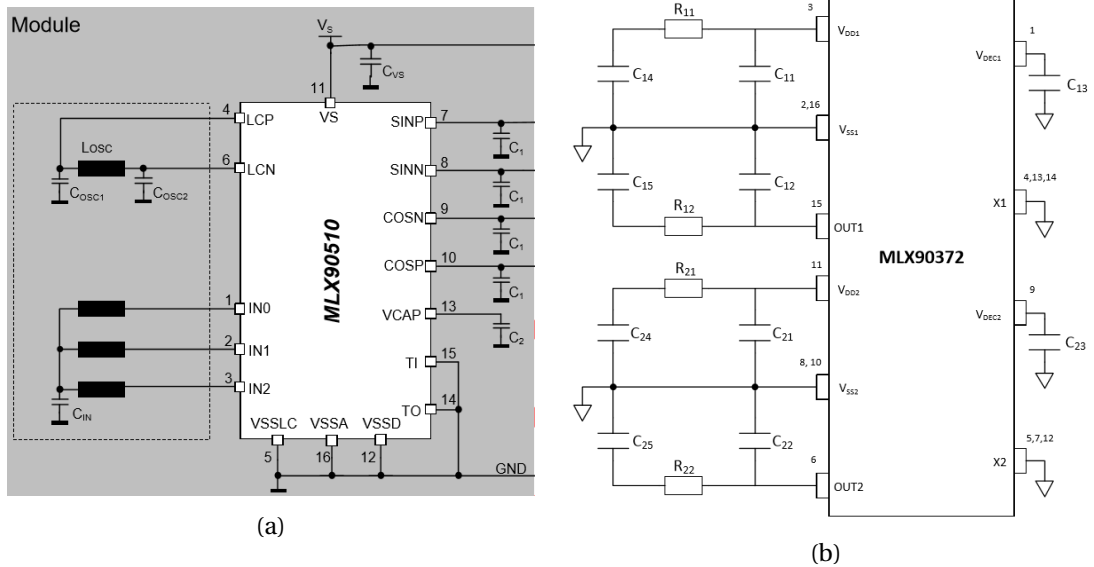
Figure 2.4 – (a) The recommended application diagrams for the inductive sensor and (b) the magnetic sensor (11) (12)

- **IN0, IN1, IN2**: these pins have to be connected to the 3 receiving coils printed on the PCB. The Rx coils have to be connected to a common reference (Starpoint) in order to build the three-phase system. The common reference of the Rx coil is connected to the common ground through a capacitor C_{IN}.

- **LCP, LCN**: LCP and LCN are the positive and negative poles to be connected to a pair of capacitors (C_{OSC1} and C_{OSC2}) and the Transmitting coil (inductance) which together will form the LC oscillating circuit. The inductance value of the Tx coil and the size of

the capacitor will determine the oscillating frequency of the generated magnetic field:

$$f = \frac{1}{2\pi\sqrt{L_{Tx}\left(\frac{C_{OSC1}C_{OSC2}}{C_{OSC1}+C_{OSC1}}\right)}} \tag{2.4}$$

- **VSSLC, VSSA, VSSD**: VSSLC is the ground for the LCO of the sensor and it will be connected to the common ground together with VSSA and VSSD

- **TI, TO**: the TI (Test_In) and TO (Test_Out) PINs in nominal working conditions for the sensor should be connected to ground. If some errors appear in the measurements we can communicate with the IC through these pins, allowing debugging and recovery of diagnostics on the problems. However, they are actually connected to 0Ω resistances connected to the ground. These 0Ω resistances can be removed if communication with the chip is required for debugging.

- **VS**: the power supply of the MLX90510, it must be connected to the PCB's power pin through a decoupling capacitor(C_{VS}).

- **SINP, SINN, COSP, COSN** These are the analog differential output for the $\sin\alpha = SINP - SINN$ and $\cos\alpha = COSP - COSN$. With these pieces of information, we are able to retrieve the value of α. Each four output PINs are connected to a capacitance and pull-up resistors close to the output connectors of the PCB.

Let's analyze now the connections for the MLX90377 [Figure 2.4b]. As previously mentioned, for this application, only one of the two dies in the package is needed and therefore the pins of chip 2 will be all grounded as advised by the data-sheet.

- **OUT1** : input-output pin used for SENT communication with the PTC-04. It is connected to a decoupling capacitor.

- **INPUT1, TEST1**: these two pins have the same function of the TI and TO pins of the MLX90510. As before, the PCB will allow connections for these pins in case some debugging is required

- **V_DEC1**: pin to be connected to a decoupling capacitor

- **VDD1**: the power supply of MLX90377, it must be connected to the PCB's power pin through a decoupling capacitor(C_{vdd}).

Another 0Ω resistance has been placed to add the possibility to separate the power supplies for the two sensors in case they can't share it during the measurements.
The list of the components that will be used is shown in Table 2.1.
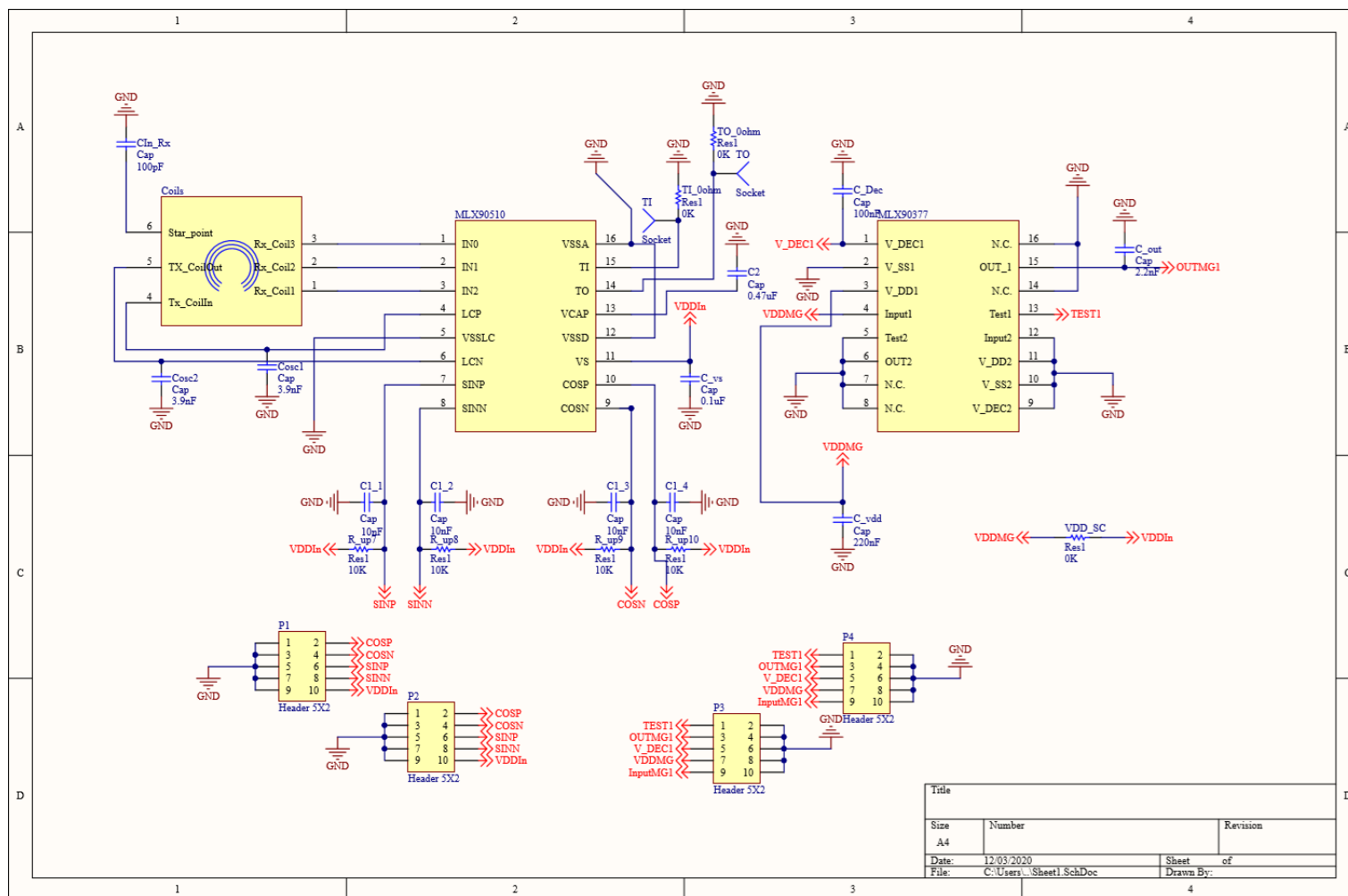
Figure 2.5 – The complete schematic of the electric circuit designed on the PCB

Type	Value	Quantity	Description
Resistor	0 Ohm	3	Used in case of debug
	10k Ohm	4	Pull-up Resitors for the output of MLX90510
Capacitor	100 pF	1	Decoupling capacitance for the inductive sensor's coils
	1.2 nF	2	Needed for the resonance of the coils' inductance
	2.2 nF	1	Output capacitance for MLX90377
	10 nF	4	Output Capacitance for MLX90510
	100 nF	2	Decoupling capacitance for the chip 1 of the MLX90377 and for the powerline of the MLX90510
	220 nF	1	Decoupling Capacitance for the powerline of the MLX90377
	470 nF	1	Decoupling Capacitance for the MLX90510
IC	MLX90510	1	Inductive sensor
	MLX90377	1	Magnetic sensor
Rx_Coils		3	Receiving coils printed on the PCB
Tx_Coils		1	Transmitting coil printed on the PCB
Connectors	Header 5x2	4	2 for the MLX90377 and 2 for the MLX90510
	Socket	2	TO and TI of the inductive sensor, for debugging

Table 2.1 – The list of components used in the PCB assembly

2.4 Layout

The PCB [Figure 2.7] was developed to satisfy the requirements of one of the fabrication class from Eurocircuits. The class used for the PCB design is 6C, employing 4 layers [Table 2.2]. Four copper layers have been used: two layers will be used for the interconnections between chips, coils and output pins, and the other two layers will be used for the Rx and Tx coils of the inductive sensor. The hybrid target (metal half-moon/magnet) will have to be centered both with the SUN structure of the chip 1 of the magnetic sensor and with the center of the inductive sensor's coil system.

Property	Size	Unit
Minimum Track width	0.15	mm
Clearance between connected parts (S_T)	0.15	mm
Via drill hole diameter size	0.35	mm
Total via diameter (metal pad included)	0.6	mm

Table 2.2 – Properties of a 6C class PCB

The PCB will have dimensions that will fit the standard slot for PCBs in the measurement station used in the laboratory (Hexapod, more in section 3.1). In particular, it will have a total width of 35.1 mm and a total length of 100 mm. If we take as the origin (0,0) the bottom left edge of the PCB, the center of the Tx coil will be in C(17.55,10), having the coordinates

expressed in mm.

Input	Comments	Values	Unit	Length in Figure 2.6
Frequency	LC oscillating frequency	3.38	MHz	
V_{Tx}	Voltage across the Tx coil	2.3	V	
r_0	Critical radius	0.217		
m	Fitting parameter	0.83		
k	Fitting parameter	10		
R_{Rx}	Radius of a single winding of the Rx coil	4	mm	2
$D_{Tx,max}$	Diameter of the outer winding of the Tx coil	16.4	mm	7 (radius in fig.)
$D_{Tx,min}$	Diameter of the inner winding of the Tx coil	15	mm	6 (radius in fig.)
$D_{Rx,ext}$	External diameter of the Rx coil	13.7	mm	3 (radius in fig.)
$D_{Rx,Int}$	Internal diameter of the Rx coil	2.3	mm	5 (radius in fig.)
D	Average diameter of the Tx coil	15.7	mm	4 (radius in fig.)
w	Total width of the Tx coil track	0.9	mm	1
W_{Tx}	Trackwidth of the Tx Coil	0.2	mm	
T_T	Average Tx coil track thickness	26.5	μm	
n_{Tx}	Turns for the Tx coil	6		
z	Air gap from the PCB	3	mm	

Table 2.3 – List of the characteristics of the PCB design.

Considering Equation 1.14, in this case we have $r = D_{Rx,int}/D_{Rx,ext} = 0.168$, lower than the critical radius r_0. By considering the values presented in Table 2.3, the formula to consider for the estimation of the the intensity of the signal across the receiving coils varying with the airgap (z) expressed in [mm] is:

$$V_{Rx} = 0.107e^{-1.14z^{0.83}} \quad [V] \tag{2.5}$$

For an airgap of 3 mm from the coils (thus 2mm from the package of the MLX90377), we retrieve $V_{Rx} = 6.35mV$ which is well above the 2.9 mV threshold stated in the inductive sensor's datasheet.

The inductance(L_{Tx}) of the Tx coils can be evaluated using using Equation 2.1. The depth of the Tx coil, l, is the sum of the thicknesses of the two copper layer used for the Tx coil (bottom layer's thickness is $18\mu m$ and middle layer's thickness is $35\mu m$) and the thickness of the insulator between the two layers (according to the build-up tool of Eurocircuit it is a total of 0.54 mm thick). Thus $l = 0.593mm$. We expect an inductance equal to $L_{Tx} = 1.14\mu H$.

The resistance of the Tx coil(R_{Tx}) can be estimated using Equation 2.3. T_T is the average thickness of the Tx coil's wires. Since we use one outer copper layer and one inner copper layer we have $T_T = (0.035 + 0.018)/2 = 0.0265mm$. We expect a resistance equal to $R_{Tx} = 1.86\Omega$. The MLX90377 will be placed above the center of the Tx coil. Since most of the chip leadframe will behave as a stray metal for the inductive part, it will act as a shield for the field coming from the metal target, that will be not perceived in that region by the Rx coils. Since the MLX90377 is overall off-centered with respect to the coil structure, in order to minimize the effects of the asymmetry on the Rx coils structure, a circular metal shield has been printed on the PCB below the magnetic sensor to increase the symmetry for the region exposed to the field of the metallic target [Figure 2.6]. The loss of the intensity of the signal due to this metal shield is low. The oscillator's capacitors (both equal to C_{osc}) have been chosen according to the inductance of the transmission coil and the operating frequency of the oscillator. Since the capacitors of the oscillators are equal, the Equation 2.4 becomes $f = 1/(2\pi\sqrt{L_{Tx}C_{osc}/2})$. From the datasheet of the MLX90510, the typical resonance frequency is $3.5MHz$. To maintain a similar frequency, it has been chosen a capacitance of $C_{osc} = 3.9nF$ for which it exists the SMD standard value available in the laboratory. The new expected frequency is 3.38 MHz. The expected Q factor(Equation 2.2) with these conditions will be equal to 13.

As mentioned in the previous section, the Rx coils are connected to a common point, called Starpoint, which is connected through a capacitor to ground. The position of the Starpoint is of crucial importance. The area inside the perimeter of the Rx coil should only include the winding-antiwinding regions inside the Tx coil. To avoid an increase in the angular error one should try to eliminate any parasitic surface of the Rx coil. This is the reason why the Starpoint has been placed very close to the inductive sensor's IC.

A single copper polygon on the first middle layer has been used for the ground plane. Of course, this metal layer must be put outside the region of the inductive coils in order to minimize the parasitic signals that would be caused by this stray metal.

For each sensor we have two identical output 5x2 Headers connectors which allow communication with the external tools. These connections have been duplicated in order to have more reference in case multiple instruments are needed to monitor the signals coming from the sensors.
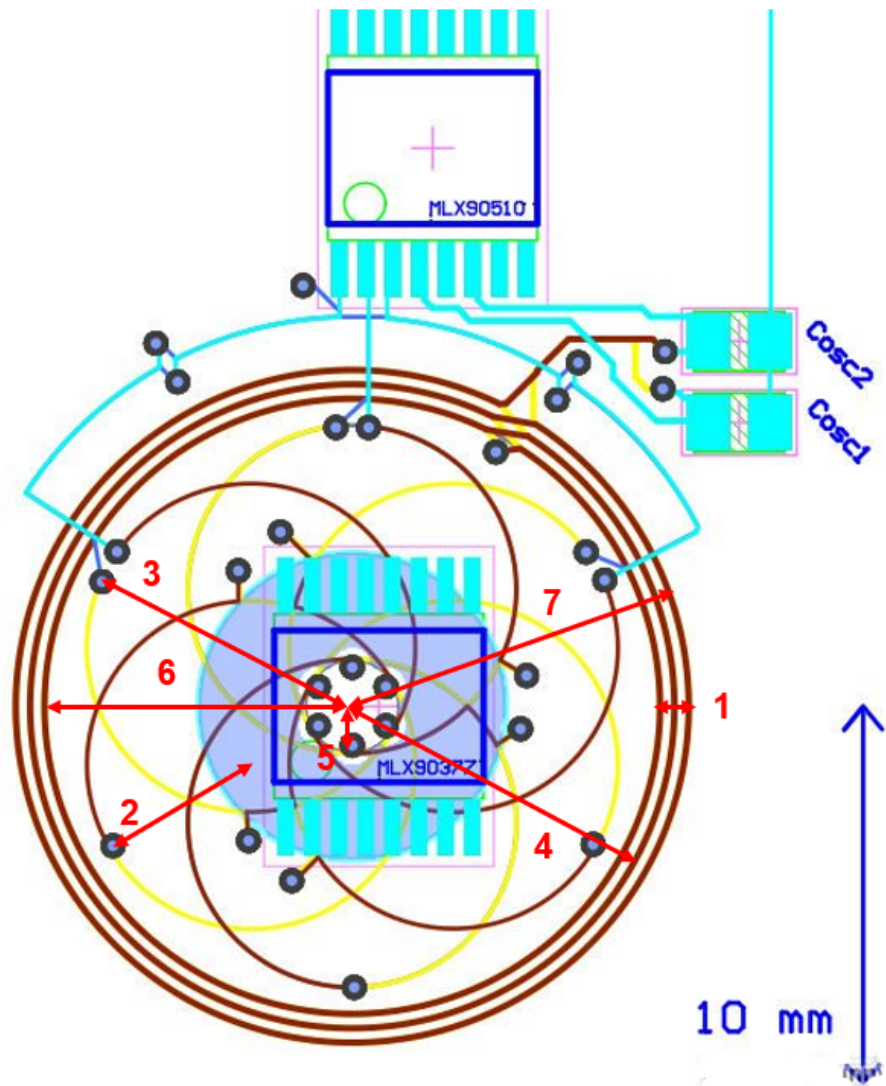
Figure 2.6 – A detail of the prototype exposing the coil system for the inductive sensor. For a description of the lengths from 1 to 7 refer to Table 2.3.
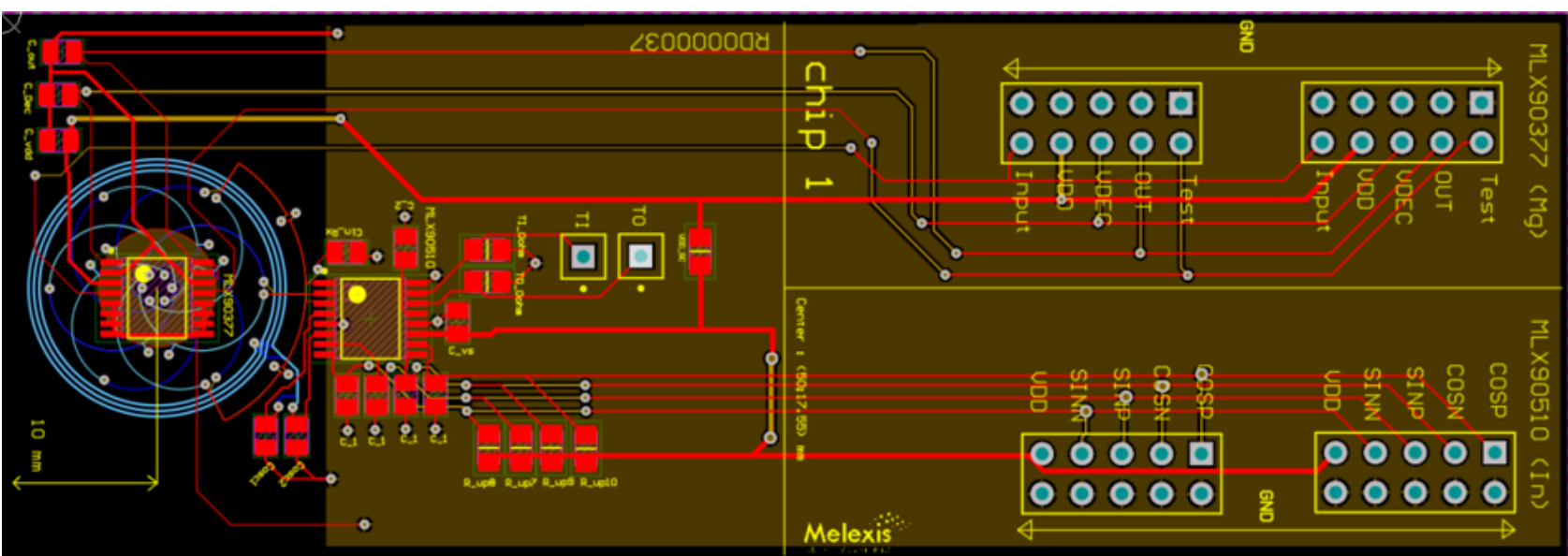
Figure 2.7 – The Layout design for the PCB

3 Hybrid sensor: characterization

Once the mounting of the PCB was completed, the board was ready to be tested. During the measurement campaign, the inductive and magnetic sensors' measurements were compared with the real rotational angle value of the hybrid target (metal target + quadrupole magnet).

The most meaningful quantity that is usually analyzed in a measurement campaign for these types of sensors is the Non-Linearity Error (NLE). The NLE is the difference between the measured angle and the actual rotation angle.

The NLE is used for the calibration of the final sensor. In fact, the NLE is subsequently saved in the memory of the sensor and it will be subtracted to the measured angle in order to obtain a far more accurate "post-linearization" angle.

Another way to refer to the angular error is trough the Range of the Non-Linearity Error (RNLE). In fact, it is usual for the NLE to have an offset if the 0 ° position of the sensor under test is not perfectly aligned with the 0 ° position of the mechanical angle. The RNLE is defined as the difference between the maximum of the NLE and the minimum of the NLE. Thus any offset is removed from the RNLE. After the offset removal the following expression is valid: $NLE = \pm RNLE/2$.

The NLE curve is usually described by its harmonic components. In the case of Figure 3.1, the strongest harmonics are the 4th and the 1st.

For all the following tests the NLE will be used as an element of comparison between different test conditions to establish the orthogonality of the two sensors composing the Hybrid sensor. In fact, the requirements in Table 3.1 show the performance of the MLX90377 as presented in its datasheet. The requirements will be met if we demonstrate that the two sensors work independently one from the other and they do not affect each other's measurements.

A normal test for a magnetic sensor would be executed exactly in the same way and condition of a test for this prototype. The only part of the hybrid sensor that could affect the measurements of the magnetic sensor is the metal target attached to the quadrupole magnet. This is the reason why the tests reported in this chapter have been performed twice: once in presence of the metal target and once without the metal target. The demonstration of the orthogonality is achieved if the result of the test does not change in the two conditions.
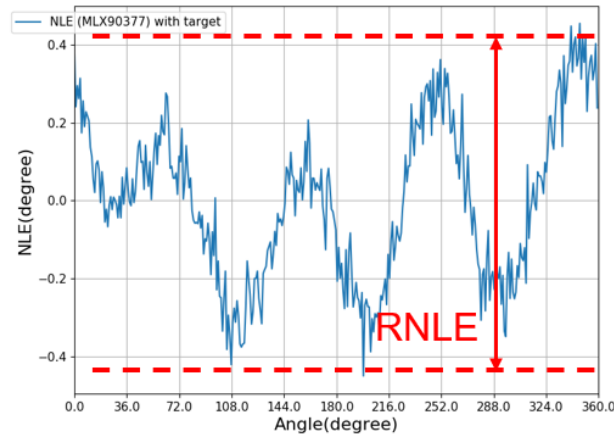
Figure 3.1 – This is a typical NLE curve for the magnetic sensor.

REQUIREMENTS	TARGET	DEMONSTRATION METHOD
Range	360 °	Test 1
Angular error	0.8 °	Orthogonality (This specific is present in the datasheet of MLX90377). Demonstrated using Test 1,2,3,4
5 mT stray field induced error	0.4 °	Orthogonality (This specific is present in the datasheet of MLX90377). Demonstrated using Test 1,2,3,4
Tilt error	<<1 °/°	Test 3
Angular error for second channel	<90 °	Test 1,2,3,4 (However a more valuable verification will be done in chapter 4)

Table 3.1 – The way each requirement will be met

3.1 Measurement setup

For the measurements, the Hexapod has been used to control air-gap (Z-axis), angle of rotation of the metal target (W-axis), tilt (U and V axes) and in-plane off-axis (X and Y axes)[Fig.3.2]. The U-axis is used to indicate the rotation around the X-axis. The V-axis stands for the rotation around the Y-axis. Finally, the W-axis describe the rotation around the Z-axis, hence the control of the hybrid target rotational position.

The Hexapod was controlled using instructions delivered trough a Python script run on the PC. Two different multimeters K2000 were connected to the two differential outputs of the MLX90510, measuring $\sin(\alpha)$ and $\cos(\alpha)$ of the angle describing the position of the metal target (α). The multimeters were connected using a GPIB connector to the PC and both were controlled using instructions from the same Python script.

Control of rotation angle

Quadrupole magnet

Metallic half moon

10 cm

3,51 cm

1 cm

PCB

Hexapod
Station

power supply
K2400

Package TSSOP-16

AO1 - (cosine)

AO1 + (cosine)

Multimeter
K2000

GPIB connector

Multimeter
K2000

MLX90510

AO2 - (sine)

AO2 + (sine)

GPIB
connector

Computer

Coarse angle
measurement

Accurate
Angle
Measurement

USB connection

PTC-04

MUPET communication

MLX90377

Package TSSOP-16

Control of mechanical misalignement

Figure 3.2 – A diagram showing the connection during the measurement process

Figure 3.3 – Picture of the built hybrid target.

A PTC-04 (universal programmer tool for sensors) has been used to establish communication between the MLX90377 and the PC. This t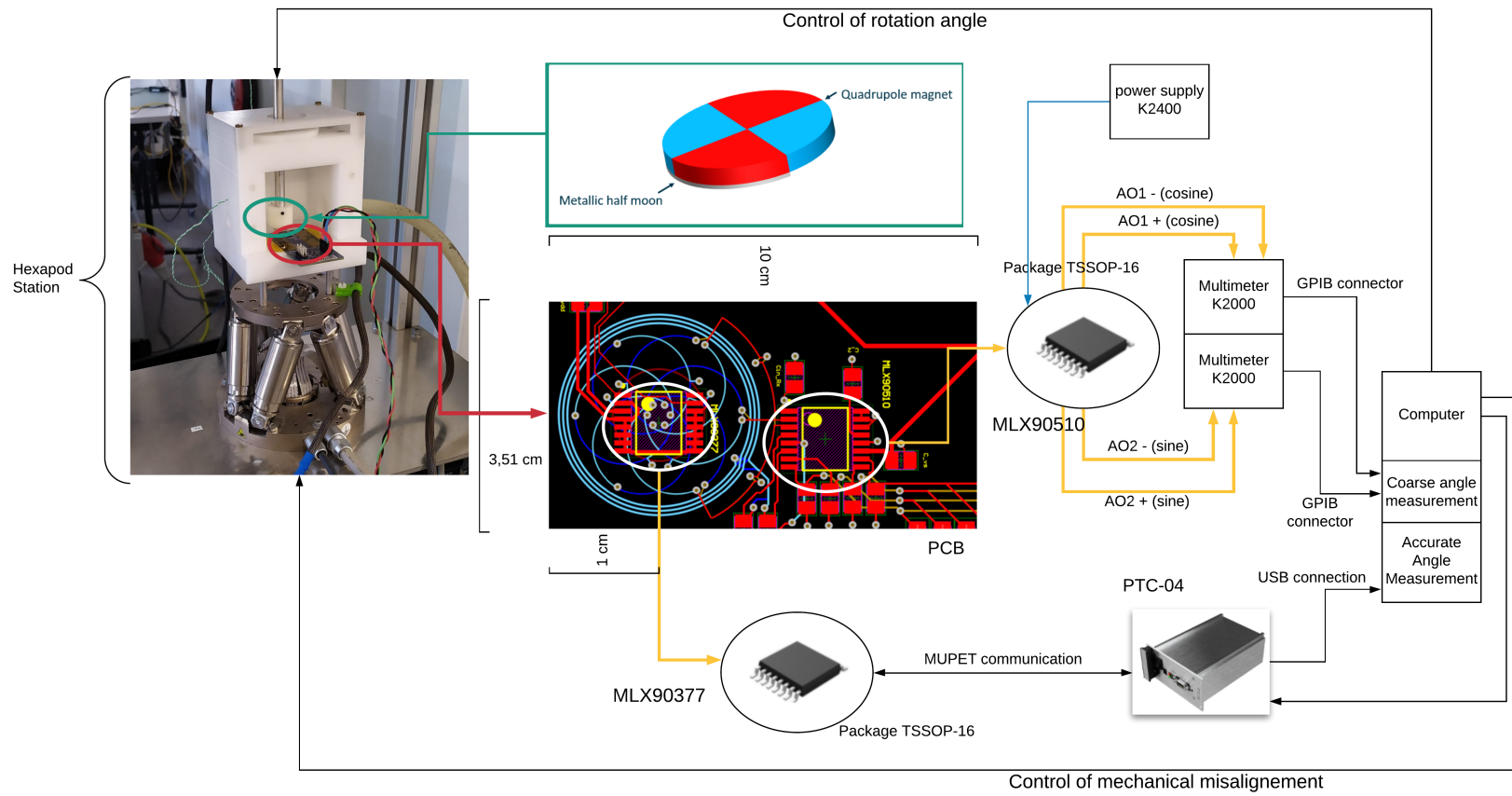ool will read the memory of the IC of the magnetic sensor and send the values to the PC. The communication with the PTC-04 can be established again with a Python script.

The powerlines of the two sensors had to be separated. In fact, during the operation of reading, the voltage supply for the MLX90377 is brought up to 9V by the PTC-04. On the other hand, the maximum voltage allowed by the MLX90510 is 6V before the automatic shutdown of the chip. The power supply for the MLX90377 remained the PTC-04 while an external power supply (K2400) set at 5V is connected to the MLX90510.

Before the first test, the inductive sensor has been calibrated using the PTC-04 in order to remove any offset related to static factors (E.g. PCB coils imperfections or close copper layer/tracks acting as stray metals). The digital offset compensation is saved inside the sensor's EEPROM and accessed during the digital processing of the signal. The magnetic sensor, on the other hand, did not need any calibration step since they are already pre-calibrated at the factory.

The hybrid target/magnet was build using a quadrupole magnet and, glued to it, a half-moon of aluminum foil. The aluminum half-moon has been glued to a plastic support which simplifies the removal during the tests. The used magnet must be a ferrite magnet, which is an insulator, in order to allow the inductive sensor to detect the signal coming exclusively from the half-moon metal target (Fig.3.3).

Before the measurement campaign started, a verification plan(summarized in Table 3.2) has been filled with a description of all the tests to be performed:

- Test 1 will demonstrate that the hybrid sensor works properly in nominal conditions
- Test 2 will demonstrate the independence of the magnetic and inductive sensor in presence of a stray field
- Test 3 will demonstrate the independence of the magnetic and inductive sensor in

presence of a stray field
* Test 4 will show the potential of this hybrid sensor, which will still work accurately even with a large error on the second channel (inductive sensor).

In Tables 3.4,3.6,3.8 and 3.10, it is shown in detail the procedure for the tests and also what is somehow the core instructions in the python scripts that are used to execute these tests.

Test number	Details
1	Room temperature, On-axis, 2mm airgap, No stray field, No stray metal
2	Room temperature, On-axis, 2.2mm airgap, With stray field, No stray metal
3	Room temperature, Mechanical misalignment, No stray field, No stray metal
4	Room temperature, On-axis, 2mm airgap, No stray field, with stray metal

Table 3.2 – The Summary of the tests that have been performed

3.2 Alignment procedure

Before starting the tests presented in Table 3.2, it is necessary to well establish the position of the magnet/target with respect to the Hall sensor at the center of the coils. The alignment will be performed on the XY plane to find the in-plane on-axis position. This alignment is critical for both the inductive and magnetic sensors. The alignment must be repeated on the UV plane to ensure that the PCB has no pre-existent tilt with respect to the hybrid target. The procedures to be performed are summarized in Table 3.3.

The aligned position corresponds to the point on the XY plane and UV plane in which the RNLE of the sensor is minimum.

The effect of a mechanical misalignment on the XY plane will cause an increase of the 1st harmonic component of the NLE curve (over a 360°range) for both magnetic and inductive sensors (see subsection 3.6.1 for the effect of the off-axis on the NLE curve of the two sensors). The in-plane aligned position has been evaluated on the two directions (X and Y) separately. In this way, the procedure is faster compared with the usual grid-like measurement points on the plane. This procedure is also equally accurate to find the aligned position since the RNLE increase has a radial symmetry with respect to the on-axis position.

Concerning the tilt alignment, the MLX90377 has very low sensitivity for tilt misalignment, while on the other hand, as explained in subsection 1.2.2, tilt misalignment is critical for 360°range inductive sensors. Tilt misalignment will cause an increase of the 1st harmonic component of the NLE curve (over a 360°range) for the MLX90510 (see subsection 3.6.1 for the effect of the tilt on the NLE curve of the two sensors). This harmonic's amplitude, which is approximately equal to the RNLE of the inductive sensor, will be used to evaluate the On-Axis tilt position.

The inductive sensor is also very sensitive to the off-axis. However, it is very unlikely that the inductive and magnetic sensors share the same center. Since the inductive sensor has to provide the coarse measurement, it is less important to have an XY perfect alignment for the

X-Axis alignment	1	All X axis measurements will be taken using Y position equal to 0
	2	A full rotation measure is taken: 36 points spaced by 10 degree and the RNLE is saved.
	3	Step 2 is repeated for X included in [-1.5,1.5] with step equal to 0.3mm. The posistion with minimum RNLE is saved in Coarse
	4	Step 2 is repeated for X included in [Coarse_X- 0.3,Coarse_X + 0.3] with step equal to 0.1 mm. The position with minimum RNLE is saved in Acc_X
Y-Axis alignment	5	All Y axis measurements will be taken using X position equal to Acc_X
	6	Steps 3-4 are performed in the same way on the Y axis and the on-axis position will be in (Acc_X,Acc_Y)
U-Axis alignment	7	All U axis measurements will be taken using V position equal to 0 and centered in (Acc_X,Acc_Y)
	8	Step 2 is repeated for U included in [-1.5,1.5] with step equal to 0.3 degree. The position with minimum RNLE is saved in Coarse_U
	9	Step 2 is repeated for U included in[Coarse_U - 0.3,Coarse_U + 0.3] with step equal to 0.1 degree. The position with minimum RNLE is saved in Acc_U
V-Axis alignment	10	All V axis measurements will be taken using U position equal to Acc_U
	11	Steps 8-9 are performed in the same way on the V axis and the no-tilt position will be in (Acc_U,Acc_V)

Table 3.3 – The Summary of the alignment procedure

MLX90510. Therefore, the MLX90377 will be used to find the on-axis position on the XY plane. Likewise, the MLX90510 will be used to evaluate the UV axis position.

The alignment procedure, or at least the accurate part, must be repeated each time the magnet is removed from the Hexapod to counter any introduced misalignment. Since the plane of the PCB is not at the same height as the Hexapod's plane, any tilt will introduce an off-axis that will have to be countered by changing the position on the XY plane [Figure 3.4].
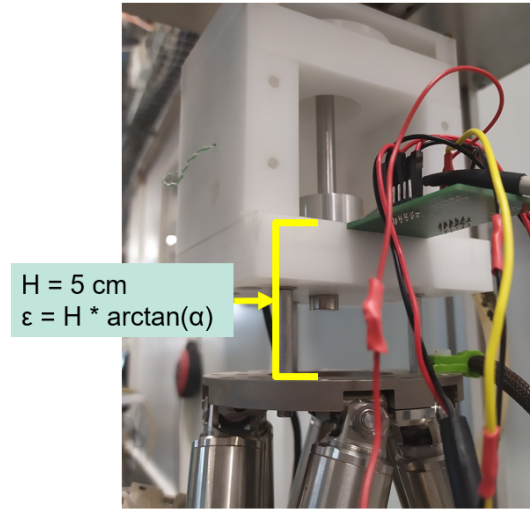
Figure 3.4 – The PCB is 5 cm above the Hexapod's plane. ϵ is the correction factor to be applied to the X axis (if tilting of α on V) or Y axis (if tilting of α on U).

3.3 Algorithm for the evaluation of the hybrid sensor's angle

The final angle calculated by the hybrid sensor is retrieved using the following algorithm:

1. The output of the inductive sensor is evaluated by extracting the arctangent of the ratio: (SINP-SINN)/(COSP-COSN). This angle will be called ϵ.
2. The output angle of the magnetic sensor is retrieved using the PTC-04. This value will be in the range 0 - 65535. The range will be modified to 0°-180°. This angle will be called α.
3. The output values of the inductive sensor are shifted by the value of ϵ when $\alpha = 0°$. The new angle will be called θ. This way, when $\theta = 0°$ also $\alpha = 0°$.
4. The final output angle of the hybrid sensor (β) is calculated using: $\beta = \alpha + \delta$ where $\delta = 0°$ if $| \alpha - \theta | < 90°$ and $\delta = 180°$ if $| \alpha - \theta | > 90°$.

Following this procedure, the range of the magnetic sensor will be extended to 360° from the previous 180°.

3.4 Test 1 - On-axis error

This test was performed in nominal working conditions: no mechanical misalignment, no stray field, and at room temperature. The test is going to demonstrate that, for this prototype, the performances will be the same as those of the MLX90377 but extended to 360°. To demonstrate this property we need to demonstrate the orthogonality with the inductive part of the hybrid sensor. Hence, we will show that the error of the magnetic sensor shall be the same for a test without the inductive part of the hybrid sensor. The inductive part that could possibly interfere with the measurement of the MLX90377 is the metallic half-moon. This is why two sets of measurements will be taken: one with and one without a metal target. This, in principle, will demonstrate the orthogonality of the two types of sensors in ideal conditions. The air gap is fixed at 2 mm. See the following Tab.3.4 for a detailed view of the test's steps.

Test 1:	
1	Calibration of inductive sensor with PTC-04
2	Mount magnet and metal target
3	Alignment procedure(Tab.3.3)
4	Set 2mm airgap
5	Define 0 position as the position providing output of MLX90377 = 0°
6	Rotate magnet of 1°
7	Store measurement of Multimeter and PTC-04 in dataframe
8	Repeat steps 6-7 until reaching full 360° range
9	Calculate angular error and store the results
10	Remove metal target
11	Repeat steps 6-9
12	Compare the two retrieved angular errors

Table 3.4 – In details all the steps performed in the measurement campaign for Test 1

3.4.1 Results

The hybrid sensor is working as expected extending the range of the magnetic sensor up to 360° using the measurements of the inductive sensor (Fig.3.5).
From the analysis of the NLE (Fig.3.6a), one can observe how the amplitude of the NLE of the inductive sensor is far below the threshold of 90°. The RNLE for the inductive sensor in this case is equal to 0.951 °. For the NLE of the MLX90510 it is clear the presence of a 2nd harmonic, maybe related to slight surface asymmetries due to feeding wires.
The RNLE of the MLX90377 is equal to 0.905° and it is clear the presence of a 4th harmonic. This harmonic is due to the non-perfect magnetization of the ferrite magnet. The curves with and without target are overlapped and show the exact same behavior. If we make the difference between these curves (Fig.3.6b) we observe a variation around 0 °of about ±0.25°. Mostly, this is a noisy component which has little to do with the presence or absence of the metal target.
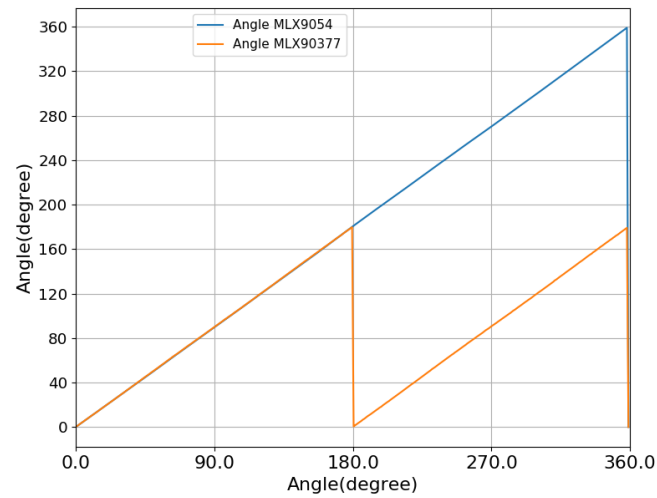
Figure 3.5 – The behavior of the signals coming from the two sensors

Parameter	sensor	Unit	Metal target	Verification Results
NLE	MLX90377	degree	Yes	±0. 45
NLE	MLX90377	degree	No	±0. 47
NLE	MLX90510	degree	-	±0. 50

Table 3.5 – Summary of the results obtained by Test 1

(a)   (b)
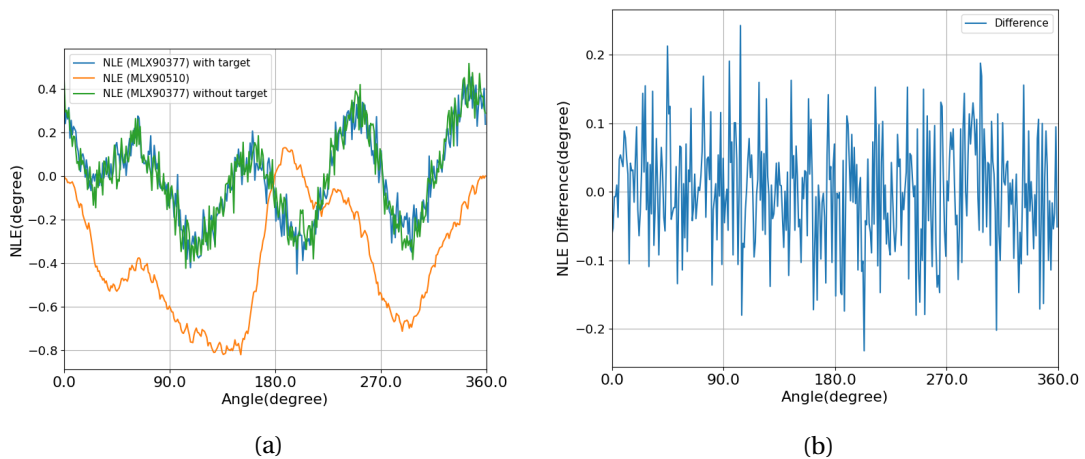
Figure 3.6 – (a)The NLE of the magnetic sensor(MLX90377) with and without metal target and the NLE of the inductive sensor(MLX90510). (b)The difference between the NLE of the magnetic sensor taken once with and once without the metal target for the inductive sensor

This test demonstrated that the hybrid sensor works properly and in the above mentioned conditions the metal target does not affect the behavior of the MLX90377.

53

3.5 Test 2- Stray field immunity

The goal of this test is to prove that the two sensors maintain their SFI when working on the same chip and that the two sensors remain orthogonal even in presence of an external magnetic field. In this case a stray field will be generated by a neodymium magnet[Figure 3.7] placed as in Figure 3.8 that will generate upon the MLX90377 a constant magnetic field.

(a)   (b)   (c)
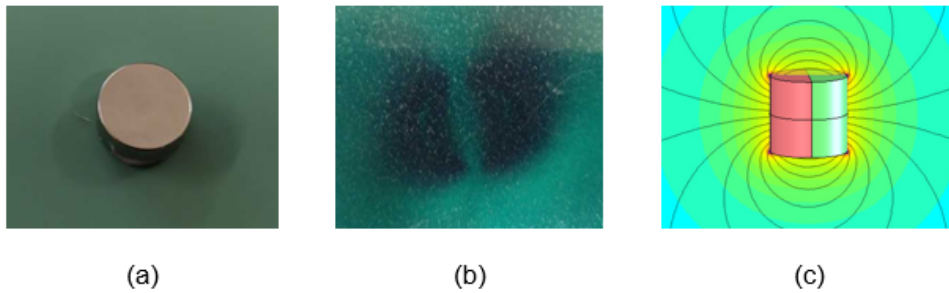
Figure 3.7 – (a)The neodymium magnet used during the experiment.(b) The polarization seen using a polarization card.(c) The field lines for this type of magnet. To minimize the gradient of the magnetic field produced at the sensing spot, the magnet has been placed as in fig.3.8
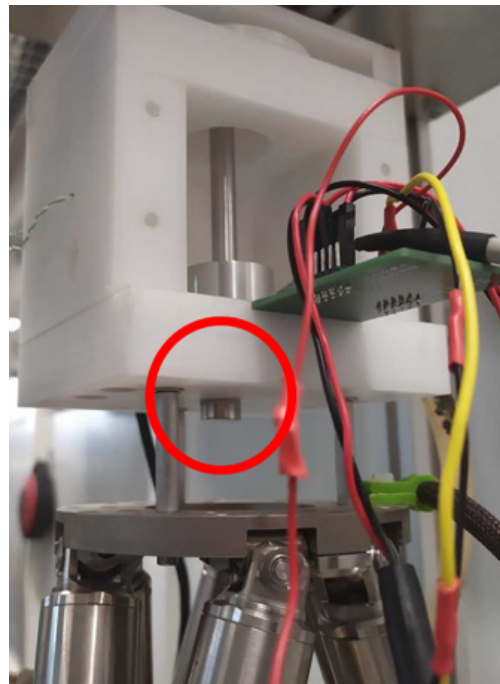
Figure 3.8 – The neodymium magnet has been glued under the testing box for the PCB

The magnet position has been chosen in order to minimize the effect of the gradient of the magnetic field, which for very powerful magnets such as neodymium ones, is very high. As presented in subsection 1.1.3, if the field is not constant and presents a gradient, two

differential HPs of the SUN structure will perceive a different value of the stray field. Therefore, the difference between the HPs' signals will not completely remove the stray field contribution. By observing the field line generated by the magnet, this position should provide mostly field lines parallel to the chip plane.

(a)

(b)
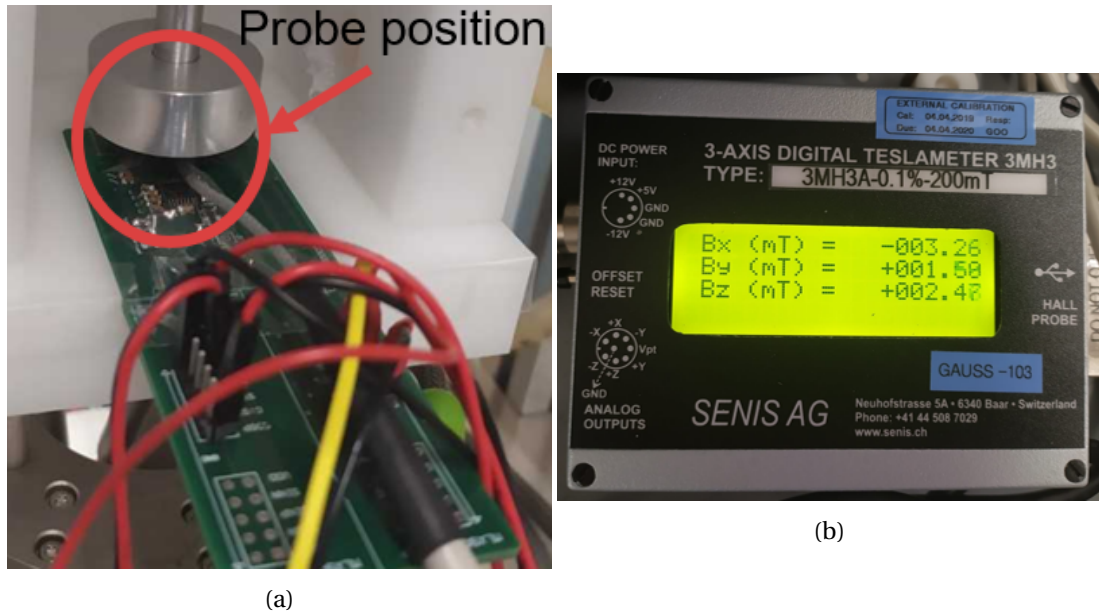
Figure 3.9 – (a) The position of the probe on the PCB. (b) On the display the amplitude of the magnetic field generated exclusively by the neodymium magnet.

The amplitude of the magnetic field has been measured using a Teslameter whose probe has been placed right on top of the MLX90377 [Figure 3.9]. The total amplitude of the field on the sensor is 4.39 mT. Since this field is lower than 5 mT, we expect from the MLX90377's datasheet the Stray field error introduced by the magnet to be lower than 0.4 °. Temperature and mechanical conditions remain ideal and the same as Test 1. See the following Table 3.6 for a detailed view of the test's steps.

Test 2:	
1	Calibration of inductive sensor with PTC-04
2	Mount magnet and metal target
3	Alignment procedure
4	Set 2.2 mm airgap
5	Define 0 position as the position providing output of MLX90377 = 0°
6	Rotate magnet of 1°
7	Store measurement of Multimeter and PTC-04 in dataframe
8	Repeat steps 6-7 until reaching full 360° range
9	Calculate angular error and store the results
10	Place magnet so to have a 5mT field in one direction on the MLX90377
11	Repeat steps 6-9
12	Calculate Stray field error
13	Remove metal target
14	Repeat steps 6-9
15	Remove magnet
16	Repeat steps 6-9
17	Compare the two Stray field error

Table 3.6 – In details all the steps performed in the measurement campaign for Test 2

3.5.1 Results

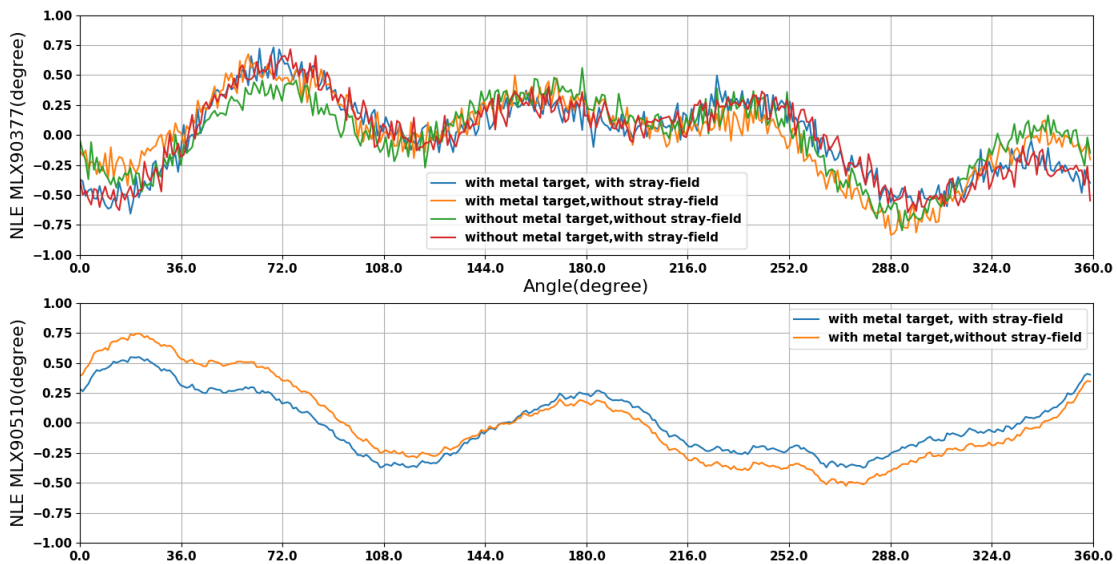Figure 3.10 – above, the NLE in the four combinations of with an without metal target and stray field. Below, the NLE for the inductive sensor

As it appears in Figure 3.10, the NLE curves follow the same trend in presence and in absence of the stray field, demonstrating that the inductive and magnetic sensors are still SFI. The orthogonality of the two measurement principles in these conditions is also demonstrated by

the curve having the same behavior in case of presence and absence of the metal target.

The NLE error of the MLX90510 shows a noticeable variation. This variation is due to the proximity of the neodymium object which, being a good conductor, behaves as a stray metal for the inductive sensor. The eddy current that will be generated inside the magnet will produce a modulated external magnetic field whose signal will be captured by the Rx coils of the inductive sensor. This contribution will affect always the same region during the metal target's rotation. The final effect of this stray metal is an increase of the 1st order harmonic of the NLE.

The stray field error(Fig.3.11a) is still present as a 2nd harmonic and it is equal to ±0.44°. The value is at the limit of the specs (±0.40°) but this is due to the fact that the stray field is not actually constant. The gradient of the magnetic field generated by the neodymium magnet is minimized by its placement, however, a small gradient will still be present and it will affect the measurement.

(a)

(b)
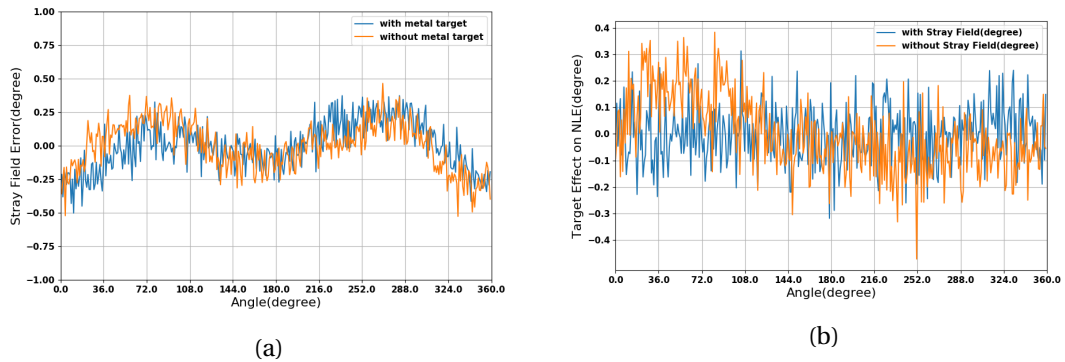
Figure 3.11 – (a) The Stray field error introduced by the neodymium magnet on the MLX90377. (b) The difference between the NLE for the measures with and without metal target

The presence of the metal target (Fig.3.11b), once again, do not change the behavior of the magnetic sensor and the difference between the two cases is just a noisy component around 0° not related to the metal target. Moreover, since both the inductive and magnetic sensors remained SFI, the combined sensor is SFI.

Parameter	Sensor	Unit	Stray Field	Metal Target	Verification Results
NLE	MLX90377	degree	Yes	Yes	±0. 69
		degree	No	No	±0. 68
		degree	Yes	No	±0. 68
		degree	No	Yes	±0. 75
	MLX90510	degree	No	-	±0. 60
		degree	Yes	-	±0. 46
Stray field error	MLX90377	degree	-	Yes	± 0.44
		degree	-	No	± 0.50

Table 3.7 – Summary of the results for Test 2

3.6 Test 3 - Mechanical misalignment

The purpose of this test is to evaluate the errors in case of mechanical misalignment. As in the previous tests, the measurements will be taken both with and without metal target in order to demonstrate the orthogonality of the two sensors also in case of mechanical misalignment. An off-axis test involves the displacement of the center of the hybrid target with respect to the center of the SUN structure of the magnetic chip. During the tilt test, the magnet will be back on-axis and it will be tilted on the U axis. The air gap will be varied in the on-axis position to evaluate its effect on the NLE both for the inductive sensor and the magnetic sensor. The test is performed at room temperature and without stray-field. See Table 3.8 for a detailed view of the test's steps.

Test 3 :	
1	Calibration of the inductive sensor with PTC-04
2	Mount magnet and metal target
3	Alignment procedure(retrieve Reference position)
4	Set 2mm airgap
5	Define 0 position as the position providing output of MLX90377 = 0°
6	Rotate magnet of 1°
7	Store measurement of Multimeters and PTC-04 in dataframe
8	Repeat steps 6-7 until reaching full 360° range
9	Calculate angular error and store the results
10	Repeat steps 6-9 for the following airgaps:[2.5,3,3.5] mm
11	Calculate Airgap error
12	Repeat steps 6-9 for the following tilt angles on the U axis: from -1.5 degree to 1.5 degree with 0.5 steps
13	Calculate Tilt error
14	Repeat steps 6-9 for the following Off-Axis values on the X direction: from -1.5 mm to 1.5 mm with 0.5 mm steps
15	Calculate X Off-Axis error
16	Repeat steps 6-9 for the following Off-Axis values on the Y direction: from -1.5 mm to 1.5 mm with 0.5 mm step
17	Calculate Y Off-Axis error
18	Remove metal target
19	Repeat steps 6-17
20	Compare errors results

Table 3.8 – In details all the steps performed in the measurement campaign for Test 3

3.6.1 Results

For each section, it will be presented the NLE curves for each value of mechanical misalignment and the relative misalignment error. The misalignment errors (off-axis error, airgap error and tilt error) are the difference between the NLE curves in presence of misalignment and the

NLE curve in nominal working conditions. These curves allow us to analyze more in detail the effects of the misalignment on the NLE.

Off-Axis

The behavior of the NLE is very similar between the X off-axis error and the Y off-axis error (Fig.3.13). Since the structure is symmetrical, we expected the same behavior for the two axes but shifted of 90 ° and therefore we can analyze just one of the two (E.g. the X direction). The MLX90377 shows a 1st harmonic error increase with the increase of the off-axis. In particular, for each mm of off-axis the NLE increase in the error's amplitude of 2°. The same trend is present for the inductive sensor (again increase of the 1st harmonic) for which the sensitivity to the off-axis is higher and reaches $4°/mm$.

Airgap

The distance of the magnet from the Hall sensor does not affect heavily the angle measurement (Fig.3.13). Since the magnetic field detected by the Hall plates will be lower, the IC will need to boost the gain for the signal which will inevitably introduce noise. The noise will reduce the precision of the signal and slightly increase the NLE for the MLX90377. The effect on the NLE of the inductive sensor is limited and will increase the amplitude of the 1st harmonic by 0.4° for each mm of air gap.
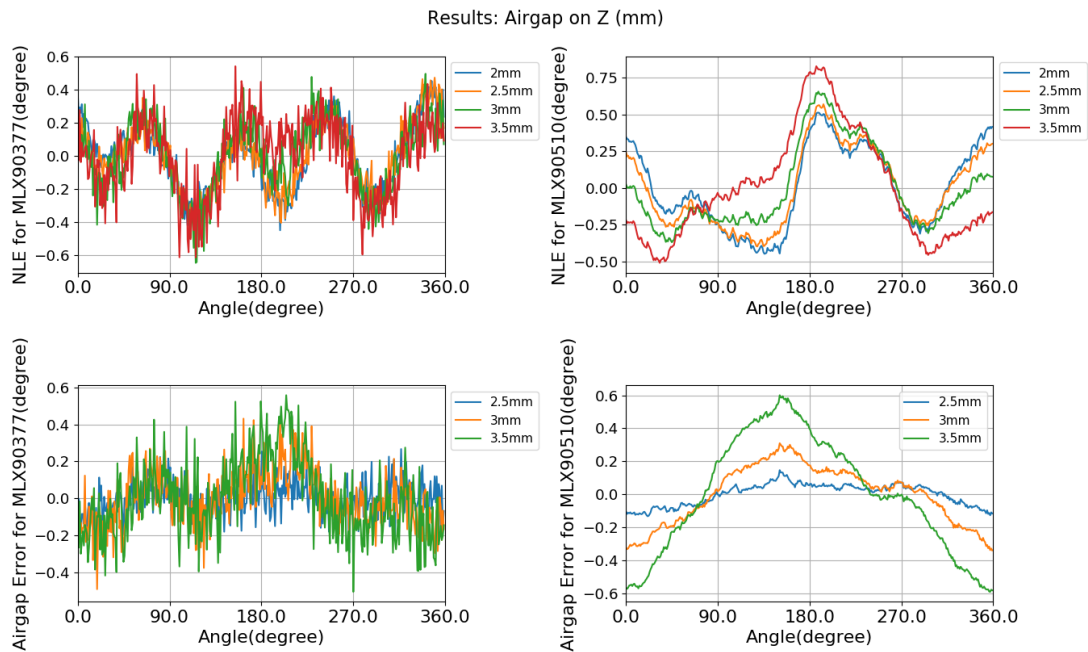
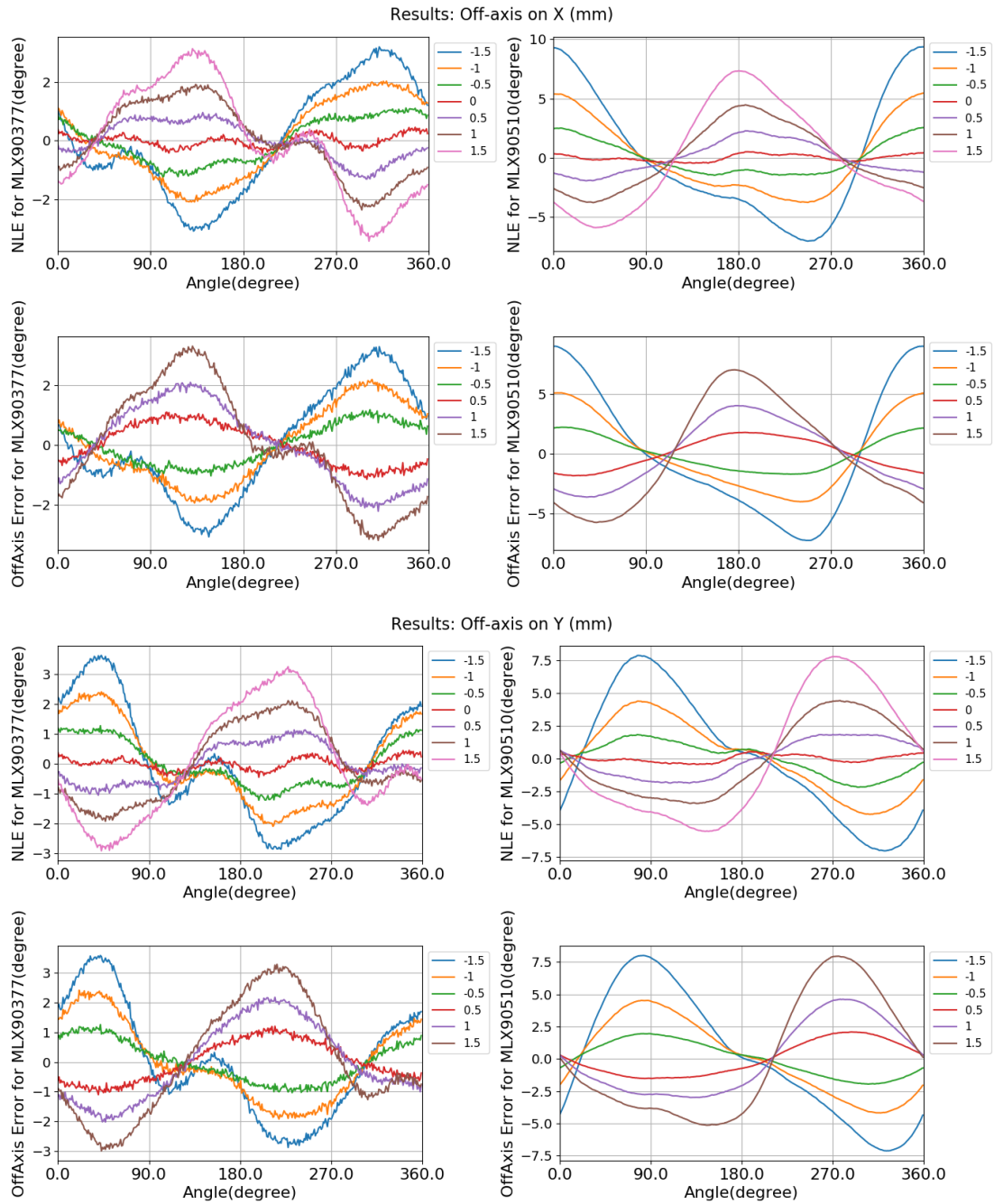Figure 3.12 – Results from the airgap variation

Figure 3.13 – Tesults of the off-axis sensitivity tests. As presented by the labels of the plots, the first column's results are related to the magnetic sensor and the second column's to the inductive sensor. For each test type, on the first row is shown the NLE of the sensors and on the second row is shown the RNLE of the sensors.

Tilt

The magnetic sensor is immune to the tilt of the magnet and therefore its tilt error will be just noisy components (Fig.3.14).
The inductive sensor is more susceptible to tilt as explained in subsection 1.2.2. The NLE will increase its 1st harmonic by 3.5°/°.
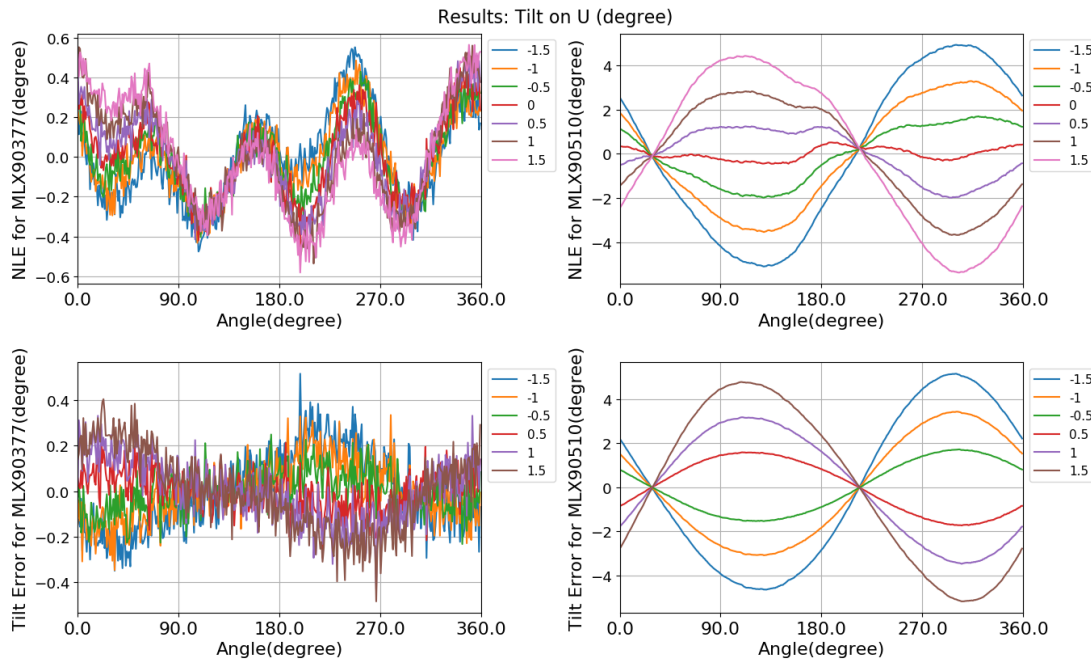
Figure 3.14 – Results from the tilt variation

Conclusions

The target does not affect the measures of the magnetic sensors in any condition of mechanical misalignment [Fig.3.15]. In fact, it is clear that the difference is always a noisy component between ±0.4° that does not depends on the presence of the metal target. **Moreover, in every misalignment case, the hybrid sensor is working correctly and the NLE of the inductive sensor is well below the 90° threshold.**
As expected, the inductive sensor is overall more sensitive to mechanical misalignment with respect to the magnetic sensor. This is another advantage of using the magnetic sensor for the accurate angle measurements. Since the NLE for the inductive sensor remained lower than 90° the hybrid sensor would have kept the accuracy of the magnetic sensor. In Table 3.9 you can find a summary of the results for this test.
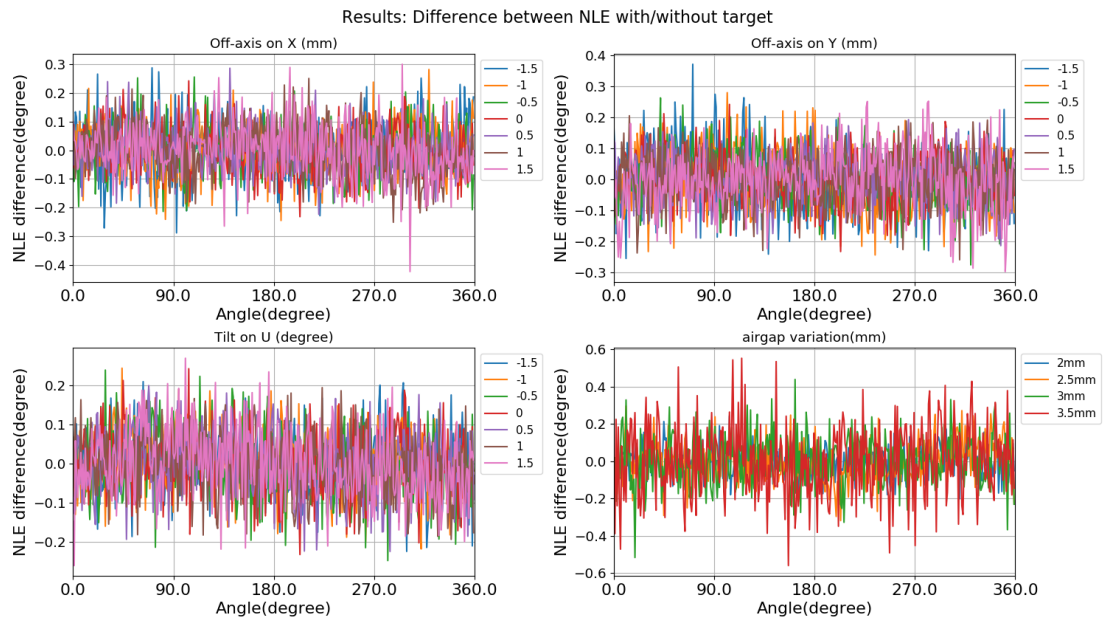
Figure 3.15 – This plot shows the results for the 4 sections of the test for what concerns the target effect on the MLX90377

Sensor	Errors			
	X off-axis	Y off-axis	Tilt	Airgap
MLX90377	2°/mm	2°/mm	Unaffected	More Noise
MLX90510	4°/mm	4°/mm	3.5°/°	0.4°/mm

Table 3.9 – Summary of the results for the mechanical misalignment

3.7   Test 4- Effect of stray metals

The purpose of this test was to demonstrate that the hybrid sensor can maintain high performances even with a large error for the inductive sensor. In fact, if the NLE of the inductive sensor is kept under 90° then the hybrid sensor will still work properly with the accuracy of the magnetic sensor.
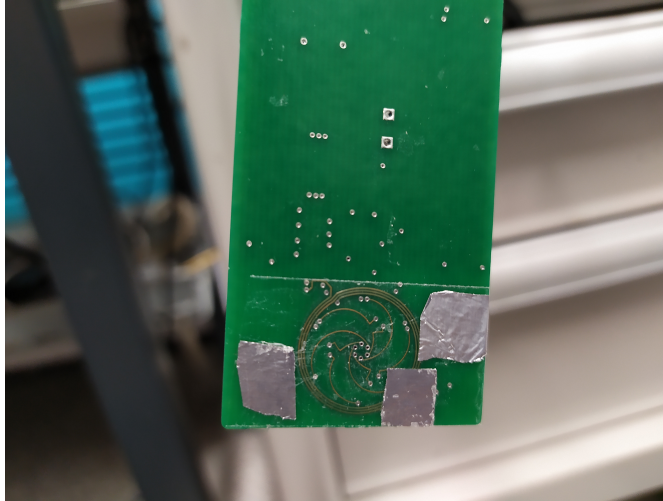
Figure 3.16 – The position of the stray metals on the inductive coils

Stray metals (aluminum foils) have been placed very close and even overlapping the coils of the inductive sensor (Fig.3.16). We expect the inductive sensor to have a very high NLE.
In fact, eddy currents will be excited in the stray metals, generating in turn angle independent signals in the Rx coils. Such signals are equivalent to an offset and are thus the source of large errors.
The MLX90377 is insensitive to stray metals so we expect that its NLE will not be affected. For a detailed description of the test, see Tab.3.10.

Test 1:	
1	Calibration of the inductive sensor with PTC-04
2	Mount magnet and metal target
3	Mount stray metals as in Fig.3.16
4	Alignment procedure(Tab.3.3)
5	Set 2mm airgap
6	Define 0 position as the position providing output of MLX90377 = 0°
7	Rotate magnet of 1°
8	Store measurement of Multimeter and PTC-04 in dataframe
9	Repeat steps 6-7 until reaching full 360° range
10	Calculate angular errors and store the results

Table 3.10 – all the steps performed in the measurement campaign for Test 4

3.7.1 Results

The NLE of the inductive sensor did not exceed the 90° threshold, therefore, the hybrid sensor is still working correctly.
The algorithm (section 3.3) is able to rebuild the accurate angle using the measurements from the magnetic sensor, maintaining a 360 °range. The error of the inductive sensor is visible even on the larger scale [Figure 3.17a]. The Range of the NLE for the inductive sensor goes up to 48.42 °.

On the other hand, The NLE for the magnetic sensor remains at $\pm0.59°$ and corresponds to the original accuracy of the hybrid sensor [Figure 3.17b].

(a)   (b)
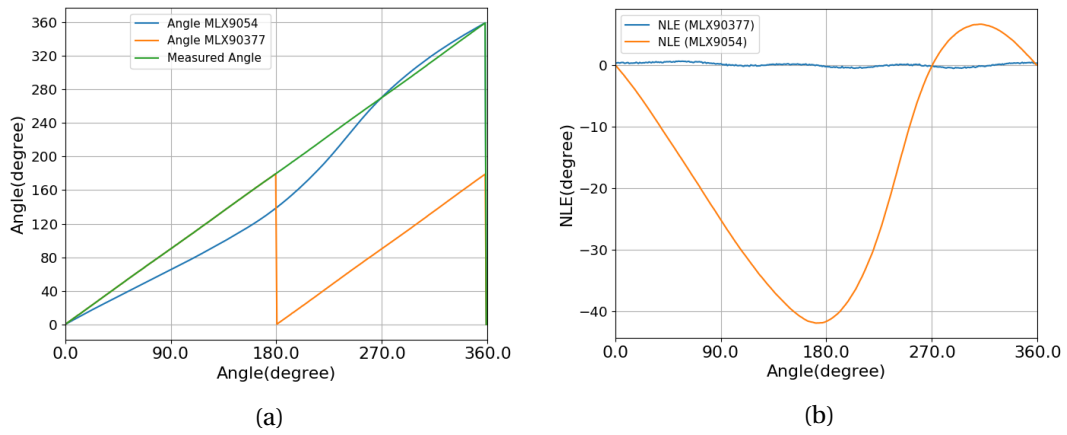
Figure 3.17 – (a) The measurements retrieved from the two sensors. (b) The NLE curves for the two sensors

3.8 Characterization Conclusions

Every requirements has been fulfilled [Table 3.11]. Since we demonstrated that the two sensors are indeed orthogonal we can use the specification directly from the datasheet of the magnetic sensor to retrieve the performances of the hybrid sensor. This is a general discussion that can be made on a general Hybrid sensor that includes both an inductive and a magnetic sensor. This approach can be followed also in other contexts in which higher accuracy is required and can be achieved by reducing the range of the main channel and using the second channel to maintain a larger range. This also applies in a complementary situation in which one may prefer using the inductive sensor as the main channel and the magnetic sensor as a support sensor. In general, using these hybrid configurations, the requirements for the second channel sensor are much less strict than in a normal configuration. This gives more freedom in terms of development and opens new design possibility for preexisting concepts.

REQUIREMENTS	TARGET	ACHIEVED	SOURCE
Range	360 °	360 °	Test 1
Angular error	0.8 °	0.8 °	Orthogonality
5 mT stray field induced error	0.4 °	0.4 °	Orthogonality
Tilt error	<<1 °	0.3 °/°	Test 3
Angular error for second channel	<90 °	<90 °	Test 1,2,3,4

Table 3.11 – All requirements are met

4 Towards a scaled-down prototype

In the previous chapter, it has been proved that the hybrid concept works as expected in the first prototype. Nevertheless, the design described in chapter 2 is a scaled-up proof of concept with respect to the final product that was imagined by Melexis [Figure 1.15]. The final goal of the project, in fact, is to redesign this hybrid sensor in order to be contained inside a single, smaller, and even PCB-less package.

The magnetic sensor we used is produced on silicon wafers and the size of the SUN structure has a radius usually around $250\mu m$. The inclusion of this sensor in the final package will not be a problem since the whole circuit and structure have already been designed with a $0.18\mu m$ technology. Hence, its design can remain very similar.

On the other hand, problems arise when we consider the inclusion of the inductive sensor in the small package. The chip used in the prototype (MLX90510) needs to be connected to the Transmitting Coil and the Receiving coils in order to work. In the first prototype, these coils were smaller with respect to a normal Tx and Rx coils design, but they were still printed on an extended region on the PCB. The dimensions of these coils affect heavily the performance of the inductive sensor as shown in subsection 1.2.2.

This chapter will focus on the consequences of down-scaling the inductive part of the hybrid sensor to fit a region that should not be larger than 5x5 mm. With these dimensions, the coils should be able to fit an SMP3 package, a standard used by Melexis.

4.1 Challenges associated with coils size reduction

The reduction of the diameter of the Tx coil will inevitably cause a reduction of its inductance. A low inductance will cause a huge current drain by the MLX90510 that could reach easily a hundred of mA [Figure 2.3]. Hence, a new oscillating circuit for the IC is in scope for the next development steps of this project. However, for the following analysis, we will try to achieve a design compatible with the already developed MLX90510.

We will consider Equation 2.1 seen in chapter 2 for the estimation of the Tx coil's inductance. The largest element of the design will be the outer diameter for the transmission coil ($D_{Tx,max}$) and it shall not exceed 5 mm. According to the datasheet of the MLX90510, L_{Tx} should not

be lower than $0.5\mu H$ to avoid too large power consumption. The number of layers to be used in the PCB for the coil structure is very important. A higher number of layers would allow distributing the Tx coil's winding in a vertical way. This means that, on average, the diameter of the windings of the Tx coil will be larger, increasing its inductance. In fact, L_{Tx} depends on $R = D/2$ in Equation 2.1. On the other hand, the price of the PCB will increase heavily if a large number of layers are used.

Having L_{Tx} greater than 0.5 μH is not sufficient to have an acceptable power consumption. In order to work with such small inductance, the quality factor of the oscillating circuit needs to be very high [Equation 2.2]. Since for such a small design the track-width is needed to be very small, the resistance of the Tx coil will be high [Equation 2.3]. For integrated versions of inductive angular sensors, the oscillating circuit is usually designed to work at high frequency in order to boost the Q factor. Nevertheless, the MLX90510 allows for a maximum frequency of 5 MHz only. Therefore, manipulating the frequency to boost the Q factor gives little results. Another important quantity which will vary with the dimensions is the signal captured by the receiving coils (described by Equation 1.14). The amplitude of this signal will affect the robustness against external disturbances and mechanical misalignment. The amplitude of the signal is exponentially affected by the size of the receiving coil, which we must assure to be the largest possible. For the miniaturized prototype, it has been chosen to print the Rx coil on different layers with respect to the Tx coil. The idea is to have the Rx coil with the same diameter as the Tx coil. This solution is used in order to boost the signal captured by the receiving coils and simplify the connections with the IC. Most of the signal captured by the Rx coil will be in the region where the two coils are not overlapping. However, part of the signal will be also present in the region where the Rx coils are overlying the Tx coil. Another trick that is used to boost the signal is to place the Rx coil's layers close to the surface of the PCB, reducing at the minimum the distance from the metal target. If we consider these conditions, Equation 1.14 becomes an underestimation of the signal of the Rx coil.

Design restrictions become very important too. A very small clearance is required in order to allow the presence of tracks and vias in a very small area. Standard providers can reach a clearance of only 0.1mm (spacing between tracks). Nevertheless, specialized providers (E.g. Contag) can allow clearance down to 0.06mm.

Since we already set $D_{TX,max}$ to be 5mm, we can find $D_{Tx,min}$ with the following expression:

$$D_{Tx,min} = D_{Tx,max} - 2 * ((K-1) * (S_T + W_{Tx}) + W_{Tx}) \tag{4.1}$$

where K is the integer part of $n_{Tx}/(N_L - 2)$ (where N_L is the number of layers we decided to use) and S_T is the minimum spacing between the tracks. We will call $D = (D_{Tx,max} + D_{Tx,min})/2$ the average diameter of the coil and $W_{Tx} = (D_{Tx,max} - D_{Tx,min})/2$ the width of the Tx coil. To have an estimation of the signal we will consider $D_{Rx,ext}$ equal to D, even if it will have ideally always the same dimension equal to $D_{Tx,max}$. This approximation is to take into account that the signal captured by the outer part of the Rx coil will be actually lower.

We can now proceed to the analysis of Q, L_{Tx} and V_{Tx} when we vary some characteristics of the PCB.

4.2 Numerical analysis

4.2.1 Track width for the Tx coil and number of layers

Increasing the width of the transmission coil will increase the quality factor of the oscillator by reducing the resistance of the coil [Figure 4.1b]. At large track width, the behavior will start to saturate since the inductance will start to decrease as well [Figure 4.1a]. The reason why W_{Tx} affects the inductance is that the average diameter (D) of the coil will be reduced. Using a wider track for the Tx coil will reduce its inductance but it might be necessary to boost the Q factor.

Using more layers is beneficial to reach higher values for L_{Tx} and the Rx coil signal. Also, the quality factor will saturate at higher values if more layers are used. The reason behind these results is that the average diameter D of the Tx coil will remain high since the windings can be distributed on many levels.

The values of the other design parameters used for this analysis are shown in Table 4.1.

Input	Value	Unit
Frequency	4.5	MHz
V_{Tx}	2.4	V
$D_{Rx,Int}$	1	mm
S_T	0.06	mm
T_T	0.035	mm
n_{Tx}	12	
z	2.5	mm

Table 4.1 – The fixed parameters used during the analysis of W_{Tx}
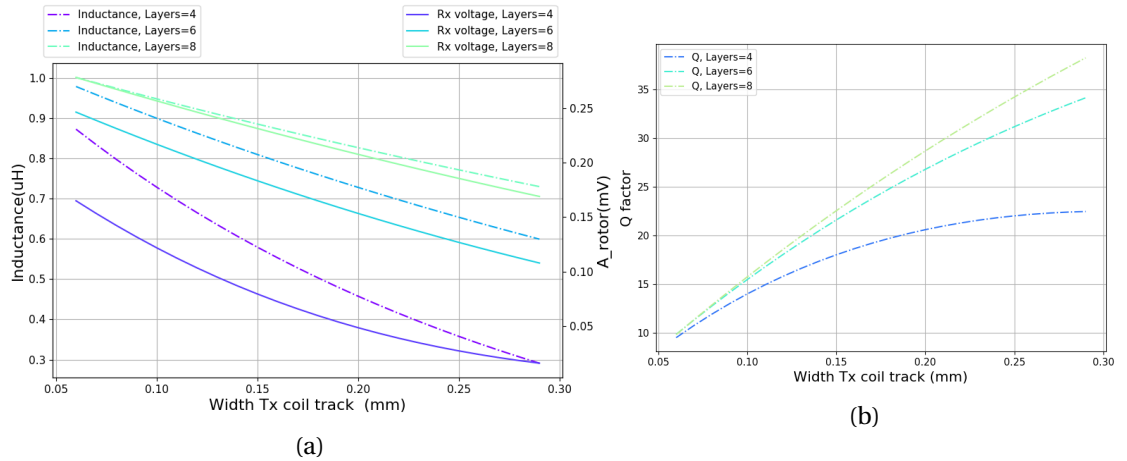

(a)

(b)

Figure 4.1 – A plot showing the variation of the three key factor with the width of the track of the transmission coil.

For the new design, and therefore for the following analyses, it has been chosen $W_T x =$

$0.14mm$.

4.2.2 Number of turns for the Tx coil

From Equation 2.1, the number of turns is the factor that will affect more heavily the value of the inductance compared to R, l and w. Actually, the final shape of the coil will be affected by the number of layers we intend to use for the Tx coil. In order to maximize D, the idea is to distribute as much as possible the turns of the coils equally on all the layers. We observe that the inductance will increase with the number of rounds of the coil (Figure 4.2a), however right after the number of turns reaches a multiple of the layers there is a sudden reduction for $D_{Tx,min}$ and therefore a reduction for the inductance.

We find that the best condition is achieved when the number of turns is a multiple of the number of layers. This is also visible in the Q factor which follows the same behavior of L_{Tx}. The values of the other design parameters used for this analysis are shown in Table 4.1 withthe addition of $W_{Tx} = 0.14mm$.
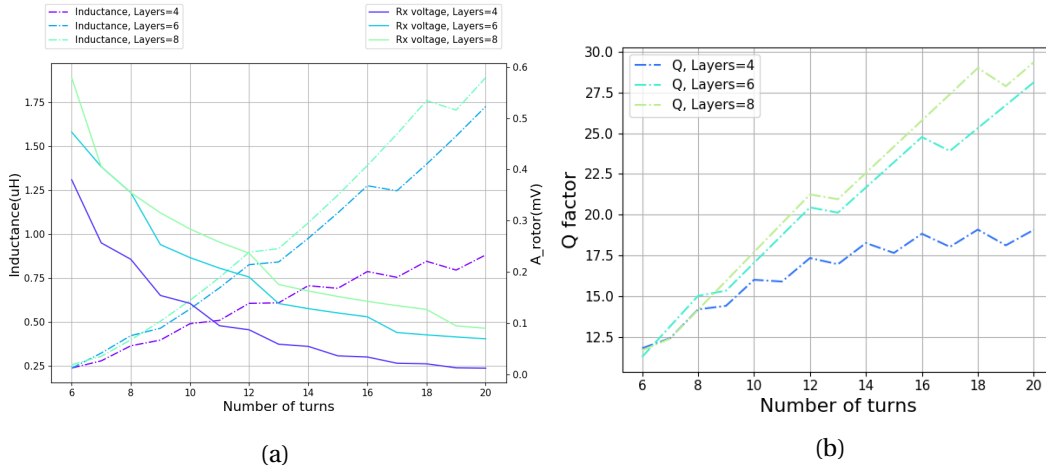
Figure 4.2 – A plot showing the variation of the three key factors with the variations of the number of layers available for the Tx coil and also the number of turns for the coil

4.2.3 Internal diameter of the Rx coil and airgap

Decreasing the internal diameter of the Rx coil or the air gap between the coils and the metal target are two ways to improve the signal of the Rx coil without changing the Q factor of the or the inductance of the Tx coil. For this analysis the fixed design parameters were the same as shown in Table 4.1 with the addition of $W_{Tx} = 0.14mm$ and $N_L = 6$.

The dependence of the signal on $D_{Rx,Int}$ is very limited [Figure 4.3], especially if $D_{Rx,Int} <$ $1.5mm$. In fact, in Equation 1.14, r, that depends on $D_{Rx,Int}$, is very close to the critical radius (r_0) and, therefore, its effect on the signal is very limited.
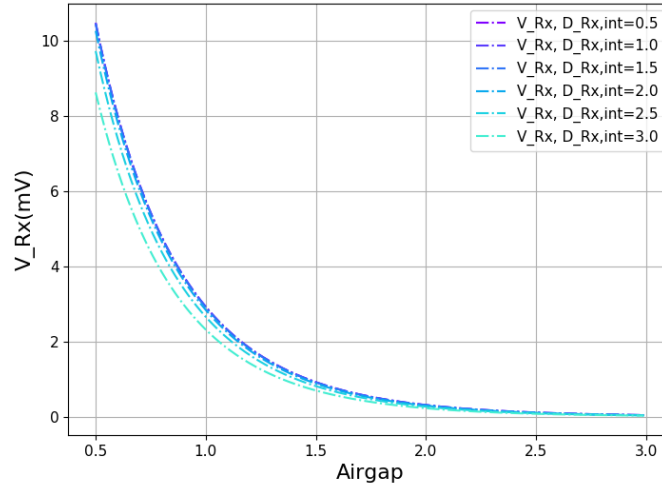
Figure 4.3 – The amplitude of the signal from the receiving coil with the variation of the air gap and the internal diameter of the Rx coils.

On the other hand, the Rx coils signal has an exponential dependence on the airgap [Equation 1.14], and the signal drops very fast with the increasing of the airgap. Moreover, the hybrid sensor shall be included in a single package and therefore the air gap will have to include also the thickness of the package and the IC of the sensor. From very low signal conditions we can expect a very noisy angle measurement and also an increment of the NLE.

4.3 A new prototype

We already discussed the impact of the down-scaling on the inductance of the Tx coil and the quality factor of the oscillating circuit. These two quantities will affect heavily the power consumption of the inductive chip and they need to be monitored to not exceed acceptable values. All these requirements are necessary because we planned to use the MLX90510. A working prototype using an already developed chip can save a lot of costs in terms of the development of a completely new IC. Naturally, in a more advanced concept, some changes will be required, especially in the oscillating circuit to withstand higher frequencies which will reduce the power consumption. Moreover, the automatic shutdown of the IC can be avoided in order to work with even lower signals coming from the Rx coils.

An experiment has been performed using the previous design [Figure 2.7] to evaluate the lowest signal that the MLX90510 can detect before the output shuts down. To test the chip in these extreme conditions, the metal target has been placed very far from the inductive coils. The test has been performed at 8mm of airgap from the inductive coils, after which the chip would have shut the outputs. The PTC-04 has been used to extract the value of A_rotor generated by the Rx coils(Table 4.2). Unfortunately, the resolution of the tool is fixed at the millivolts since it is very unusual for inductive sensors to work with such small signals.

Airgap(mm)	A_rotor (mV)
2	10 ± 0.5
3	5 ± 0.5
4	3 ± 0.5
5	2 ± 0.5
6	1 ± 0.5
7	1 ± 0.5
8	0 ± 0.5

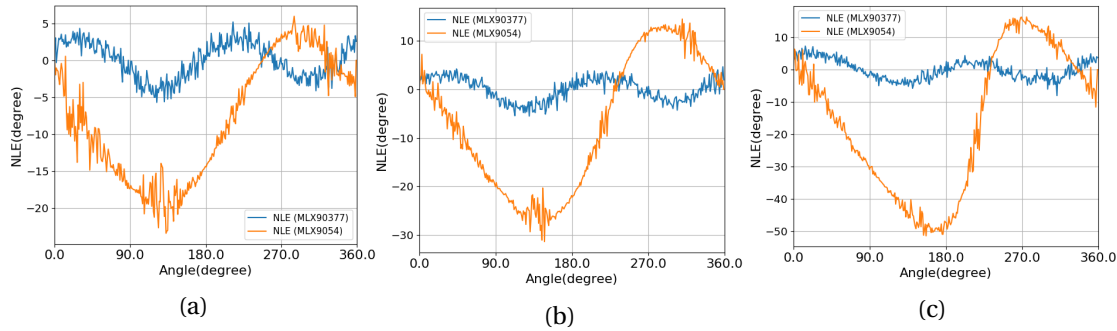Table 4.2 – The measures retrieved using the PTC-04

(a)

(b)

(c)

Figure 4.4 – (a)NLE in on-axis conditions at 8mm of airgap,(b)NLE in precence of a 1°of tilt at 8mm of airgap, (c)NLE in presence of 1.5 mm of off-axis at 8mm of airgap

At 8mm of airgap the MLX90510 still works and it can even stand the presence of mechanical misalignments(Figure 4.4). For this airgap, according to the analytical model (Equation 1.14), we should have $A\_rotor = 311\mu V$ and $V_{Rx} = 180\mu V$. Therefore we have a chance to find a set of values for the scaled-down prototype which would gives us a signal above this threshold.

4.3.1 Suitable values

After an evaluation of the results obtained in the previous sections, it has been chosen to pick the features shown in Table 4.3. The resulting values for this configuration are shown in Table 4.3. Moreover, it is shown the expected variation of the amplitude of A_rotor with the increase of the air gap [Figure 4.5].

The signal appears to be very weak for this configuration, however, Equation 1.14 is usually an underestimation of the real signal perceived by the coils. The power consumption on the other end is expected to be even lower than the first prototype's.

Input	Affecting	Values	Unit
Frequency	Q	3.5	MHz
V_{Tx}	V_{Rx}	2.4	V
r_0	V_{Rx}	0.217	
p	V_{Rx}	2.39	
m	V_{Rx}	0.832	
k	V_{Rx}	10	
$D_{Tx,max}$	Q , V_{Rx} ,L_{Tx}	5	mm
$D_{Tx,min}$	Q , V_{Rx} ,L_{Tx}	3.92	mm
$D_{Rx,ext}$	V_{Rx}	4.46	mm
$D_{Rx,Int}$	V_{Rx}	1	mm
D	Q , V_{Rx} ,L_{Tx}	4.46	mm
S_T	Q , V_{Rx} ,L_{Tx}	0.06	mm
W_{Tx}	Q , V_{Rx} ,L_{Tx}	0.14	mm
T_T	Q , V_{Rx} ,L_{Tx}	0.021	mm
n_{Tx}	Q , V_{Rx} ,L_{Tx}	17	
Layers	Q , V_{Rx} ,L_{Tx}	8	

Table 4.3 – The set of values considered to be the optimal configuration

Output	Value	Unit
L_{Tx}	1.75	μH
R_{Tx}	2.98	Ω
Q	12.9	
C_{osc}	2.37	nF

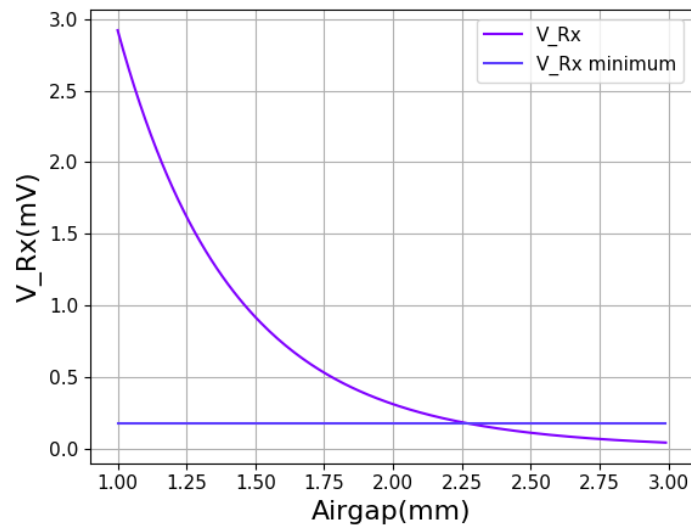Table 4.4 – The results from Table 4.3 configuration

Figure 4.5 – The signal of the receiving coil varying the airgap between target and coils and the threshold for the shut down.

4.3.2 New layout and COMSOL simulation

For the design of the second prototype, it has been decided to use the design parameters presented in Table 4.3. The coil structure used for the MLX90510 is shown in Figure 4.6.

The second prototype will also include a fake lead-frame of the future package. The lead-frame is a metal structure used to connect the pin of the internal IC with the outside of the package. This metal structure is present in one of the two layouts only to investigate the effect of these stray metals on the signal of the Rx coils.

This PCB will mount only the inductive part of the hybrid sensor. The connections between the coil system and the MLX90510 will be the same as the first prototype.
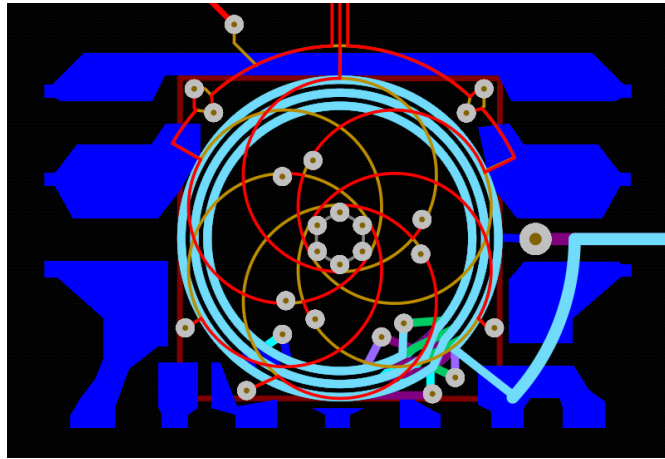

Figure 4.6 – The detail of the new prototype in which is visible the coil structure. The lead frame was placed on the bottom of the PCB. The diameter of the outer winding of the Tx coil is 5mm long.

The layout designed with Altium has been imported into Comsol in order to simulate the behavior of the coil structure of the new prototype. In Table 4.5, the results of the simulation are compared with the results given by the analytical model. Only the coil structure has been simulated and therefore the lead frame and the connections have been removed from the model. The model for the evaluation of the impedance of the Tx coil is a good approximation of the simulated behaviour. However, the estimation of the Rx coils' signal turned out to be an underestimation of the real signal captured by the receiving coils.

Overall, the results of the simulation are very promising and, therefore, it has been decided to proceed with the fabrication of the new design.

Output	Model		Unit
	Analytical	COMSOL	
L_{Tx}	1.79	1.73	μH
R_{Tx}	2.23	2.5	Ω
Q	14.5	15	
A_rotor(@ 2mm airgap)	404	1652	μV

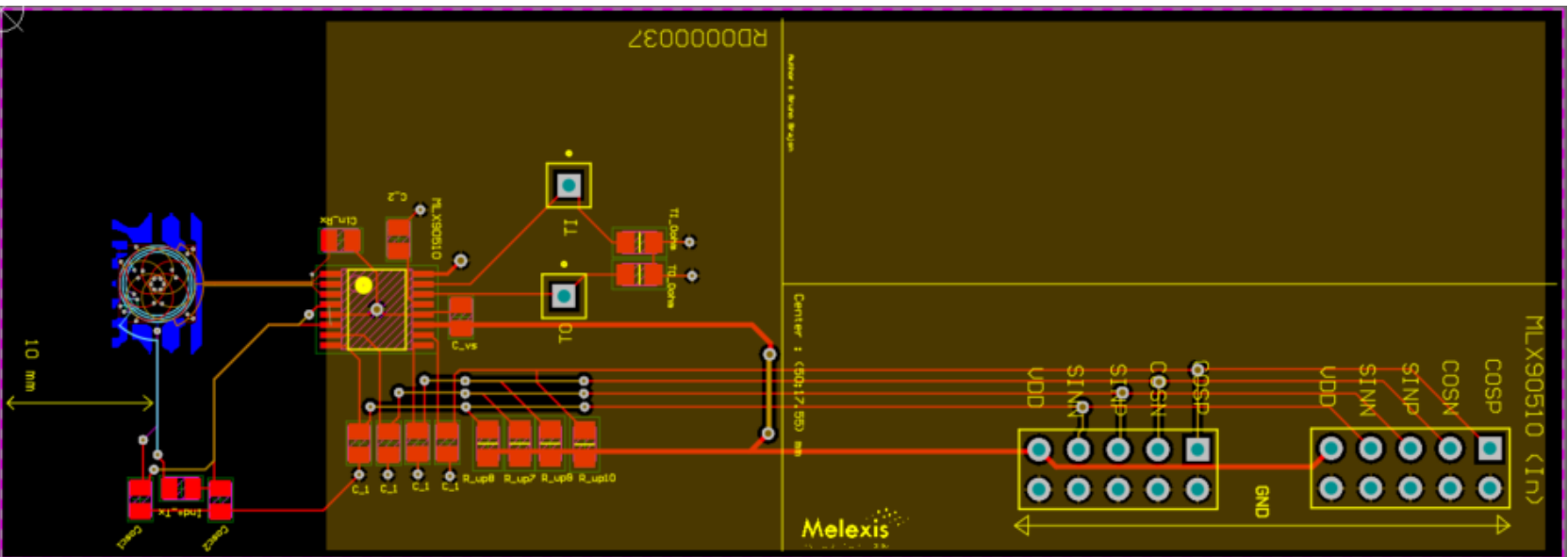Table 4.5 – Comparison of the results from the simulation and the analytical model.

Figure 4.7 – The Layout design for the second PCB prototype

4.4 New prototype characterization

4.4.1 Measurement Setup

A similar setup used for the previous characterization [section 3.1] was used. In this case, we only needed to calibrate the MLX90510 with the PTC-04. We used the same power supply (K2400) and multimeters (K2000) of the previous experiments connected as in Figure 4.9.

For this new set of measurements, a new hybrid target was used. This new hybrid target was designed together with one of the world's leading manufacturers of plastic-bonded permanent magnets.

The alignment procedure has remained the same except that this time both the XY-plane alignment and the UV-plane alignment has been performed using the inductive sensor.

4.4.2 Test 1 - On-Axis

This test was performed in nominal working conditions: without mechanical misalignment or stray fields and at room temperature. The test procedure is the same as the one shown in Table 3.4 The metal target is placed 2mm above the coils. This test is going to demonstrate that the scaled-down version of the inductive sensor can maintain a NLE lower than 90°, necessary feature in order to be employed in the hybrid sensor.

(a) (b)
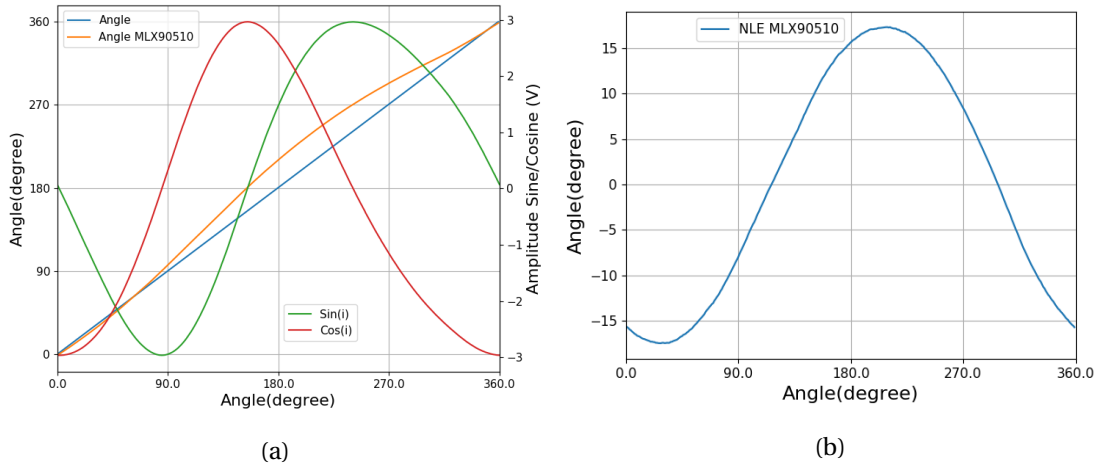
Figure 4.8 – (a)The differential output of the inductive sensor together with the measured angel and the mechanical angle. (b) the NLE of the Test 1.

The NLE curve [Figure 4.8] shows the presence of a strong 1st harmonic. This harmonic is due to the very low signal which is provided by the Rx coil.

The NLE for this measurement is equal to $\pm 17.4°$, well below the 90° threshold proving it suitable for the integration in an SMP3 package.

Figure 4.9 – The measurement set up for the second experimental campaign

4.4.3 Test 2 - Mechanical misalignment

This test was performed in the presence of mechanical misalignments such as off-axis, tilt and air-gaps. The test procedure is the same presented in Table 3.8. The respective mechanical errors are computed in the same way as Test 3 presented in chapter 3. The aim of this test is to assess the 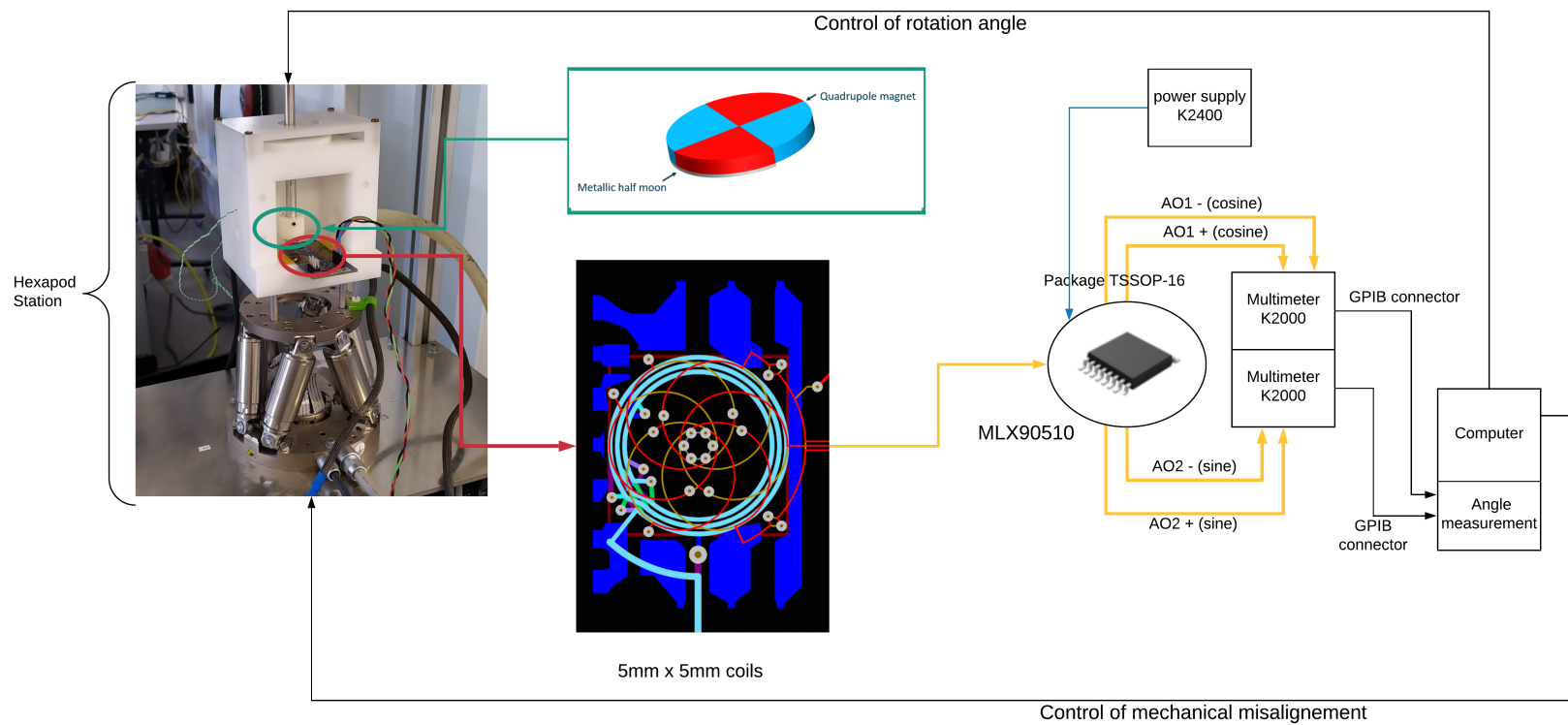robustness of the inductive sensor with respect to mechanical misalignments. Due to the size reduction, we expect a greater sensibility to off-axis with respect to the first prototype. Moreover, due to the exponential dependence on the air gap of the Rx coils signal's amplitude, which is already low due to the small dimensions, we expect to have a much higher sensitivity to the air gap with respect to the previous prototype.

Off-Axis

As expected the Off-axis error is much worse than in the case of the previous prototype [Figure 4.10]. Due to the reduced size of the coil structure, the effect for the same value of the off-axis is enhanced with respect to the 15x15 mm version. In the case of a 5x5mm coil structure, a shift of 1mm in one direction have to be compared with a 3mm shift for a 15x15mm coil structure.
In this case there is also to take into account the very low signal that the sensor perceives when the target is in its furthest position with respect to the coil center. The positions in which the signal is very low are clearly recognizable by the noise spikes on the NLE plot.
Despite the very large NLE shown by the inductive sensor, under no circumstances the threshold of 90°is violated. **Therefore in each one of these cases the hybrid sensor should have worked.**
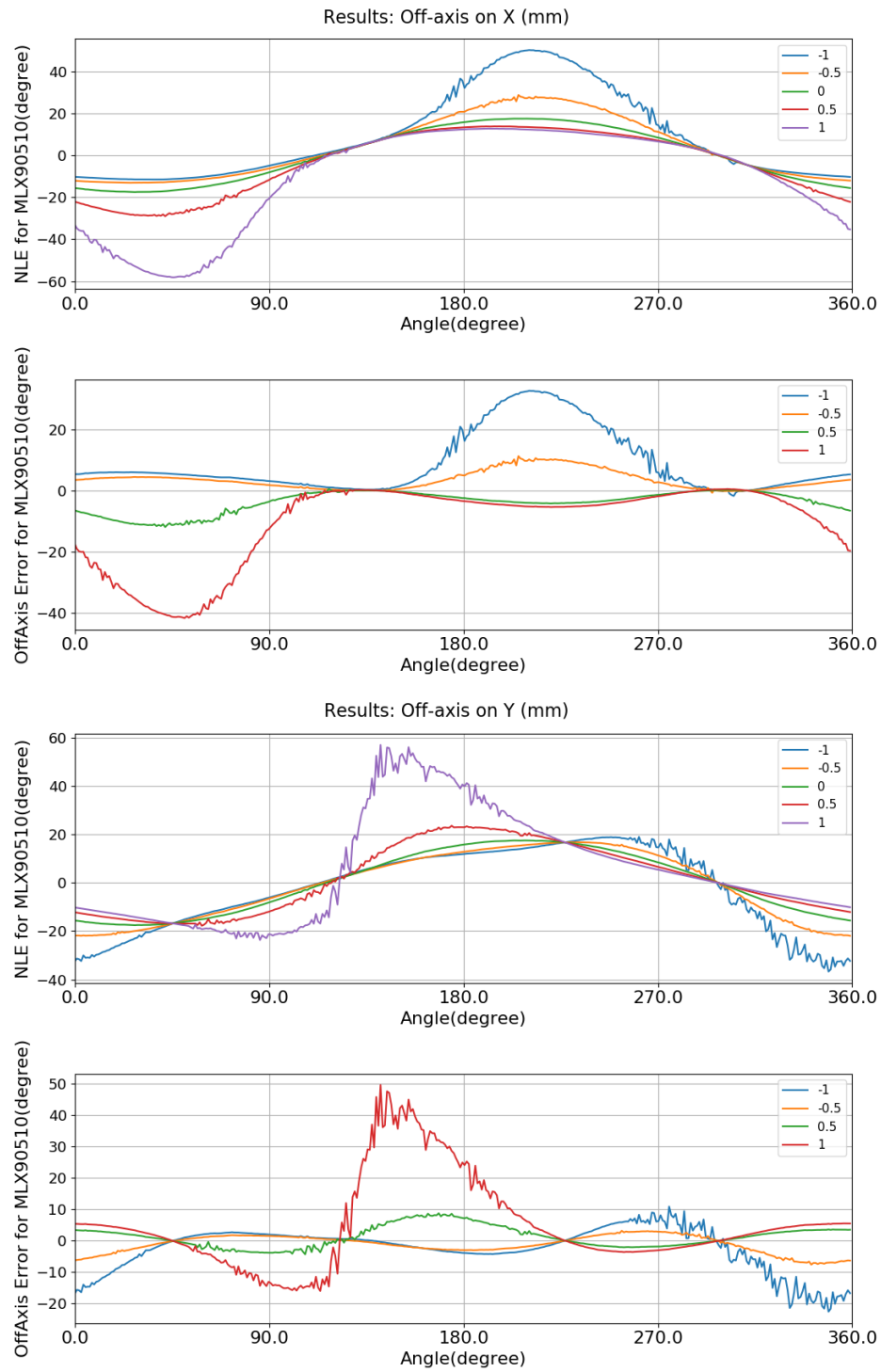
Figure 4.10 – These plots show how the NLE varies in presence of off axis on both the X axis and Y axis

Air gap
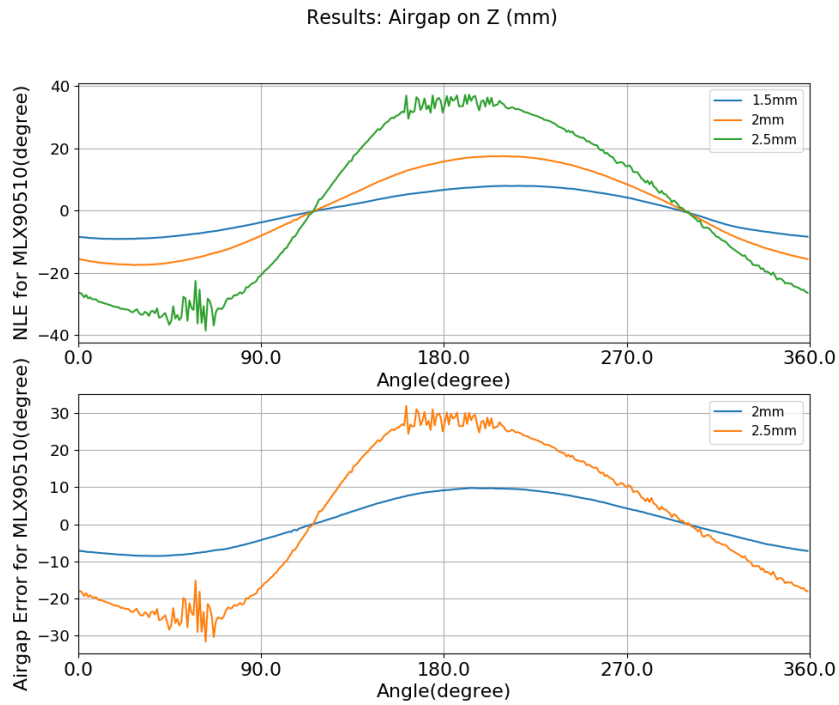
Figure 4.11 – NLE variation at several air gaps

As in the case of the first prototype, we observe an increase in the first harmonic [Figure 4.12]. However, the amplitude of such harmonic is much higher than in the 15x15mm case. This is due to the exponential dependence on the air gap of the signal's amplitude. **However, also in this case we never overcome the 90°threshold, meaning that the sensor could have still worked correctly in the hybrid structure.**

Tilt

In this case, the effect of the misalignment is not amplified by the small coil structure's dimensions. The tilt error has remained basically the same as the one saw in Test 3 of chapter 3: about 2.5°/°. **The sensor behaves really well in case of tilt and also in this case we do not cross the 90°threshold.**
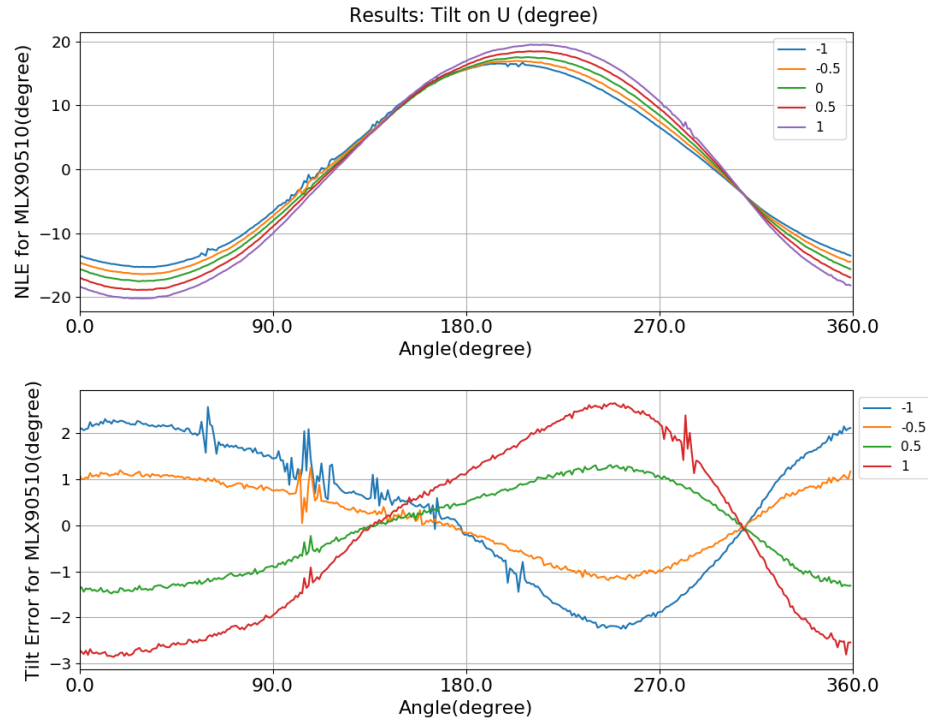
Figure 4.12 – NLE variation at several tilts on the U axis

4.5 Conclusions

The results obtained with the last measurement campaign were very positive and promising. We demonstrated that the developed scaled-down version of the inductive sensor is very much suitable for hybrid sensor design. The miniaturization of the inductive sensor was the biggest risk source for the project and now it is clear that it is possible to implement. In fact, since in chapter 3 we demonstrated the orthogonality of the working principles of inductive and magnetic sensors, the two measurement channels can be developed and evaluated separately. Moreover, these satisfying results were also obtained using the already developed MLX90510, meaning that the future IC of the inductive part of the hybrid sensor can be developed taking inspiration from this pre-existing design.

5 Conclusions and perspectives

This internship increased the Technology Readiness Level (TRL) of the hybrid 360°SFI angular sensor project from level 2 to level 3 by creating the first proof of concept prototype. The concept as shown in Figure 5.1 has been tested and is working as intended. This report demonstrated that the working principle of the inductive sensor and the magnetic sensor are completely orthogonal. This is a fundamental property which is one of the main advantages of these magnetic-inductive hybrid sensors, allowing a separated development of these two parts.

Another achievement of this internship is the development of a functional scaled-down version of the inductive part of the hybrid sensor, which may be used for a future complete implementation.
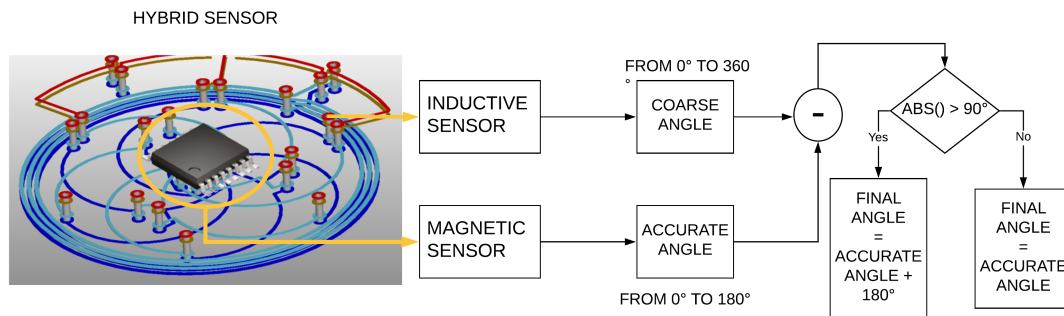
Figure 5.1 – The working principle behind the Hybrid sensor.

To summarize the current development of the project we can use Figure 5.2. The hybrid target has been ordered and has been tested on the second prototype. The interaction between the inductive and magnetic sensors was studied. A version of the coil system that could be included in an electronic package was tested in the second prototype. The remaining parts required to build the first integrated hybrid sensor are a new IC and the Lead-frame.

The path to a fully developed hybrid 360°SFI angular sensor is still long and there are still very large steps to be taken in this project.
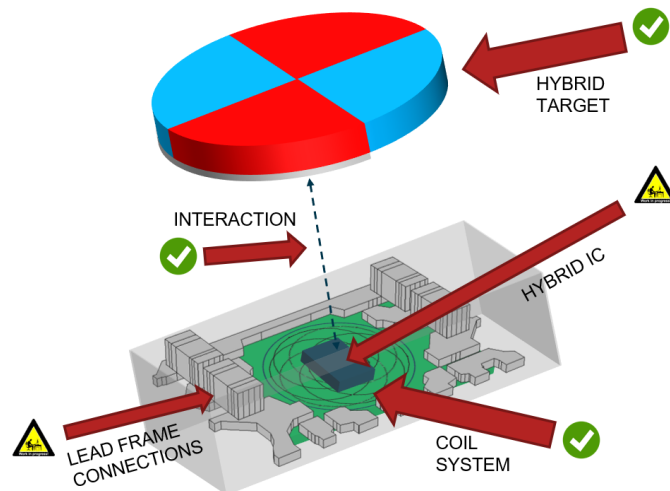
Figure 5.2 – A summary of the developments achieved in this thesis as well as a representation of the missing parts

5.1 The next steps

Despite the fact that the work done in this internship was a consistent step forward for the development of this sensor, there are many missing pieces left to be developed in the future. In order to develop a standalone sensor in a single package, a new IC has to be developed first. This IC will need to be able to coordinate the behavior of the magnetic and inductive parts of the hybrid sensor. It is not needed to develop the new IC from scratch, a good part of the design can be directly shared with preexisting designs. As an example, the MLX90510 is actually well suitable for the hybrid sensor, however, some changes could increase its performances. For example, a new oscillation circuit for the Tx coil could work with lower inductance and drain less current from the chip. Moreover, the IC can be made ad-hoc to handle very low signal levels coming from the Rx coil by increasing the level of amplification. The new part of the IC will have to include the communication part between the two channels and the output of the final measured angle.

In addition to the development of the IC, one has to study the feasibility of merging a design on a PCB with a silicon wafer produced chip and the lead-frame of the final package.

Once a first single package version of the hybrid sensor is achieved we can start a detailed error analysis which can include thermal drift error or High Temperature Operating Life (HTOL) analysis. Also, high-speed tests can be performed in order to understand the limits of the concept. Finally, functional safety aspects also have to be explored, considering the redundancy of the measurement in a dual die version to increase such safety.

The final chip will have also to be tested in the environments it is meant to work in, which in our case is an automotive environment. It will have to be able to withstand the temperature variations and aging.

Finally all these steps are considered if Melexis can find a good market for this kind of sensor and see clearly a business opportunity in this project.

A Technology Readiness Level (TRL)

Technology Readiness Levels (TRL) are a type of measurement system used to assess the maturity level of a particular technology. Originally developed by NASA for space applications in the 70s, it has been adopted as a general measure of the progress of a project in every technology from nanotechnology to informatics and communication technology[Figure A.1].

TRL 9
•Actual system "flight proven" through successful mission operations

TRL 8
•Actual system completed and "flight qualified" through test and demonstration (ground or space)

TRL 7
•System prototype demonstration in a space environment

TRL 6
•System/subsystem model or prototype demonstration in a relevant environment (ground or space)

TRL 5
•Component and/or breadboard validation in relevant environment

TRL 4
•Component and/or breadboard validation in laboratory environment

TRL 3
•Analytical and experimental critical function and/or characteristic proof-of-concept

TRL 2
•Technology concept and/or application formulated
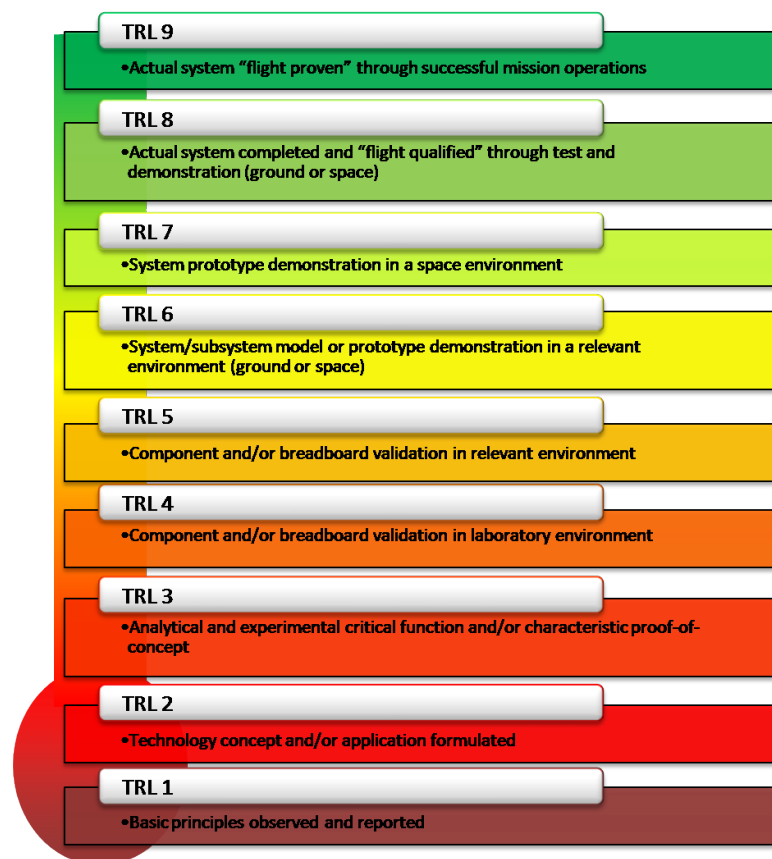
TRL 1
•Basic principles observed and reported

Figure A.1 – The meaning of each level of the TRL system. Of course, the description of each TRL have to be adapted to the field of the project in consideration.

Bibliography

[1] D.B. Pengra, J. Stoltenberg, R. Van Dyck, and O. Vilches. The hall effect. *Washington courses*, 2015.

[2] Hadi Heidari, Nicoleta Wacker, Scott Roy, and Ravinder Dahiya. Towards bendable cmos magnetic sensors. 07 2015.

[3] Jörg Bretschneider, Andreas Wilde, Peter Schneider, H.-P Hohe, and U. Kohler. Design of multi-dimensional magnetic position sensor systems based on hallinone® technology. *Fraunhofer EAS*, 07 2010.

[4] R. S. Popovic. High resolution hall magnetic sensors. In *2014 29th International Conference on Microelectronics Proceedings - MIEL 2014*, pages 69–74, 2014.

[5] R.S Popovic, Z Randjelovic, and D Manic. Integrated hall-effect magnetic sensors. *Sensors and Actuators A: Physical*, 91(1):46 – 50, 2001. Third European Conference on Magnetic Sensors Actuators.

[6] Nicolas Dupré, Olivier Dubrulle, Samuel Huber, Jan-Willem Burssens, Christian Schott, and Gael Close. Experimental demonstration of stray-field immunity beyond 5 mt for an automotive-grade rotary position sensor. *Proceedings*, 2(13):763, Dec 2018.

[7] Antonius Duisters. High speed inductive position sensor for e-machines, 2 2020.

[8] Richard Phillips Feynman, Robert Benjamin Leighton, and Matthew Sands. *The Feynman lectures on physics; New millennium ed.* Basic Books, New York, NY, 2010. Originally published 1963-1965.

[9] Lorenzo Lugani. O shaped coils based inductive sensors. 2020.

[10] Melexis. Submitted patent for hybrid sensor. 2020.

[11] Melexis. *MLX90377 Datasheet*, 2 2020. Confidential.

[12] Melexis. *MLX90510 Datasheet*, 11 2019. Confidential.

[13] H. A. Wheeler. Simple inductance formulas for radio coils. *Proceedings of the Institute of Radio Engineers*, 16(10):1398–1400, 1928.

Acronyms

CMOS Complementary Metal–Oxide–Semiconductor. 6

DAC Digital to Analog Converters. 35

DSP Digital Signal Processing. 33

EMC Electromagnetic Compatibility. 35

HP Hall Plate. 2, 10

HTOL High Temperature Operating Life. 84

IC Integrated Circuit. 33

IMC Integrated Magnetic Concentrator. 12

NEMFsd Noise-Equivalent Magnetic Field spectral density. 12

NLE Non-Linearity Error. 45

PCB Printed Circuit Board. 25

PTC Programming Tool for Characterization. 33

RAM Random Access Memory. 34

RNLE Range of the Non-Linearity Error. 45

Rx Receiving. 21

SD Single Disc. 29

SENT Single Edge Nibble Transmission. 33

SFI Stray Field Immune / Stray Field Immunity. 14, 83

SMD Surface Mounted Device. 34, 42

SOIC Small Outline integrated circuit. 33

TRL Technology Readiness Level. x, 3, 30, 83, 85

TSSOP Thin-Shrink Small-Outline Package. 33

Tx Transmitting. 21

Bruno BRAJON

Electronic Engineer,
Nanotech Master Student

- November 25, 1996
- Via protagora 36, Rome, Italy
- brunobrajon@yahoo.it
- Italian

Social Network ———

- LinkedIn

Language skills ———

🇮🇹	Italian	● ● ● ● ●
🇬🇧	English	● ● ● ● ○
🇫🇷	French	● ● ○ ○ ○

Computer Skills ———

JAVA	● ● ○ ○ ○
C	● ● ● ○ ○
MATLAB	● ● ● ● ○
COMSOL	● ● ● ○ ○
PSPICE	● ● ● ○ ○
KICAD	● ● ● ● ○
MPLAB	● ● ● ○ ○
VIRTUOSO(Cadence)	● ● ● ● ○
VHDL	● ● ● ● ○
ANSYS	● ● ○ ○ ○
ATHENA	● ● ● ○ ○
ALTIUM	● ● ● ● ○
PYTHON	● ● ● ○ ○

Hobby ———

Climbing
Piano

Education

2018 – NOW
MASTER'S DEGREE IN MICRO AND NANO TECHNOLOGIES FOR INTEGRATED SYSTEMS — PoliTo/Phelma/EPFL

The first semester at the Politecnico of Turin (Italy) is dedicated to a leveling of fundamental and advanced knowledge of solid-state physics. The second semester in the Phelma institute in Grenoble (France) is particularly focused on nanotechnological subjects and the description of physical phenomena at the nanoscale. The final semester in the EPFL (Switzerland) deepens and completes the knowledge acquired in micro and nanoelectronics with special focus on simulations and projects.

2015 – 2018
ELECTRONIC ENGINEERING BACHELOR DEGREE — University of Rome "Roma TRE"

Three years degree focused on the learning of the basics of Mathematics and Physics useful in an engineering environment with primary attention on electronics, chemistry, signals analysis, quantum mechanics, electromagnetic fields, Biomedical applications, photonics, circuits, and electronic measurements.
Final grade: 110/110 with honors.

Experience

2020
ENGINEER INTERN — MELEXIS, Bevaix CH
- Supervised the development of a next-generation position sensor for automotive application (from TRL2 to TRL3)
- PCB design (Altium) of test boards for ICs
- Automatic testing using Python scripts
- Successful study of miniaturization consequences.

2019
ASSISTANT RESEARCHER — ECTM Group, TU Delft
- Circuit design for simultaneous sensing and actuation of an Ionic Polymer–Metal Composite cantilever.
- PCB design (KiKad) of the designed circuit
- App developed with MATLAB for real-time sensing

2018
THESIS APPRENTICE — CNR-ARTOV, ROMA - ITALY
- Development of a firmware for an electronic interface for gas sensors
- C language used in MPLAB environment to program a Microchip PIC100
- Manipulation of DAC and ADC on the board to achieve impedance spectroscopy

2017 – 2018
MANAGER ASSISTANT, RECEPTIONIST — ROMA TRE Univesity, ROMA - ITALY

Part-time job at the library of scientific-technological domains. Here I learnt to interact with customers and acquired management skills.

2016 – 2020
Other projects
- Design and Layout of booth radix-4 multiplier
- Layout of ALU 8-bit
- Followed fabrication process of a piezoresistive pressure sensor in Minatec's cleanroom
- Project on sportive wearable electronics (TRL1 - TRL2)
- Design of a current generator successfully employed in electroplating process

Training

91

2019
PROCESS INTEGRATION TRAINING — ELSE KOOI LAB-TU DELFT
This training took place inside the cleanroom and it was focused on the safety measures and working principles of the various tools inside the EKL.